

2

NAVAL POSTGRADUATE SCHOOL

Monterey, California

AD-A257 886



DTIC
ELECTE
DEC 8 1992
S C D

THESIS

DEFINITION OF MEAN ENVIRONMENTAL STEERING FLOW FOR
TCM-90 TROPICAL CYCLONES

by

Richard H. Bohner Jr.

September 1992

Thesis Advisor:

Russell L. Elsberry

Approved for public release; distribution is unlimited

92-31050



REPORT DOCUMENTATION PAGE			
1a. REPORT SECURITY CLASSIFICATION UNCLASSIFIED		1b. RESTRICTIVE MARKINGS	
2a. SECURITY CLASSIFICATION AUTHORITY		3. DISTRIBUTION/AVAILABILITY OF REPORT Approved for public release; distribution is unlimited.	
2b. DECLASSIFICATION/DOWNGRADING SCHEDULE			
4. PERFORMING ORGANIZATION REPORT NUMBER(S)		5. MONITORING ORGANIZATION REPORT NUMBER(S)	
6a. NAME OF PERFORMING ORGANIZATION Naval Postgraduate School	6b. OFFICE SYMBOL (if applicable) MR	7a. NAME OF MONITORING ORGANIZATION Naval Postgraduate School	
6c. ADDRESS (City, State, and ZIP Code) Monterey, CA 93943-5000		7b. ADDRESS (City, State, and ZIP Code) Monterey, CA 93943-5000	
8a. NAME OF FUNDING/SPONSORING ORGANIZATION	8b. OFFICE SYMBOL (if applicable)	9. PROCUREMENT INSTRUMENT IDENTIFICATION NUMBER	
8c. ADDRESS (City, State, and ZIP Code)		10. SOURCE OF FUNDING NUMBERS	
		Program Element No.	Project No.
		Task No.	Work Unit Accession Number
11. TITLE (Include Security Classification) Definition of Mean Environmental Steering Flow for TCM-90 Tropical Cyclones			
12. PERSONAL AUTHOR(S) Bohner, Richard H., Jr.			
13a. TYPE OF REPORT Master's Thesis	13b. TIME COVERED From To	14. DATE OF REPORT (year, month, day) 1992, September	15. PAGE COUNT 91
16. SUPPLEMENTARY NOTATION The views expressed in this thesis are those of the author and do not reflect the official policy or position of the Department of Defense or the U.S. Government.			
17. COSATI CODES		18. SUBJECT TERMS (continue on reverse if necessary and identify by block number)	
FIELD	GROUP	SUBGROUP	
		limited region/global analysis, mean environmental flow, TCM-90, tropical cyclone motion, wavenumber bandpass filtering	
19. ABSTRACT (continue on reverse if necessary and identify by block number)			
<p>A definition for the environmental steering flow in the vicinity of the TCM-90 tropical cyclones is sought by bandpass filtering the Naval Operational Global Atmospheric Prediction System deep-layer mean u- and v- velocity and geopotential height fields. One-dimensional and two-dimensional Fourier decompositions in a limited region (120 deg. long) and in a global region are compared with six wavenumber bandpass filters (1-6, 1-9, ..., 1-21). The measure of goodness of the environmental steering flow interpolated to the storm position was to determine the minimum standard deviations of the propagation vector (defined as difference between storm motion and the steering estimate) for all six storms and the ensemble. The best results were found for either the limited region and global one-dimensional Fourier analyses of the u and v wind fields with a bandpass filter that included only wavenumbers 1 - 15. The six TCM-90 tropical cyclones were subsequently analyzed using this definition of the steering flow to estimate the propagation vectors and to examine the linear shear and relative vorticity gradients of the environmental flow. Except for early stages of storms in low latitudes, the bandpass filtered analyses provided steering vectors consistent with the changing translation directions. However, the translation speeds tended to exceed the storm motion and lead to more westward propagation vectors than expected. These propagation vectors tended to be almost perpendicular to the absolute vorticity gradient vector.</p>			
20. DISTRIBUTION/AVAILABILITY OF ABSTRACT <input type="checkbox"/> UNCLASSIFIED/UNLIMITED <input type="checkbox"/> SAME AS REPORT <input type="checkbox"/> DTIC USERS		21. ABSTRACT SECURITY CLASSIFICATION UNCLASSIFIED	
22a. NAME OF RESPONSIBLE INDIVIDUAL R.L. Elsberry		22b. TELEPHONE (Include Area code) 408-646-2373	22c. OFFICE SYMBOL MR/Es

Approved for public release; distribution is unlimited.

Definition of the Mean Environmental Steering Flow for TCM-90 Tropical Cyclones

by

Richard H. Bohner, Jr.
Lieutenant Commander, United States Navy
B.S., United States Naval Academy, Annapolis, Maryland, 1982

Submitted in partial fulfillment
of the requirements for the degree of

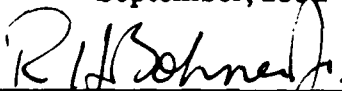
MASTER OF SCIENCE IN Meteorology and Physical Oceanography

from the

NAVAL POSTGRADUATE SCHOOL

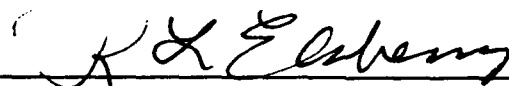
September, 1992

Author:

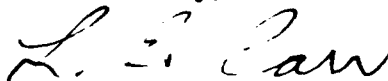


R.H. Bohner, Jr.

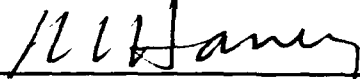
Approved by:



R.L. Elsberry, Thesis Advisor



L.E. Carr, Second Reader



R.L. Haney, Chairman
Department of Meteorology

ABSTRACT

A definition for the environmental steering flow in the vicinity of the TCM-90 tropical cyclones is sought by low-pass filtering the Naval Operational Global Atmospheric Prediction System deep-layer mean u- and v-velocity and geopotential height fields. One-dimensional and two-dimensional Fourier decompositions in a limited region (120° long) and in a global region are compared with six wavenumber low-pass filters (1-6, 1-9, ..., 1-21). The measure of goodness of the environmental steering flow interpolated to the storm position was to determine the minimum standard deviations of the propagation vector (defined as difference between storm motion and the steering estimate) for all six storms and the ensemble. The best results were found for either the limited region and global one-dimensional Fourier analyses of the u and v wind fields with a low-pass filter that included only wavenumbers 1 - 15. The six TCM-90 tropical cyclones were subsequently analyzed using this definition of the steering flow to estimate the propagation vectors and to examine the linear shear and relative vorticity gradients of the environmental flow. Except for early stages of storms in low latitudes, the low-pass filtered analyses provided steering vectors consistent with the changing translation directions. However, the translation speeds tended to exceed the storm motion and lead to more westward propagation vectors than expected. These propagation vectors tended to be almost perpendicular to the absolute vorticity gradient vector.

1981

Accession For	
NEIS CRISI	<input checked="" type="checkbox"/>
DPAC TAB	<input type="checkbox"/>
Unannounced	<input type="checkbox"/>
Justification	
By	
Distribution/	
Availability Codes	
Dist	Avail and/or Special
A-1	

TABLE OF CONTENTS

I.	INTRODUCTION	1
A.	BACKGROUND	1
B.	THE THREE-COMPONENT PARTITION	5
C.	OBJECTIVES	6
II.	PROGRAM DEVELOPMENT	7
A.	MOTIVATION	7
B.	ERRICO DETRENDING PROCEDURE	8
C.	FILTER PROGRAM DESCRIPTION	9
D.	WAVENUMBER FILTERING	10
III.	DATA ANALYSIS	16
A.	INTERPOLATION OF FILTERED FIELDS TO STORM POSITION	16
B.	SELECTION OF OPTIMUM ANALYSIS METHOD AND FILTER	19
IV.	STEERING FLOWS FOR TCM-90 STORMS	25
1.	Typhoon Winona	25
2.	Typhoon Yancy	32
3.	Typhoon Zola	41
4.	Typhoon Dot	47
5.	Typhoon Ed	54
6.	Supertyphoon Flo	61
V.	CONCLUSIONS AND RECOMMENDATIONS	70
	APPENDIX A: DISCUSSION ON FFT2D/FFT2B SUBROUTINES	73

LIST OF REFERENCES 76

INITIAL DISTRIBUTION LIST 78

LIST OF TABLES

Table I. PARAMETERS CALCULATED FOR EACH BEST TRACK STORM POSITION.	17
Table II. DATE AND TIME (00 UTC OR 12 UTC) OF ANALYSES OF TCM-90 TROPICAL CYCLONES.	18
Table III. MEANS AND STANDARD DEVIATION VALUES FOR X-COMPONENT (TOP NUMBER), Y-COMPONENT (BOTTOM NUMBER), AND MAGNITUDE OF PROPAGATION VECTORS DERIVED FOR 16 MAP TIMES DURING TYPHOON ED.	21
Table IV. NUMERICAL SUMMARY OF TCM-90 TROPICAL CYCLONE ANALYSIS BY WAVENUMBER LOW-PASS FILTER AND ANALYSIS METHOD.	23
Table V. SUMMARY OF TCM-90 TROPICAL CYCLONE ANALYSIS OF U, V WINDS VS GEOSTROPHIC WINDS, ANALYSIS METHOD, AND WAVENUMBER LOW-PASS FILTER BY STORM.	24

LIST OF FIGURES

Figure 1. Original field of layer-mean geopotential heights for TCM-90 analysis domain for 00 UTC 17 August 1990. 12

Figure 2. Wavenumbers 1 - 6 low-pass filtered layer-mean geopotential heights in the TCM-90 analysis domain for 00 UTC 17 August 1990. 13

Figure 3. Wavenumbers 1 - 15 low-pass filtered layer-mean geopotential heights in the TCM-90 analysis domain for 00 UTC 17 August 1990. 14

Figure 4. Combined zonal wavenumbers 1 - 6 and meridional wavenumbers 1 - 3 low-pass filtered layer-mean geopotential heights in the TCM-90 analysis domain for 00 UTC 17 August 1990. 15

Figure 5. Environmental steering flow for Typhoon Yancy during 9 - 21 August using LIMREG1D analysis method with a wavenumber 1 - 15 low-pass filter. 26

Figure 6. Environmental steering flow as in Fig. 5 except using GLOBAL1D analysis method. 27

Figure 7. Best track for Typhoon Winona from JTWC (ATCR 1990). 28

Figure 8. Direction and speed (top), environmental steering flow using the GLOBAL1D analysis method (middle), and derived propagation vectors for Typhoon Winona from 4 - 11 August 1990. 29

Figure 9. Relative vorticity (top) calculated from wind field (solid) and geostrophically (dotted) and total horizontal wind shear for Typhoon Winona from 4 - 11 August. 30

Figure 10. Y components (solid) and geostrophic (dashed) y components of relative vorticity gradients, and plus/minus beta values, for Typhoon Winona during 4 - 11 August 1990. 31

Figure 11. X components (solid) and geostrophic (dashed) x components of relative vorticity gradients, and plus/minus beta values, for Typhoon Winona during 4 - 11 August.	32
Figure 12. Propagation vectors (double arrow) and the gradients of absolute vorticity (dashed arrow) at four selected date-times for Typhoon Winona, based on relative vorticity gradients in Figs. 10 and 11.	33
Figure 13. Best track for Typhoon Yancy from JTWC (ATCR 1990). . .	34
Figure 14a. Translation vectors, environmental steering and propagation vectors as in Figure 8, except for Typhoon Yancy during 12 UTC 9 August through 00 UTC 15 August 1990.	35
Figure 14b. As in Fig. 14a, except for Typhoon Yancy during 12 UTC 15 August through 12 UTC 21 August.	36
Figure 15a. Relative vorticity and horizontal wind shear as in Fig. 9, except for Typhoon Yancy during 12 UTC 9 August through 00 UTC 15 August 1990.	37
Figure 15b. Same as in Fig. 15a, except for Typhoon Yancy during 12 UTC 15 August through 12 UTC 21 August.	38
Figure 16a. Relative vorticity gradients in y direction as in Fig. 10, except for Typhoon Yancy during 12 UTC 9 August through 12 UTC 15 August 1990.	39
Figure 16b. Same as in Fig. 16a, except for Typhoon Yancy during 12 UTC 15 August through 12 UTC 21 August.	40
Figure 17a. Relative vorticity gradients in x direction as in Fig. 11, except for Typhoon Yancy during 12 UTC 9 August through 12 UTC 15 August 1990.	41
Figure 17b. Same as in Fig. 17a, except for Typhoon Yancy during 12 UTC 15 August through 12 UTC 21 August.	42
Figure 18. As in Fig. 12, except for seven selected date-times for Typhoon Yancy.	43
Figure 19. Best track for Typhoon Zola from JTWC (ATCR 1990). . .	44

Figure 20. Translation vectors, environmental steering flow and propagation vectors as in Fig. 8, except for Typhoon Zola during 12 UTC 15 August through 12 UTC 22 August 1990.	45
Figure 21. Relative vorticity and horizontal wind shear as in Fig. 9, except for Typhoon Zola during 12 UTC 15 August through 12 UTC 22 August 1990.	46
Figure 22. Relative vorticity gradient in y direction as in Fig. 10, except for Typhoon Zola during 12 UTC 15 August through 12 UTC 22 August 1990.	48
Figure 23. As in Fig. 22, except for relative vorticity gradient in x direction.	49
Figure 24. As in Fig. 12, except for seven selected date-times for Typhoon Zola.	50
Figure 25. Best track for Typhoon Dot from JTWC (ATCR 1990).	51
Figure 26. Translation vectors, environmental steering flow, and propagation vectors as in Fig. 8, except for Typhoon Dot during 12 UTC 2 September through 12 UTC 8 September 1990.	52
Figure 27. Relative vorticity and horizontal wind shear as in Fig. 9, except for Typhoon Dot during 12 UTC 2 September through 12 UTC 8 September 1990.	53
Figure 28. Relative vorticity gradient in y direction as in Fig. 10, except for Typhoon Dot during 12 UTC 2 September through 12 UTC 8 September 1990.	54
Figure 29. As in Figure 28, except for relative vorticity gradient in x direction.	55
Figure 30. As in Figure 12, except for five selected date-times for Typhoon Dot.	56
Figure 31. Best track for Typhoon Ed from JTWC (ATCR 1990).	57
Figure 32. Translation vectors, environmental steering flow and propagation vectors as in Fig. 8, except for Typhoon Ed during 00 UTC 12 September through 12 UTC 19 September 1990.	58

Figure 33. Relative vorticity and horizontal wind shear as in Fig. 9, except for Typhoon Ed during 00 UTC 12 September through 12 UTC 19 September 1990.	59
Figure 34. Relative vorticity gradient in y direction as in Fig. 10, except for Typhoon Ed during 00 UTC 12 September through 12 UTC 19 September 1990.	60
Figure 35. As in Fig. 34, except for relative vorticity gradient in x direction.	61
Figure 36. As in Fig. 12, except for seven selected date-times for Typhoon Ed.	62
Figure 37. Best track for Supertyphoon Flo from JTWC (ATCR 1990).	63
Figure 38. Translation vectors, environmental steering flow and propagation vectors as in Fig. 8, except for Supertyphoon Flo during 00 UTC 12 September through 12 UTC 19 September 1990.	64
Figure 39. Relative vorticity and horizontal wind shear as in Fig. 9, except for Supertyphoon Flo during 00 UTC 12 September through 12 UTC 19 September 1990.	66
Figure 40. Relative vorticity gradient in y direction as in Fig. 10, except for Supertyphoon Flo during 00 UTC 12 September through 12 UTC 19 September 1990.	67
Figure 41. As in Fig. 40, except for relative vorticity gradient in x direction.	68
Figure 42. As in Fig. 12, except for seven selected date-times for Supertyphoon Flo.	69

ACKNOWLEDGEMENTS

I would like to publicly thank the many individuals who made this work possible. First and foremost, I would like to thank Dr. Elsberry for his gifted art of teaching. His patience and wise counsel to keep the big picture helped encourage and direct me. Paul Dobos and Lcdr. Dave Titley deserve more credit than I can put into words for their expert guidance and instruction in computer programming. Their patience, understanding, and availability turned many seemingly hopeless situations into profitable learning experiences. I would also like to thank Lcdr. Les Carr for his review of the manuscript. Thanks are also due to Rich Donat, Neil Harvey, and Dennis Mar of the W. R. Church Computer Center of the Naval Postgraduate School for their time and help in debugging numerous Fortran programs.

I also owe Professors Pat Harr, Teddy Holt, and Tom Murphree of the Naval Postgraduate School Meteorology Department a heart full of appreciation for their responses to many "spur of the moment" requests for some instruction in statistics and dynamics.

Last, but certainly not least, I owe a great deal of gratitude to my wonderful wife, Connie, and my three priceless children, Aimee, David, and Rebekah, for their many prayers and selfless encouragement and support throughout this project. They were always so understanding, and it truly would have been infinitely more difficult without them. This work is dedicated to my family, who I love more than anything else on this earth.

I. INTRODUCTION

A. BACKGROUND

In recent years, an emphasis has been placed upon the study and research of tropical cyclone motion. Through the sponsorship of the Office of Naval Research Marine Meteorology Program, a five-year accelerated research initiative on this subject was commenced in October 1986, and culminated in a field experiment (Elsberry 1990) in August and September 1990 known as Tropical Cyclone Motion 90 (TCM-90). Other components of this initiative included analytical and numerical modelling studies and analysis of existing data sets.

Although tropical cyclones can be considered to be advected by a large-scale environmental flow, recent observational and numerical studies indicate that the motion can deviate significantly at times from this large-scale flow. This difference between the tropical cyclone motion vector, V_c , and the steering flow vector, V_s , is known as the propagation vector, V_p . Specification, understanding, and prediction of V_p have been primary objectives of recent tropical cyclone motion research (Elsberry and Abbey 1991).

The calculation of the propagation vector magnitude and direction via $V_c - V_s$ is strongly dependent upon the definition of the environmental steering flow. One definition of V_s came from the rawinsonde composite studies (e.g., George and Gray 1976, Chan and Gray 1982, Gray 1989) under Professor William Gray. These studies have defined the steering flow as radial-band averages of vertically-integrated wind observations at various radial distances from the cyclone center. Based upon this definition, the storm motion generally was found to be to the left of and faster than the steering flow, regardless of whether the vertical averaging was over the entire troposphere or only the layer between the boundary and the outflow layers. This definition of steering, however, rotates clockwise and

decreases in magnitude at increasing radii in the Northern Hemisphere. Therefore, the departure of the tropical cyclone motion from the defined steering flow depends upon which radial bands are used for averaging. The common choice has been the 5° - 7° lat. radial band.

Chan (1985) did further steering flow studies using radial-band averages of operational wind field analyses, and he found large differences in flow fields among groups of westward-, northward-, and northwestward-moving cyclones. Except for the westward-moving storms, the steering motion relationships he found agreed with the rawinsonde composites of Chan and Gray (1982).

Carr and Elsberry (1990) converted the composite rawinsonde studies of Chan and Gray (1982), along with similar composites by Holland (1984) of Australian cyclones, into a north-oriented, earth-relative coordinate system. Although both of the original studies defined the steering flow using 5° - 7° lat. radial bands, slightly different layer depths were used. Carr and Elsberry found that the propagation vector magnitudes generally ranged from 1 - 2.5 m/s, with directions that tended to be westward and poleward.

A second environmental steering flow is the geostrophic steering as defined in a series of studies initiated by Neumann (1979). Neumann (1979) and Keenan (1982) calculated the geostrophic steering flow from operational height field analyses and showed that the Atlantic and Australian region tropical cyclones tended to move with the speed and direction of the deep-layer environmental flow from such height fields.

Dong and Neumann (1986) reanalyzed the relationship between tropical cyclone motion and the environmental geostrophic flow by using various gridpoint values of geopotential heights at 5° - 10° lat. distances from the cyclone center to calculate the geostrophic steering components. They found significant differences between the steering for eastward-moving and westward-moving Atlantic cyclones. One noticeable difference is that the basic flow in the westerlies increases with height up to 200 mb, whereas

the basic flow in the easterlies decreases with height up to approximately 400 mb. In general, the storm motion is found to be to the left of the deep-layer steering in the westerlies and to the right in the easterlies, but the departures from the steering at individual pressure levels are quite significant. Based on correlation coefficients for geostrophic steering, Dong and Neumann found 400 mb to be the optimum single level for both westward- and eastward-moving Atlantic hurricanes, whereas 700 mb was optimum for tropical storms. The optimum deep-layer mean for hurricanes is up to 100 mb. Although the correlation coefficients are slightly higher for the deep-layer mean, the track forecast errors at 24 h for a steering prediction based on the optimum level are not much smaller.

A recent innovation in environmental steering flows is known as cyclone intensity-dependent steering. Velden and Leslie (1991) in the Australian basin, Gross (1991) using the Beta Advection Model (BAM) in the East Pacific basin, and various other studies conducted in the Atlantic basin, have revealed that the layer depth of the environmental steering flow should be increased with increased tropical cyclone intensity. That is, a deeper layer should be used to account for the deeper cyclonic circulation associated with the more intense storms.

Some individual storms have also been studied in an attempt to correlate storm motion with the environmental flow. During their Synoptic-Flow Experiments, the Hurricane Research Division (HRD) of the National Oceanic and Atmospheric Administration (NOAA) obtained wind fields for several cases of tropical cyclones by deploying Omega dropwindsondes from a flight level of around 400 mb. Lord and Franklin (1987) described the three-dimensional, nested analysis of these wind fields. Franklin (1990) describes the evolution of the environmental wind field over three successive days around the developing hurricane Josephine. Although the storm moves in the general direction of the flow at approximately 700 mb, the translation speed is closer to the 500 mb flow, or the layer mean flow from the surface to 100 mb. The radial-band

averages around Josephine, almost without exception, rotate clockwise rapidly with increasing distance from the storm. During the three-day analysis, as the 5° - 7° lat. radial-band average rotates clockwise, the storm motion also rotates clockwise to maintain a relatively consistent vector difference, defined as the propagation vector: 1.8 m/s toward 289°, 2.4 m/s toward 319°, and 3.7 m/s toward 317° respectively.

Kaplan and Franklin (1991) applied the same technique to analyze dropwindsonde data in tropical storm Florence. They found that the smallest propagation vector occurred for the 850 - 500 mb layer (2.7 m/s toward 012°), with the storm motion to the left and faster than the 5° - 7° lat. radial-band average. Feuer and Franklin (1991) show for hurricane Gloria that the difference between the storm motion and the mid-tropospheric flow was toward the northwest at 2 - 3 m/s.

Marks et al. (1991) have used airborne Doppler radar data to study the 3-dimensional wind field in the inner core of some tropical cyclones. Although noting that the horizontal average of the inner core wind velocities varied with height due to vertical wind shear, they discovered that the storm motion appeared to correlate well with the vertical mean of the average wind velocities. Roux and Marks (1991) proposed a new processing technique to derive the wind field from Doppler velocity measurements along a single flight leg. They found that their measurements in hurricane Hugo confirmed that the tropical cyclone is translating with the depth-averaged wind velocity in the inner core region.

In conclusion, numerous attempts have been made to define the environmental steering flow around tropical cyclones in an effort to discover consistent relationships to the tropical cyclone motion. Although the motion does appear to deviate significantly at times from this flow, as it is defined in each case, the forecasting of tropical cyclone motion seems to hinge upon a consistent definition of environmental steering.

B. THE THREE-COMPONENT PARTITION

One approach to obtain the environmental steering flow is a three-component partitioning of the total wind flow. The three parts are the symmetric vortex, a large-scale environmental flow and an asymmetric circulation that includes wavenumber one gyres. Although tropical cyclones blend continuously with their environment, this partitioning can be quite informative if the spatial and temporal scales of each component are different. The "Three-Component Partition" was used by Holland and Evans (1991) in their study of the structural changes associated with the interaction of a barotropic vortex with an idealized subtropical ridge.

An alternative two-component partitioning method is the removal of the symmetric vortex that represents the cyclone, and assuming that all of the remaining flow represents the environment. A problem associated with this approach is the inclusion in the environment of any time-dependent symmetric or asymmetric features that may be associated with the cyclone. The converse can also occur, wherein environmental gradients can be aliased into the symmetric vortex, as illustrated in Figure 2 of Holland and Evans.

In the Three-Component Partition, the environmental flow is initially removed by one of various methods. The remaining flow can be further partitioned into a time-dependent symmetric cyclone and asymmetric components. After the symmetric circulation is removed, the asymmetric circulation (wavenumber one gyres) would then be left. For numerical model simulations such as Fiorino and Elsberry (1989), the uniform flow between these wavenumber one gyres is equal to the propagation vector, and in the absence of a mean flow represents the total motion of the tropical cyclone. One advantage of this method as opposed to the symmetric vortex partition is that the resulting "tropical cyclone" left after the environment is removed can be studied and compared with similar cyclones that may have evolved in differing environments.

One condition that must be met for this partitioning method to be effective is that the environmental flow changes more slowly in time than both the symmetric cyclone and the asymmetric circulation. In particular, it is assumed that most of the environmental changes are due only to the translation of the tropical cyclone within the very slowly evolving environmental velocity field.

C. OBJECTIVES

The purpose of this study is to evaluate a definition for the environmental steering flow based upon Fourier-analyzed global and limited region Naval Operational Global Atmospheric Prediction System (NOGAPS) wind and height fields. The results should provide a quick determination of long wave filtered environmental data. In this study, the steering flows on a global and limited region scale will be compared using both one- and two-dimensional Fourier filtering. Additional comparisons will be made between steering flows defined directly from the analyzed winds and calculated indirectly based on geostrophic winds using analyzed height fields.

If this environmental steering flow can be unambiguously identified and removed from the total wind field as part of the three-component partitioning, then the remaining symmetric cyclone and asymmetric circulations can be more readily studied. From a forecasting perspective, a quick first-order estimate to the tropical cyclone motion may be obtained by the addition of a consistent propagation vector to the derived environmental steering flow. Although not evaluated as part of this study, it is possible that the evolution of the environmental steering flow might be described by applying the same low-pass filtering techniques to the NOGAPS forecast fields. Then a track forecast over longer times could be derived by adding a propagation vector to the steering estimates from filtered NOGAPS forecast fields.

II. PROGRAM DEVELOPMENT

A. MOTIVATION

The natural representation of any field on a sphere is in terms of spherical harmonics. Once a particular environmental field has been transformed into its spectral coefficients, that complete set of spectral coefficients can be used to reconstruct the analyzed or the forecast field. This can be readily done with global spectral models, such as NOGAPS.

The Fleet Numerical Oceanography Center (FNOC) does not archive spectral coefficients, but instead stores the analyzed fields, including winds and geopotential heights, on a 2.5° lat. by 2.5° long. grid. Consequently, an harmonic analysis in terms of a one-dimensional (around latitude circles) or two-dimensional Fourier decomposition will be used to represent the FNOC analyses. The longest waves (smallest wavenumbers) represent the large-scale environmental flow that advects the tropical cyclone. Conversely, the tropical cyclone circulation is represented primarily by shorter wavelengths (larger wavenumbers). The difficulty in diagnosing a steering flow is choosing a low-pass filter that selectively removes the wavelengths representing the tropical cyclone circulation. Various summations of wavenumbers will be tested to determine which summation best represents the large-scale environmental flow that advects the tropical cyclone.

The harmonic analyses are derived using one- and two-dimensional Fourier decompositions over the entire globe. An alternative is to do the harmonic analyses within a limited region from 60°E to 180°E , and from 10°S to 60°N . Such limited region analyses may serve as a better representation of the advection of the tropical cyclone by the large-scale environmental flow, since the global harmonic analyses may be contaminated with environmental values far from the western North Pacific that have no

influence on the tropical cyclone due to their spatial separation. The size of the limited region is chosen to completely encompass the development and decay regions of the western North Pacific tropical cyclones studied during TCM-90. Furthermore, the zonal extent of this domain is exactly one-third of the globe, which facilitates zonal wavenumber comparisons.

B. ERRICO DETRENDING PROCEDURE

The absence of periodicity introduces a problem for Fourier analysis on limited region fields. A detrending method is used here that was originally developed by Errico (1985), and subsequently used by Errico and Baumhefner (1987) in a modelling study of mesoscale predictability. The detrending procedure was applied both zonally and meridionally in the two-dimensional analyses (except zonally in the global analysis), and only zonally in the one-dimensional limited region analysis.

To illustrate this procedure, consider a field of M equally spaced elements zonally and N equally spaced elements meridionally. Elements in the field are identified as F_{ij} , where i and j are the zonal and meridional indices. Since the procedure is independent of the order in which the trends are removed, the field is detrended first in the meridional direction. The domain-wide meridional slope is given by

$$S_{yi} = (F_{i,N} - F_{i,1}) / (N - 1) , \quad i = 1, M.$$

The resulting detrended field is expressed as

$$F'_{ij} = F_{ij} - 0.5 * S_{yi} * (2 * j - N - 1) , \quad i = 1, M , j = 1, N.$$

Similarly, the domain-wide zonal slope is

$$S_{xj} = (F'_{M,j} - F'_{1,j}) / (M - 1) , \quad j = 1, N$$

and the resulting final detrended field is

$$F_{Dij} = F'_{ij} - 0.5 * S_{xj} * (2 * i - M - 1) , \quad i = 1, M , j = 1, N.$$

As this detrended field is now periodic in both the zonal and meridional directions, a one- or two-dimensional Fourier analysis can readily be calculated. When the inverse Fourier transform is applied to reconstruct

the fields, the trends that were removed must be replaced. Therefore, the final analyzed field with the trend restored can be expressed as

$$F_{Tij} = F_{Dij} + 0.5 * S_{yi} * (2 * j - N - 1) \\ + 0.5 * S_{xj} * (2 * i - M - 1) , \quad i = 1, M , j = 1, N.$$

C. FILTER PROGRAM DESCRIPTION

The NOGAPS data were provided on cartridge tapes in a compressed format. A Fortran program entitled NEDNREAD, written by LCDR Dave Titley, converted the u and v velocities to meters per second and the geopotential heights to meters. The initial test NOGAPS data set covered the time period 12 September 1990 through 19 September 1990 at 12-h intervals. This test period was chosen to coincide with the TCM-90 data collected during tropical cyclones Ed and Flo. Other time periods were later analyzed that coincided with TCM-90 data collected on tropical cyclones Winona, Yancy, Zola and Dot. NOGAPS analysis and forecast fields out to 72 h in 12-h increments were available on a 2½° lat./long. grid. Only the analyses will be used in this research, although the procedures could also be used for the forecast fields to evaluate how well NOGAPS predicts different wavelength features.

For the global fields, there are 73 gridpoints in the meridional direction and 144 gridpoints in the zonal direction. The fields are archived on a grid from 90°N to 90°S with 60°E as the first gridpoint in longitude. For convenience in the display routines, the latitudinal indices were reversed so that the first gridpoint in latitude was 90°S. For the limited region from 60°E - 180°E and from 10°S - 60°N, the longitude gridpoints range from 1 to 49, and the latitude gridpoints are 33 to 61 on the global grid. The one-dimensional analysis for the limited region was between 60°E and 177.5°W, using gridpoints 1 - 50 to comply with subroutine specifications.

Although analyses and forecasts are available at 12 mandatory pressure levels, only layer-mean values are utilized here. That is, pressure-

weighted mean values are calculated using the 850 mb, 700 mb, 500 mb, 400 mb, and 300 mb u and v velocities and geopotential heights. These layer-mean values are considered to apply within the 925 - 250 mb layer, and represent a basic current that advects the tropical cyclone. Both the boundary layer and outflow layers are excluded by this definition of the steering layer.

Four harmonic analyses were applied to the NOGAPS fields: limited region using a one-dimensional Fourier analysis (LIMREG1D); limited region using a two-dimensional Fourier analysis (LIMREG2D); global domain using a one-dimensional Fourier analysis (GLOBAL1D); and global domain using a two-dimensional Fourier analysis (GLOBAL2D). The Errico "detrending" routine was applied to both limited grids and the GLOBAL2D. The Fourier analyses were calculated using IMSL subroutines (IMSL Library Vol 2, Ch F, Ed 9.2, IMSL Math/Library Vol 2, Ch 6, Ver 1.1): FFTSC for the one-dimensional analysis, the FFT2D/FFT2B combination for the two-dimensional analyses. In the FFTSC, a single array of even dimension (N) is input, and the output is two arrays of sine and cosine coefficients of dimension $N/2 + 1$. A brief description of the FFT2D/FFT2B is given in Appendix A. The filtering was carried out by manipulating the coefficients derived from the appropriate subroutines. Specifically, the undesired coefficients were simply ignored in the one-dimensional programs. For the two-dimensional programs, the coefficients of various sets of shorter wavelengths were set to 0, since the entire array of coefficients was required in the matrix multiplication to reconstruct the filtered fields. Once the desired coefficients had been filtered, the trend removed by the Errico "detrending" procedure was restored.

D. WAVENUMBER FILTERING

Six global wavenumber low-pass filters were studied to determine which best represented the environmental flow that advects the tropical cyclone: wavenumbers 1 - 6; 1 - 9; etc. through wavenumbers 1 - 21 in increments of

3. In the two-dimensional analyses, similar groups of meridional wavenumbers were generated.

In the limited region, the higher wavenumber of the longitudinal filter is one-third of the analogous global wavenumber filter, since the zonal extent of the limited region is exactly one-third of the globe. Consequently, the longitudinal wavenumber filter in the limited region is equivalent to the global wavenumber filter. Thus, both results can be directly compared.

As an example, the deep-layer mean of the NOGAPS geopotential analyses for 00 UTC 17 August is shown in Fig. 1. This geopotential height field illustrates the circulation of Typhoon Yancy to the southeast of Taiwan, and the beginning stage of Typhoon Zola farther to the southeast. Retaining only the first six wavenumbers in the low-pass filter (Fig. 2) strongly smooths the features in the midlatitudes and also flattens the geopotentials around Yancy. However, the low-pass filter retaining the first 15 wavenumbers (Fig. 3) retains more of the short-wave circulations in the midlatitudes and more of the trough around Yancy that are likely to be important in the steering flow. A combination of a wavenumber 1 - 3 meridional low-pass filter with a zonal low-pass filter retaining wavenumbers 1 - 6 is shown in Fig. 4. The extreme smoothing of the geopotential height gradients between 35°N and 60°N would severely alter the calculated geostrophic wind velocities that are computed using these geopotential height gradients. An extreme flattening of the geopotentials near Yancy is also noted. Because the filtering in the meridional direction severely degrades the geopotential height gradients, no filtering will be done in this direction.

In summary, the input into each of the four analysis programs was global arrays of layer-mean NOGAPS u-velocity, v-velocity, and geopotential height data. The output was arrays of low-passed filtered data of these respective fields. The global fields were compared with the limited region fields in the western Pacific region of TCM-90.

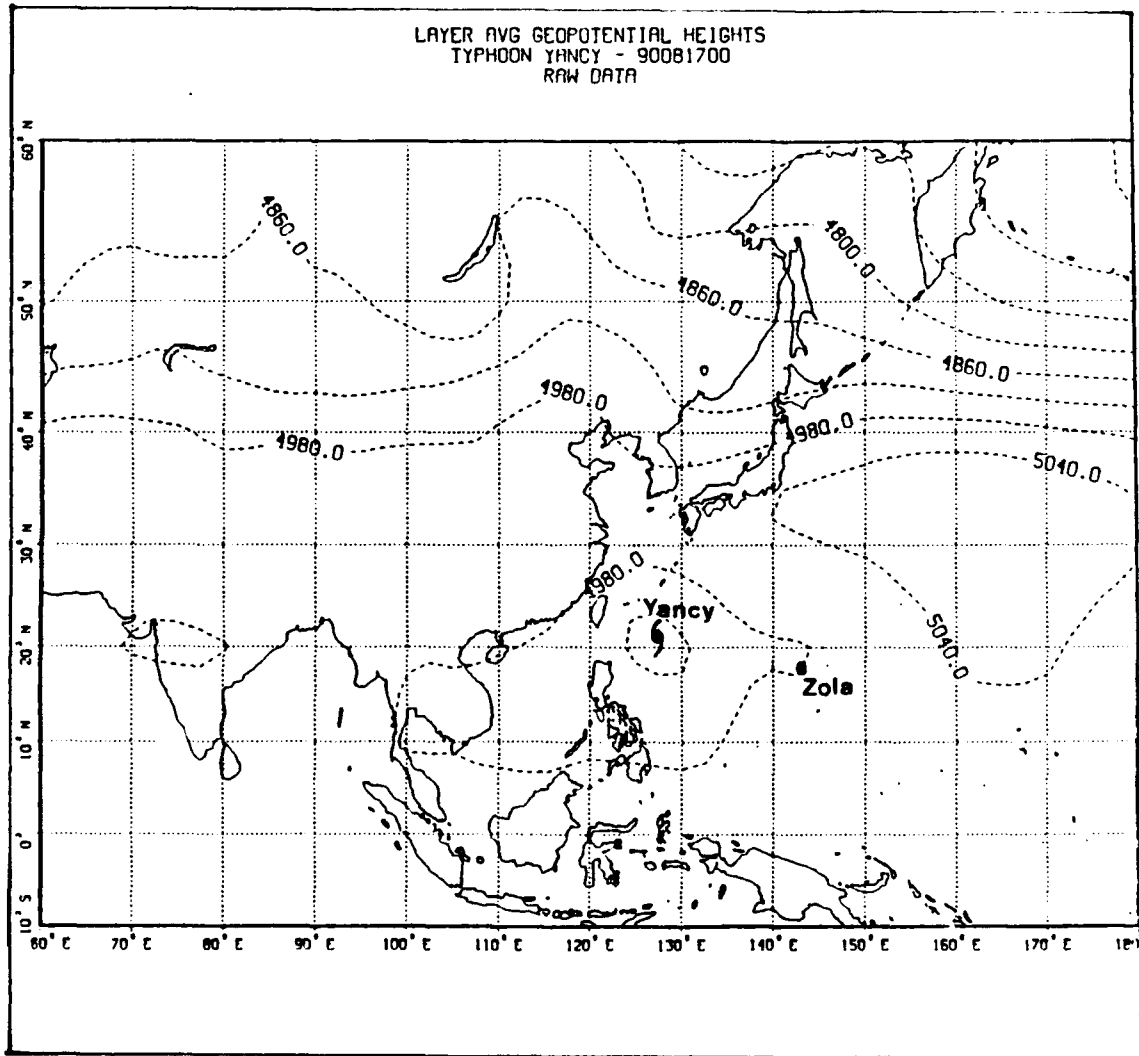


Figure 1. Original field of layer-mean geopotential heights for TCM-90 analysis domain for 00 UTC 17 August 1990.

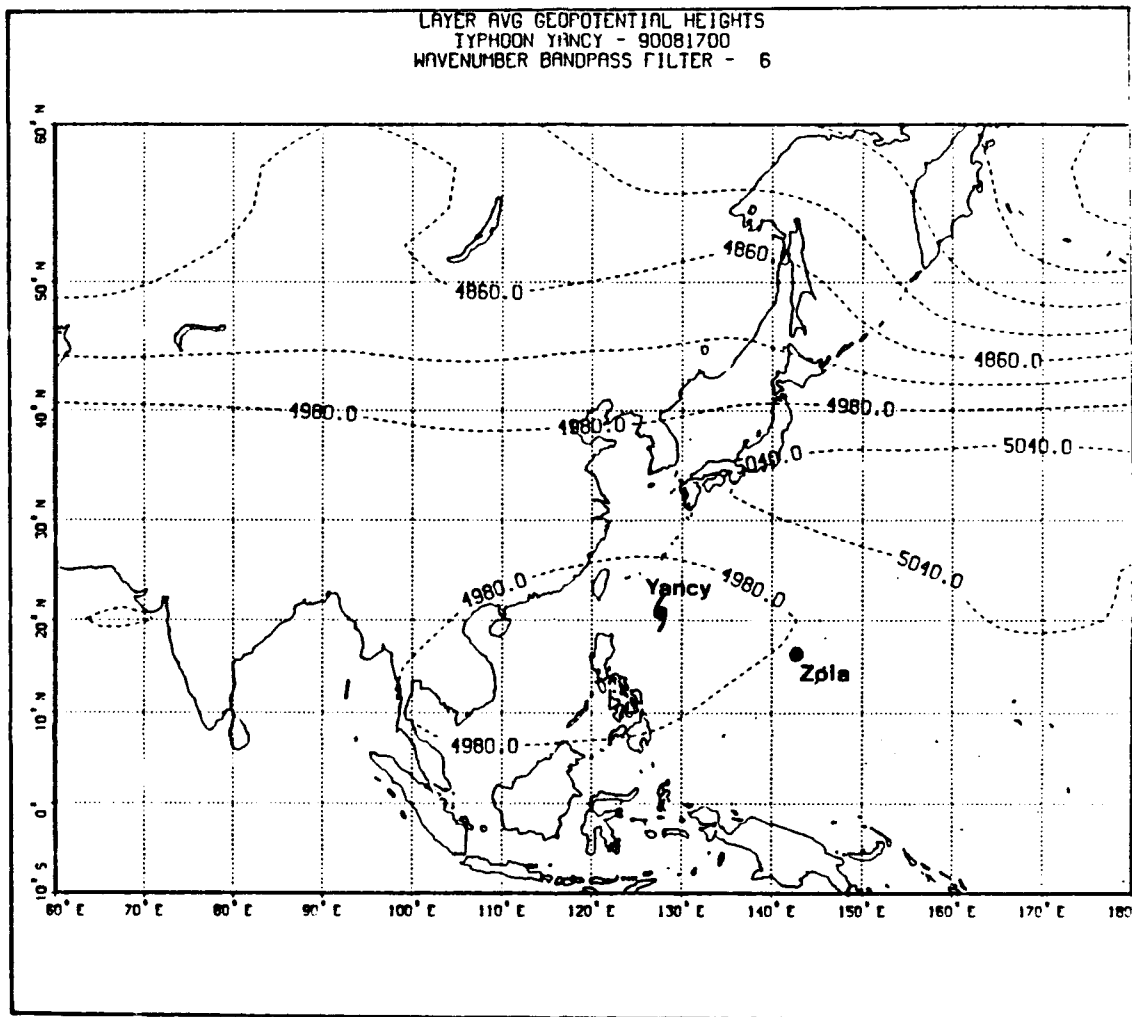


Figure 2. Wavenumbers 1 - 6 low-pass filtered layer-mean geopotential heights in the TCM-90 analysis domain for 00 UTC 17 August 1990.

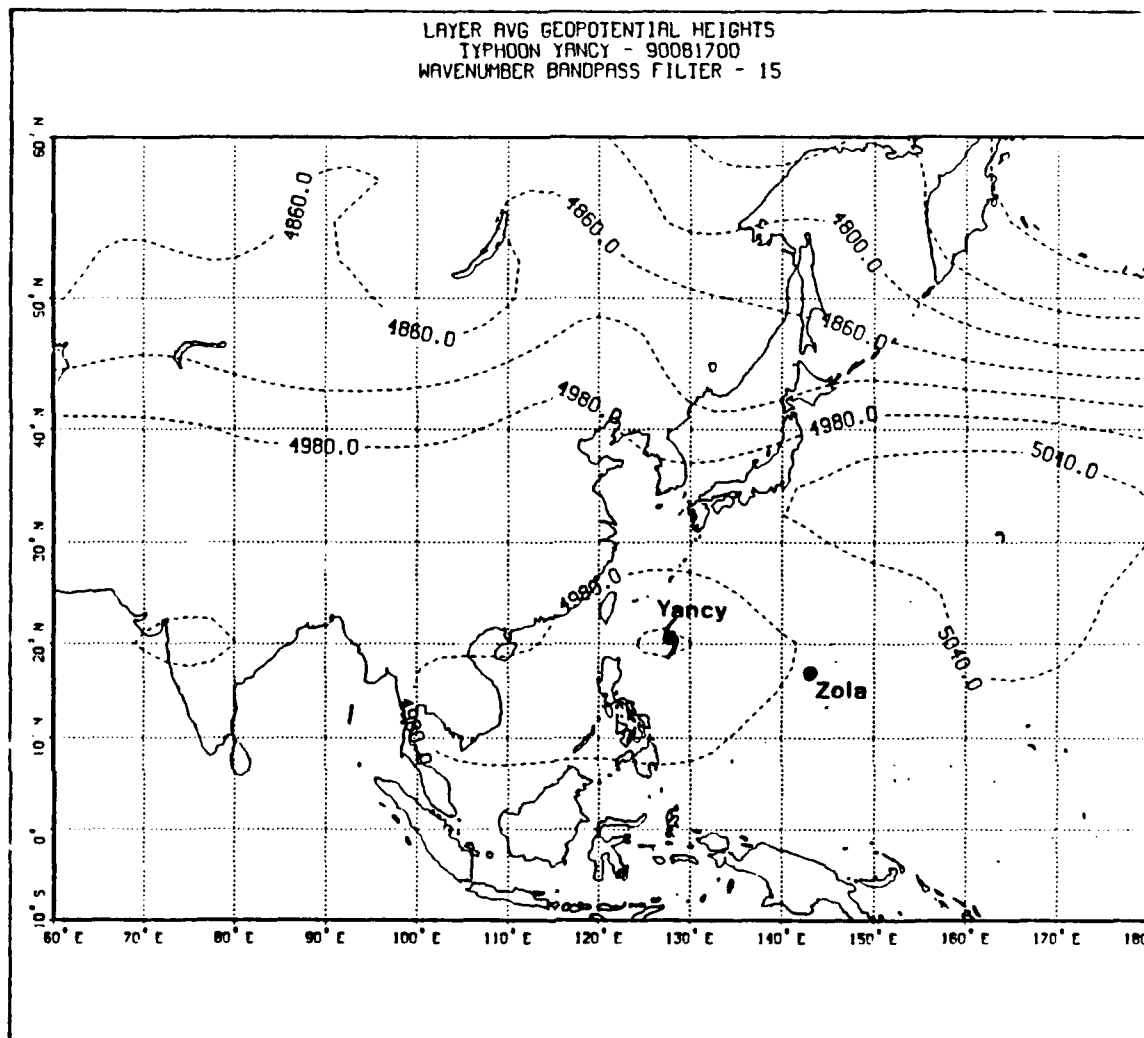


Figure 3. Wavenumbers 1 - 15 low-pass filtered layer-mean geopotential heights in the TCM-90 analysis domain for 00 UTC 17 August 1990.

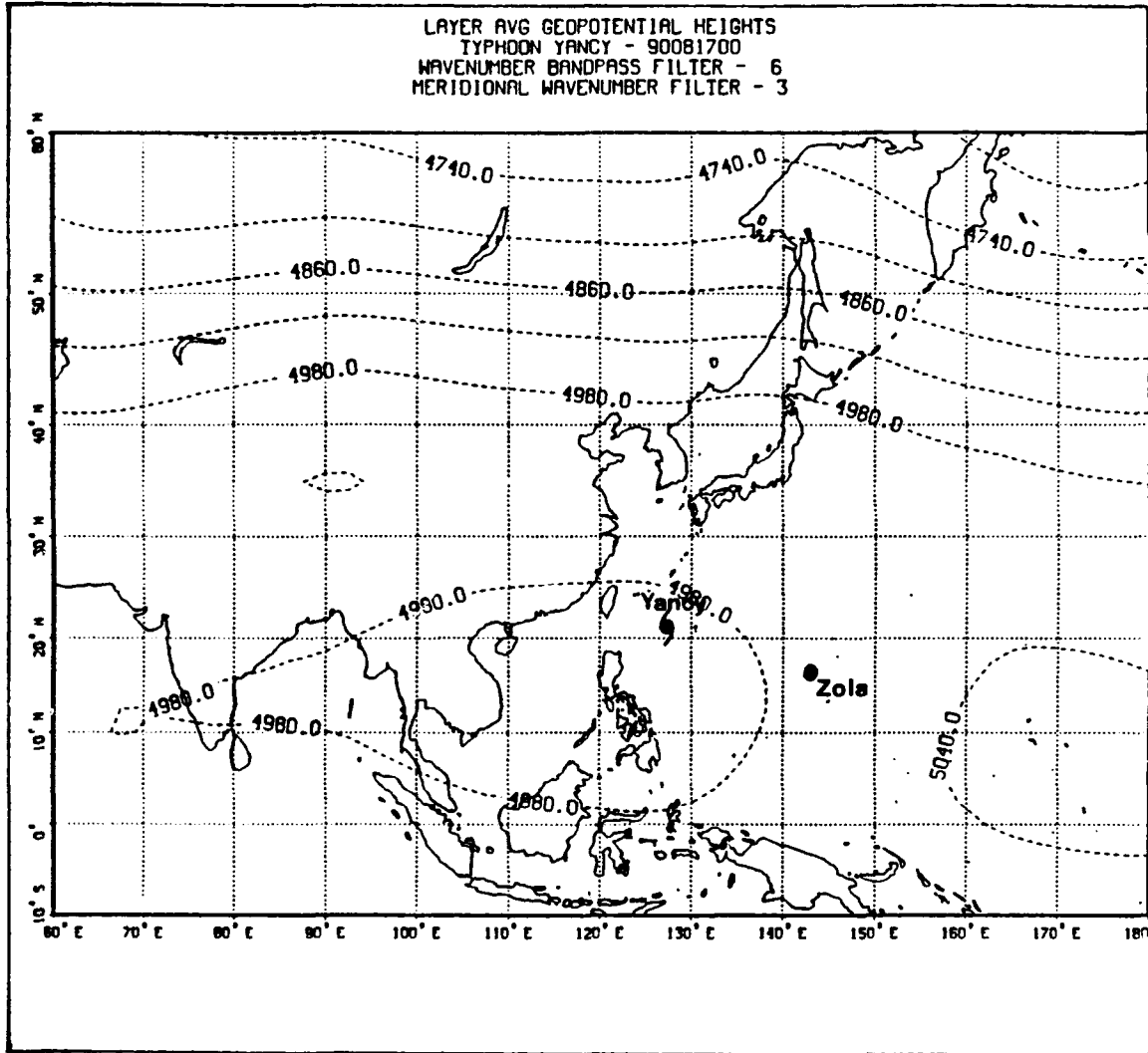


Figure 4. Combined zonal wavenumbers 1 - 6 and meridional wavenumbers 1 - 3 low-pass filtered layer-mean geopotential heights in the TCM-90 analysis domain for 00 UTC 17 August 1990.

III. DATA ANALYSIS

A. INTERPOLATION OF FILTERED FIELDS TO STORM POSITION

The wind fields filtered with the six low-passes over the global and limited regions described previously constitute 24 options for defining the steering motion of tropical cyclones. This section will describe the evaluation of these options to select the optimum analysis method and filter to represent the large-scale environmental flow advecting the tropical cyclones. The outputs of layer-mean u-velocity, v-velocity, and geopotential height generated by the four analysis methods were used to calculate 29 parameters of interest (Table I) at the 00 UTC and 12 UTC Joint Typhoon Warning Center (JTWC) best-track positions for each of the six TCM-90 tropical cyclones. The date-time groups analyzed for each storm are listed in Table II.

The layer-mean u- and v-velocities interpolated to the best-track position directly represent the environmental steering flow. The values at each storm position from the limited region grid were interpolated using the IMSL subroutine QD2VL (IMSL Math/Library Vol. 2, Ch. 3, Ver. 1.1). This subroutine interpolates a table of values using quadratic polynomials and returns an approximation to the tabulated function by using six neighboring interior grid points. The gridpoints have the same resolution as the NOGAPS data.

The layer-mean geopotential heights (z) were used to calculate the environmental geostrophic steering flow, using the geostrophic equations on a constant pressure surface

$$U_g = - (g / f) (\partial z / \partial y) \quad \text{and}$$

$$V_g = (g / f) (\partial z / \partial x),$$

where g and f are the gravitational acceleration and the Coriolis parameter respectively. The Coriolis parameter was calculated at each storm position using

Table I. PARAMETERS CALCULATED FOR EACH BEST TRACK STORM POSITION.

1. Layer-mean u-velocity
2. Layer-mean v-velocity
3. Layer-mean geopotential height
4. Coriolis parameter
5. Layer-mean geostrophic u-velocity
6. Layer-mean geostrophic v-velocity
7. X shear of layer-mean u-velocity
8. Y shear of layer-mean u-velocity
9. X shear of layer-mean v-velocity
10. Y shear of layer-mean v-velocity
11. X shear of layer-mean geostrophic u-velocity
12. Y shear of layer-mean geostrophic u-velocity
13. X shear of layer-mean geostrophic v-velocity
14. Y shear of layer-mean geostrophic v-velocity
15. Relative vorticity
16. Geostrophic relative vorticity
17. Total wind shear
18. Total geostrophic wind shear
19. X gradient of relative vorticity
20. Y gradient of relative vorticity
21. X gradient of geostrophic relative vorticity
22. Y gradient of geostrophic relative vorticity
23. Beta
24. X component of tropical cyclone motion
25. Y component of tropical cyclone motion
26. X component of propagation vector
27. Y component of propagation vector
28. X component of geostrophic propagation vector
29. Y component of geostrophic propagation vector

$$f = 2 \Omega \sin(\phi),$$

where Ω represents the earth's angular velocity, and ϕ is the latitudinal position of the storm. The derivatives were computed using another IMSL quadratic polynomial subroutine QD2DR (IMSL Math/Library Vol. 2, Ch. 3, Ver. 1.1). This subroutine performs an interpolation as in QD2VL, and then calculates the derivative at the point of interpolation. Since the derivative was returned from the subroutine in units per degree, the correction factor of 111 km per degree was applied to convert the derivative into units per meter. The IMSL subroutines assume a rectangular grid rather than latitudes and longitudes. However, the difference in latitudes and longitudes is small in tropical latitudes, and the maximum interval over which the interpolation and derivative are calculated is no more than three gridpoints. The derivative in the x

Table II. DATE AND TIME (00 UTC OR 12 UTC) OF ANALYSES OF TCM-90 TROPICAL CYCLONES.

TROPICAL CYCLONE	BEGINNING DATE-TIME	ENDING DATE-TIME	NUMBER OF DATE-TIME GROUPS
WINONA	90080400	90081100	15
YANCY	90080912	90082112	25
ZOLA	90081512	90082212	15
DOT	90090212	90090812	13
ED	90091200	90091912	16
FLO	90091200	90091912	16
TOTAL			100

direction included a cosine of latitude factor to compensate for the decreasing interval with increasing latitude. The direct u- and v-velocity interpolation of the environmental steering flow is later compared to the geostrophic representation as part of the study.

The x and y shears of the u- and v- velocities at each storm position, as well as their geostrophic counterparts, were calculated using the subroutine QD2DR described above. These values were used to calculate both the relative vorticity and the total wind shear at the storm position. Relative vorticity was calculated by subtracting the y shear of the u-velocity from the x shear of the v-velocity. The total wind shear was determined by vectorially summing the x and y shears of both the u- and v-velocities.

The x and y gradients of the relative and geostrophic relative vorticities at each storm position were also calculated using the QD2DR subroutine. The sum of beta, which is the y shear of the Coriolis parameter, and the relative vorticity gradient is the absolute vorticity gradient. In this analysis, beta was calculated using an exact expression at each storm position

$$\text{beta} = 2 \Omega \cos(\phi) / a,$$

where 'a' represents the radius of the earth ($6.37 \cdot 10^6$ m).

Kasahara and Platzman (1963) showed that a cyclonic vortex will have one component of propagation in the direction of the absolute vorticity gradient and another propagation component 90° to the left (Northern Hemisphere) of that gradient. Such an orientation of the propagation vectors in the presence of environmental relative vorticity gradients was later confirmed by DeMaria (1985). Therefore the estimates of absolute vorticity gradients are later compare with the propagation vectors.

The x and y components of the tropical cyclone motion vector at each storm position were derived from the 6-h JTWC positions before and after the analysis time. Zonal and meridional components of the propagation vector (geostrophic propagation vector) are calculated by subtracting the actual (geostrophic) steering components from the x and y components of the storm motion. That is, the propagation vector is defined by subtracting the environmental steering flow estimate from the low-pass filtered NOGAPS analyses from the actual storm motion.

B. SELECTION OF OPTIMUM ANALYSIS METHOD AND FILTER

Based on the raw global NOGAPS u and v and geopotential fields, deep-layer mean values in Table I for the storms in Table II are now available for the four analysis methods and six wavenumber low-pass filters. The propagation vectors will be used to determine the most consistent and representative method of analysis and wavenumber filter. The basic assumption is similar to prior attempts to define the steering motion. That is, the steering flow estimate that is closest to the actual motion of the tropical cyclone over a large ensemble should be the most representative value. Since the propagation vector is the difference between the motion vector and the steering vector, this procedure is to search for the analysis and filtering combination that has the smallest standard deviation about the mean value of the propagation vector. Thus,

the mean x component, mean y component, and mean magnitude for both the direct estimate and the geostrophic estimate of the propagation vectors, as well as the standard deviations, were calculated for the six tropical cyclones separately and for the overall sample.

The first comparison was whether the standard deviation values of the propagation vectors derived from the deep-layer mean steering vectors were smaller than the values derived from geostrophic steering based on the geopotential fields. With only two exceptions, the standard deviation values derived from the u- and v-velocities from tropical cyclones Winona, Yancy, Zola, Dot, Ed, and the ensemble of storms were smaller than the geostrophic values. In Supertyphoon Flo, eight of the 12 geostrophic standard deviation values were lower than those based on the u- and v-velocity values. Because Flo was a relatively large storm with a northern track, the geostrophic approximation may be an equally representative estimate of the steering flow. However, based on this sample of storms, the deep-layer mean u- and v-velocities directly interpolated from the NOGAPS fields better represent the environmental steering flow than do geostrophic wind velocities calculated from the geopotential height fields.

The next comparison was among the four combinations of global and limited regions with one- and two-dimensional harmonic analyses (see Section II). An example of the values obtained from Typhoon Ed are given in Table III. These means and standard deviation values were derived using different low-pass filtered u- and v-velocities. Minimum standard deviation values are shaded separately for x and y components and for the magnitudes in each of four analysis possibilities. The number of these 12 mean standard deviation values that occur for different low-pass filter choices is given at the bottom. Similar tables were prepared for the filtered geostrophic velocities for Ed, the filtered u- and v-velocities and geostrophic velocities for the other five storms, and the same for the ensemble. In addition to searching for the analysis that had the largest

Table III. MEANS AND STANDARD DEVIATION VALUES FOR X-COMPONENT (TOP NUMBER), Y-COMPONENT (BOTTOM NUMBER), AND MAGNITUDE OF PROPAGATION VECTORS DERIVED FOR 16 MAP TIMES DURING TYPHOON ED.

Component X = y =		WAVENUMBER LOW-PASS FILTER					
		6	9	12	15	18	21
L I M R E G 1 D	Comp Means	-1.513 -0.101	-1.273 0.175	-1.058 0.394	-0.508 0.194	-0.856 -0.527	-1.118 -0.361
	Comp St Devs	1.897 0.817	2.196 0.828	1.907 1.599	1.746 1.076	1.855 1.168	1.972 1.383
	Mag Means	1.517	1.285	1.129	0.544	1.005	1.175
	Mag St Devs	1.440	1.614	1.765	1.617	1.538	1.649
L I M R E G 2 D	Comp Means	-1.332 -0.147	-1.294 0.209	-0.995 0.330	-0.494 0.183	-0.865 -0.273	-0.187 -0.016
	Comp St Devs	2.149 1.909	2.363 1.432	1.893 1.481	1.799 0.997	1.856 1.168	2.007 1.514
	Mag Means	1.330	1.310	1.010	0.527	0.897	1.087
	Mag St Devs	2.058	1.889	1.714	1.661	1.589	1.786
G L O B A L 1 D	Comp Means	-2.277 -0.555	-1.218 0.163	-1.298 0.304	-0.633 -0.003	-0.883 -0.678	-1.216 -0.506
	Comp St Devs	1.960 1.079	2.155 0.736	1.971 1.519	1.755 1.039	1.830 1.290	1.987 1.443
	Mag Means	2.344	1.229	1.333	0.633	1.113	1.317
	Mag St Devs	1.461	1.605	1.690	1.609	1.529	1.628
G L O B A L 2 D	Comp Means	-2.284 -0.624	-1.202 -0.003	-1.298 0.190	-0.624 -0.079	-0.879 -0.654	-1.207 -0.428
	Comp St Devs	1.965 1.616	2.157 1.344	1.972 1.626	1.763 1.123	1.832 1.264	1.988 1.429
	Mag Means	2.368	1.203	1.312	0.629	1.096	1.281
	Mag St Devs	1.612	1.754	1.733	1.647	1.518	1.644
	WINNERS	3	1	0	6	2	0

number of minimum standard deviations of the propagation vectors for the storm, other standard deviation values within 0.1 m/s of the minimum standard deviation were considered to be equivalent to the minimum values and were included in a second summation. For each of the six storms and the combination of storms, the GLOBAL1D and LIMREG1D analysis methods yielded the better representations for the environmental steering flow (see Table IV). The LIMREG2D method was the worst representation of the four.

The final objective was to determine the wavenumber low-pass filter that best represented the environmental flow. As in the analysis test above, one summation was for the wavenumber that most frequently had the minimum standard deviation values for the six storms and the ensemble over all four analysis methods. For example, wavenumber low-pass filter 1 - 15 had the largest number of minimum standard deviation values in Table III for Typhoon Ed, using the directly derived layer-mean u- and v-velocity wind fields. A second summation as described above included all of the values within 0.1 m/s of the minimum standard deviation for each storm. These summations showed that the low-pass filter in wavenumbers 1 - 15 provided the best representation of the environmental steering flow. Although the low-pass filter for wavenumbers 1 - 12 was clearly the best filter for the ensemble, its performance in the individual storms was not as convincing (see Table V). Low-pass filters of wavenumbers 1 - 9, 1 - 6, 1 - 12, and 1 - 18 were all grouped closely together for the second, third, fourth, and fifth best representations respectively, with the low-pass filter of wavenumbers 1 - 21 a clear last.

In conclusion, Tables IV and V give an overall summary of the analysis. Based upon the summary, further analysis of the six TCM-90 tropical cyclones is done using the u- and v-velocities filtered in wavenumbers 1 - 15 for both the LIMREG1D and GLOBAL1D analysis methods.

Table IV. NUMERICAL SUMMARY OF TCM-90 TROPICAL CYCLONE ANALYSIS BY WAVENUMBER LOW-PASS FILTER AND ANALYSIS METHOD.

WAVENUMBER LOW-PASS FILTER		ANALYSIS METHOD	
Number of Minimum St Dev values (Number within 0.1 of Lowest St Dev values)			
# 6	15 (6)	LIMREG1D	7 (10)
# 9	17 (4)	LIMREG2D	2 (8)
# 12	14 (7)	GLOBAL1D	10 (7)
# 15	26 (8)	GLOBAL2D	3 (10)
# 18	10 (10)	SUM 22	
# 21	2 (5)		
SUM	84		

Table V. SUMMARY OF TCM-90 TROPICAL CYCLONE ANALYSIS OF U, V WINDS VS GEOSTROPHIC WINDS, ANALYSIS METHOD, AND WAVENUMBER LOW-PASS FILTER BY STORM. (LIM1 = LIMREG1D, LIM2 = LIMREG2D, GL1 = GLOBAL1D, GL2 = GLOBAL2D).

	U, V winds GEOSTROPHIC	ANALYSIS METHOD X Comp Y Comp Mag	WAVENUMBER LOW-PASS FILTER
		Most Minimum St Dev values (within 0.1 of Minimum St Dev values)	Number of Minimum St Dev values (number within 0.1 of minimum St Dev values)
WINONA	U, V	LIM2 (GL1, LIM1, GL2) GL1 (GL2) GL1 (GL2, LIM2)	# 15 12 (0) # 6 0 (1)
YANCY	U, V	LIM1 (LIM2) GL1 (LIM2, LIM1) LIM1 (LIM2)	# 6 9 (1) # 12 3 (3) # 9 0 (2) # 21 0 (2)
ZOLA	U, V	GL1 (GL2) GL1 (LIM1) GL1	# 9 7 (1) # 15 3 (1) # 12 1 (1) # 6 1 (1)
DOT	U, V	LIM1 (GL1) LIM1 (GL1) GL2 (GL1, LIM1)	# 9 8 (0) # 18 3 (1) # 15 1 (0)
ED	U, V	LIM1 (GL1, GL2, LIM2) GL1 (LIM1) LIM1 (GL1, GL2)	# 15 6 (1) # 6 3 (1) # 18 2 (4) # 9 1 (0) # 12 0 (1)
FLO	Geostrophic	LIM2 (LIM1) GL2 (LIM1) LIM1 (GL1, GL2, LIM2)	# 18 5 (1) # 15 4 (0) # 6 2 (0) # 9 1 (0) # 21 0 (1)
ENSEMBLE	U, V	GL1, GL2 (LIM1, LIM2) GL1 (LIM1, GL2, LIM2) GL1 (GL2, LIM1)	# 12 10 (2) # 21 2 (2) # 15 0 (5) # 18 0 (4) # 6 0 (2) # 9 0 (1)

IV. STEERING FLOWS FOR TCM-90 STORMS

Detailed analyses of the steering flows for the six TCM-90 tropical cyclones were based on the 1 - 15 low-pass filtered NOGAPS fields. The goals of this analysis were to evaluate the internal consistency of the steering flows at subsequent times and how well the calculated propagation vectors agreed with prior studies of tropical cyclone motion. Particular areas of interest include: how smoothly the environmental steering flow and propagation vectors varied in time; and how consistently the three-component decomposition represented the total wind field in the region of the TCM-90 tropical cyclones.

In these deep-layer mean, low-passed analyses, the LIMREG1D and GLOBAL1D were in remarkable agreement in virtually every area. All trends were identical with very few exceptions. For example, the LIMREG1D and GLOBAL1D analyses of the environmental steering flow are shown in Figs. 5 and 6 respectively for Typhoon Yancy. The insignificant vector differences demonstrate the internal consistency between the two analysis methods for the specific purpose of deriving the environmental steering flow near a tropical cyclone. Consequently, the GLOBAL1D and LIMREG1D fields will alternately be presented below.

1. Typhoon Winona

Typhoon Winona formed on 4 August 1990 in a monsoon trough over the East China Sea, which was farther north than usual (ATCR 90). Another unusual feature about Winona was the southeastward track between 5 - 8 August (Fig. 7). On 8 August Winona began moving northward, and an anticyclonic circulation to the east of Winona also began migrating northward. Winona reached a maximum intensity of 65 kt on 9 August just before landfall into southern Japan at 00 UTC 10 August. Subsequent to landfall, Winona weakened and tracked to the northeast.

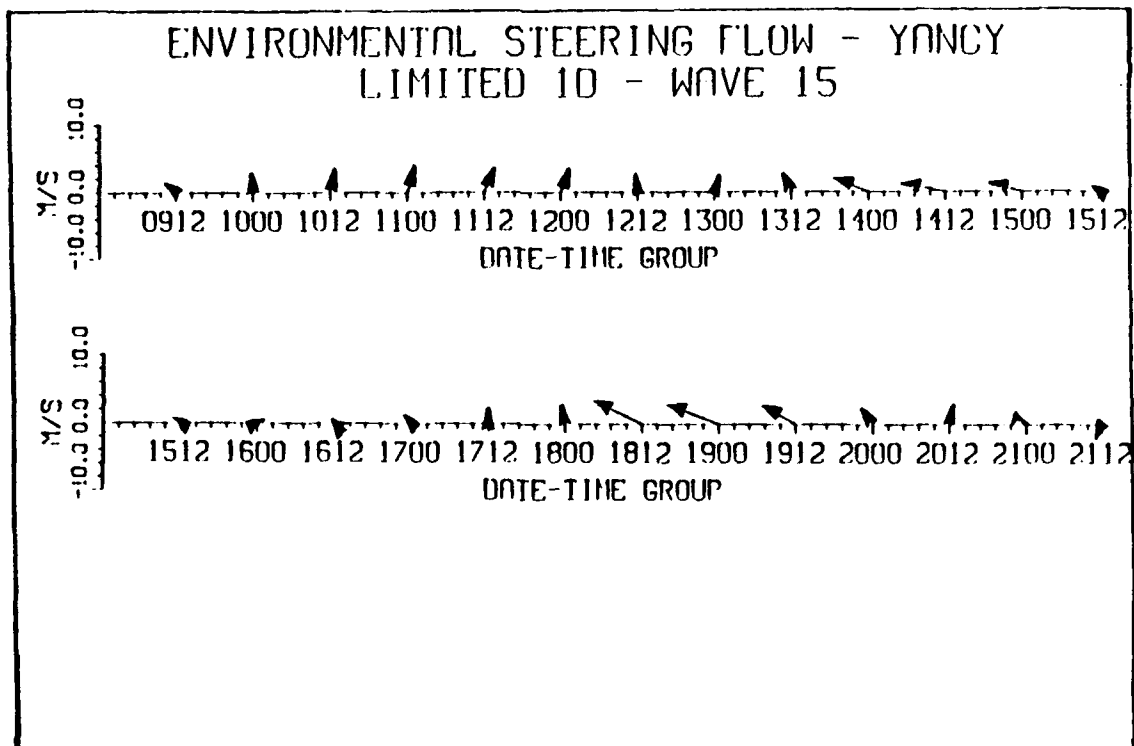


Figure 5. Environmental steering flow for Typhoon Yancy during 9 - 21 August using LIMREG1D analysis method with a wavenumber 1 - 15 low-pass filter.

The Typhoon Winona translation vectors and low-passed environmental steering flow and propagation vectors are compared in Fig. 8. The early northeastward motion period, the anomalous southeastward track period and the rapid turn to the north on 00 UTC 8 August are reflected in the translation vectors in Fig. 8. Similar directions and magnitudes of environmental steering flow are shown during each of these periods, which indicates that the steering was the primary factor in each track portion. Of particular note with respect to the propagation vectors is the rapid change in directions associated with the sharp track changes around 00 UTC 6 August and around 00 UTC 8 August.

Horizontal wind shear and the relative vorticity at the positions of Typhoon Winona are derived from the gradients of low-pass-filtered

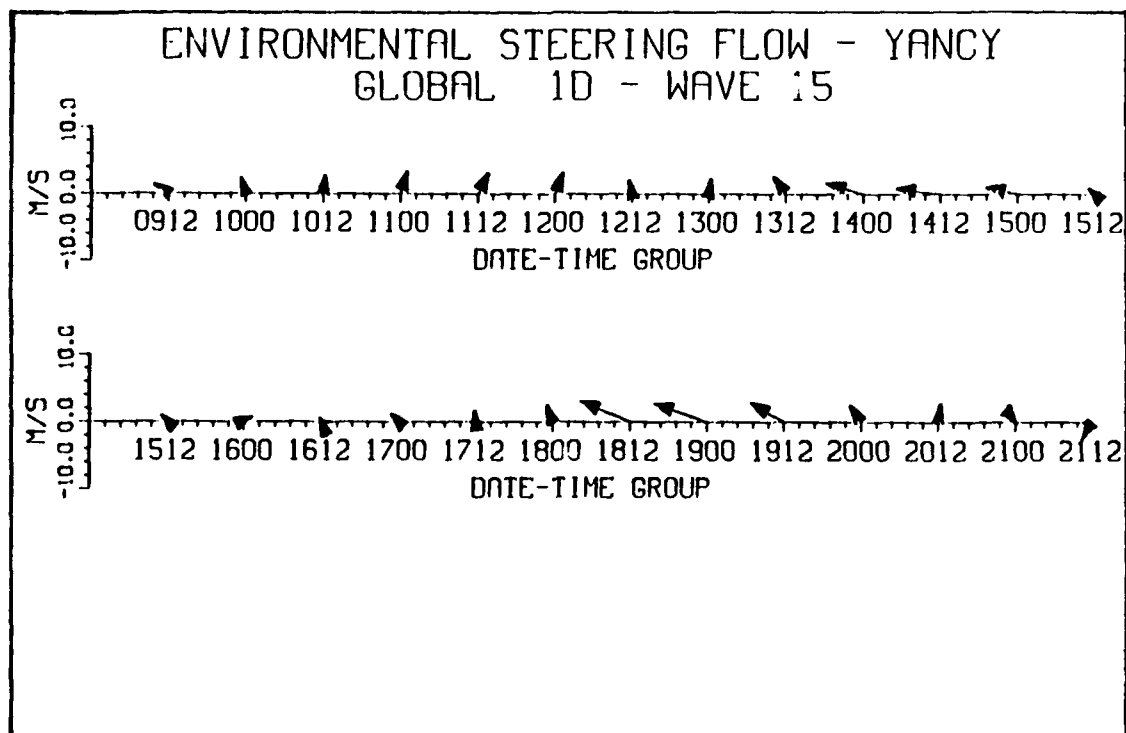


Figure 6. Environmental steering flow as in Fig. 5 except using GLOBAL1D analysis method.

environmental fields (Fig. 9). The magnitude of Coriolis at each storm position is denoted on the relative vorticity plot to provide a reference value. Positive values of relative vorticity are generally expected as tropical cyclones form in regions of cyclonic shear, such as the monsoon trough. The decrease in relative vorticity at 12 UTC 7 August could be associated with Winona's interaction with anticyclonic circulations both southwest and southeast of its position. The steady increase in relative vorticity subsequent to 12 UTC 8 August is probably due to interaction with an approaching midlatitude trough from the northwest as Typhoon Winona tracked northward. The horizontal wind shear also influences the direction of the propagation vector (Elsberry and Abbey 1991). An anticyclonic wind shear tends to produce a more northward propagation

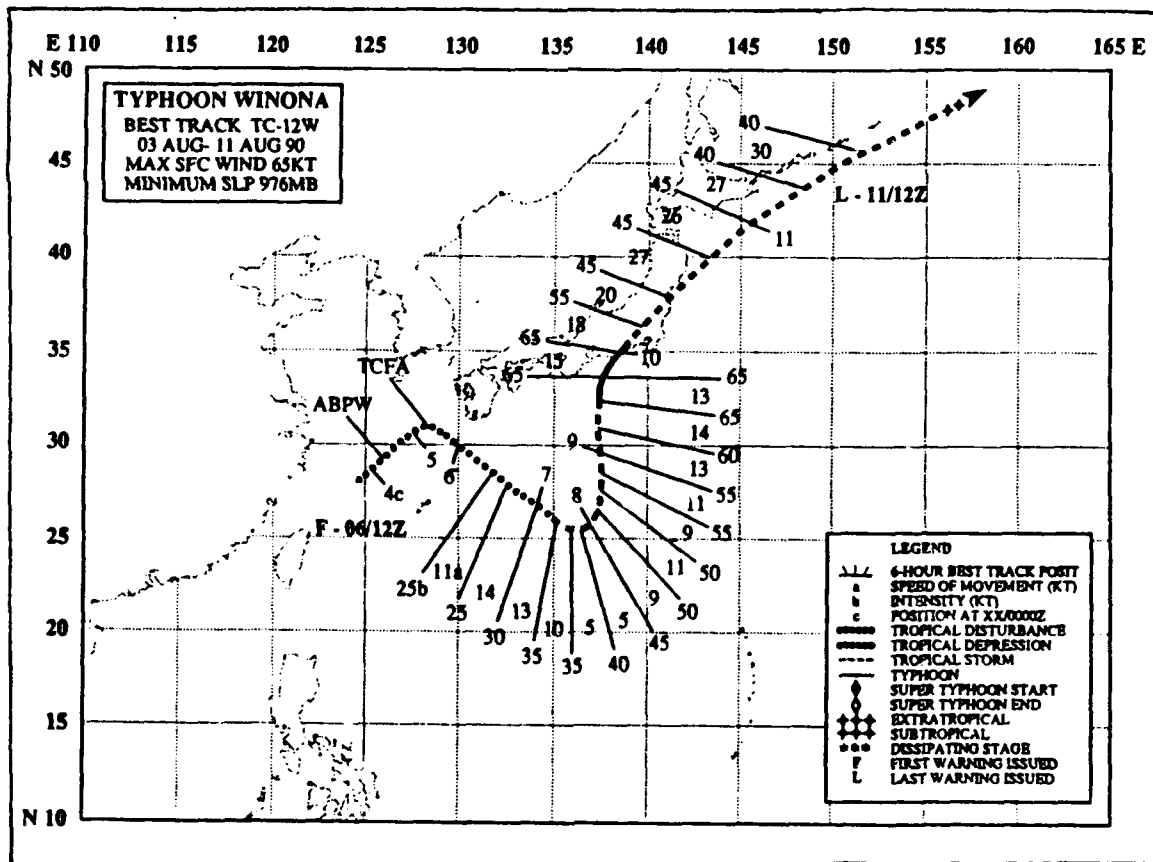


Figure 7. Best track for Typhoon Winona from JTWC (ATCR 1990).

vector, whereas a cyclonic wind shear causes a rotation toward a more westward direction.

The relative vorticity gradients in the y and x directions are shown in Figs. 10 and 11 respectively. Whereas the beta term is always positive (toward the north in the Northern Hemisphere), the y -gradient of relative vorticity may either add or subtract from beta. Prior to 00 UTC 7 August, the y gradient of relative vorticity generally opposes beta, as does the 12 UTC 8 August gradient. Exceptions to this trend occur at 12 UTC 4 August and 00 UTC 6 August. The more westward or southwestward orientation of the propagation vectors during the early period would be consistent with this opposition of relative vorticity gradient and beta. Between 00 UTC 7 August and 00 UTC 8 August, and subsequent to 12 UTC 8 August, the y gradient of relative vorticity complements beta. The

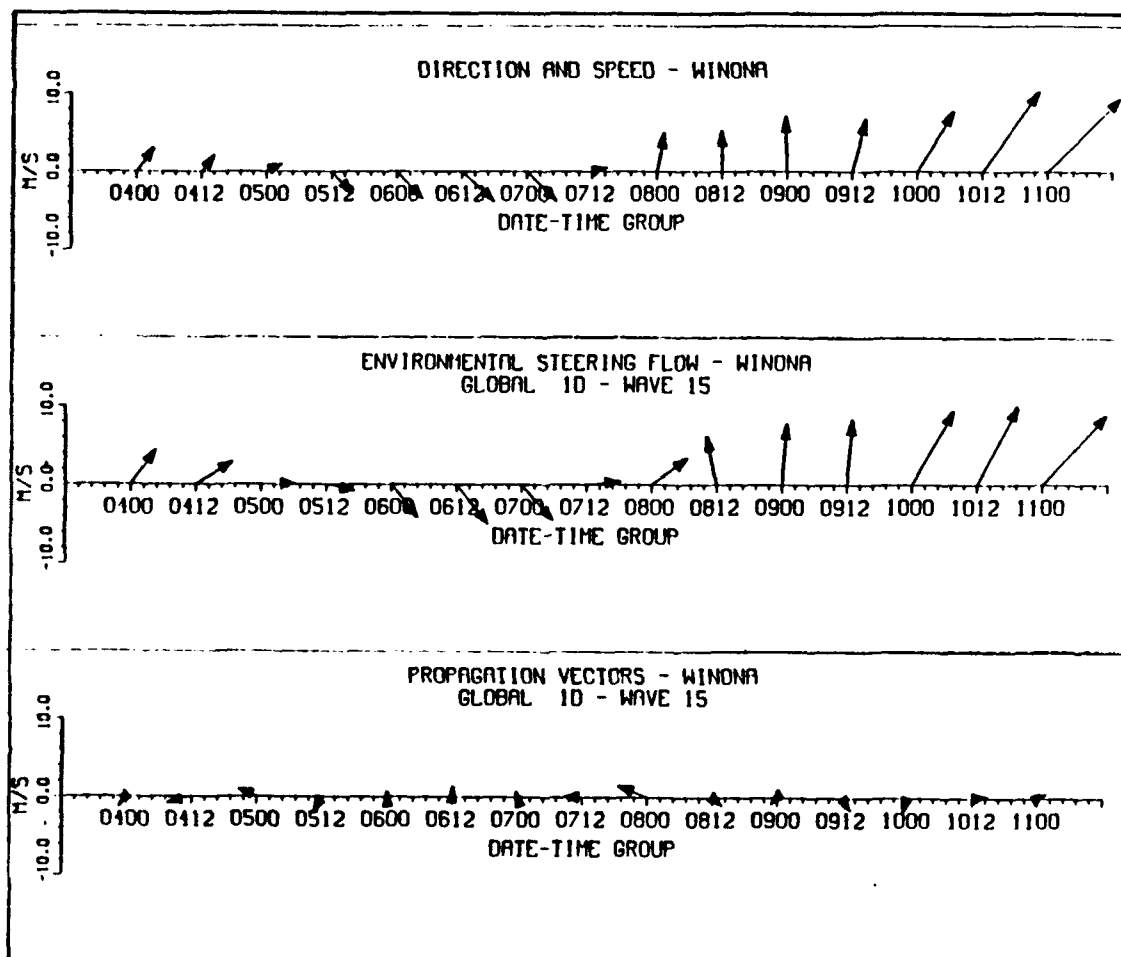


Figure 8. Direction and speed (top), environmental steering flow using the GLOBALID analysis method (middle), and derived propagation vectors for Typhoon Winona from 4 - 11 August 1990.

geostrophic relative vorticity gradient in the y direction generally is more consistent in time than the gradient calculated from the wind fields for this case at relatively higher latitudes than the other TCM-90 storms.

Normally the x gradient term has been omitted in simplified environmental shear cases with relative vorticity gradients only in the meridional direction (e.g., DeMaria 1985). Prior to 12 UTC 7 August, the x gradient (Fig. 11) has a significantly large positive value, whereas afterwards it assumes a large negative value. The geostrophic relative vorticity gradients agree rather well with the gradients from the wind fields. The key point in Fig. 11 is that the x gradient is of the same

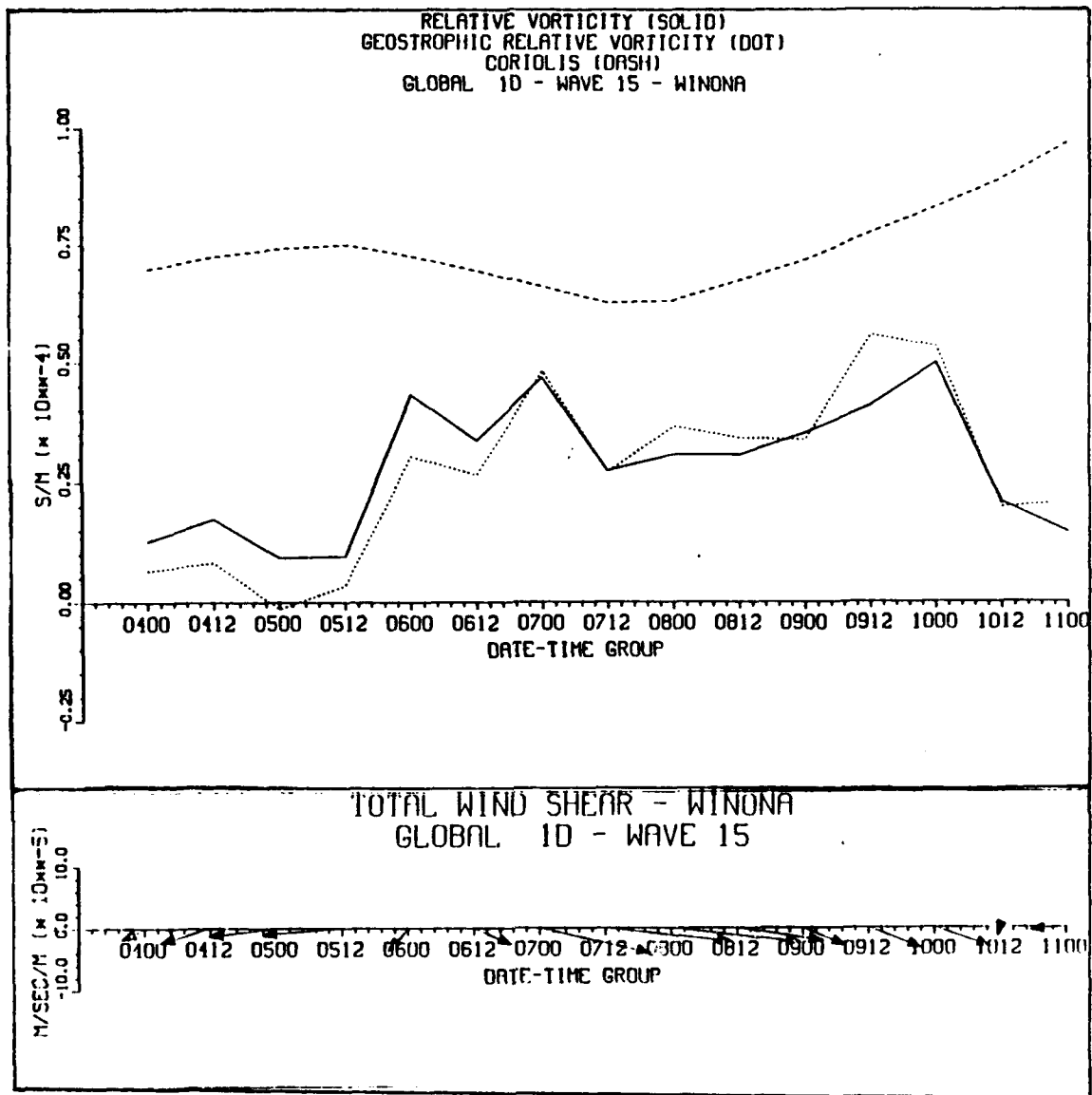


Figure 9. Relative vorticity (top) calculated from wind field (solid) and geostrophically (dotted) and total horizontal wind shear for Typhoon Winona from 4 - 11 August.

order of magnitude as beta, and thus should not be neglected in the calculation of the propagation vector. The x-gradient of relative vorticity is vectorially added to the sum of beta and the y gradient to give the absolute vorticity gradient. The propagation vector should fall within this absolute vorticity gradient and 90° to the left of it (Elsberry and Abbey 1991). Four date-times from Figs. 10 and 11 were

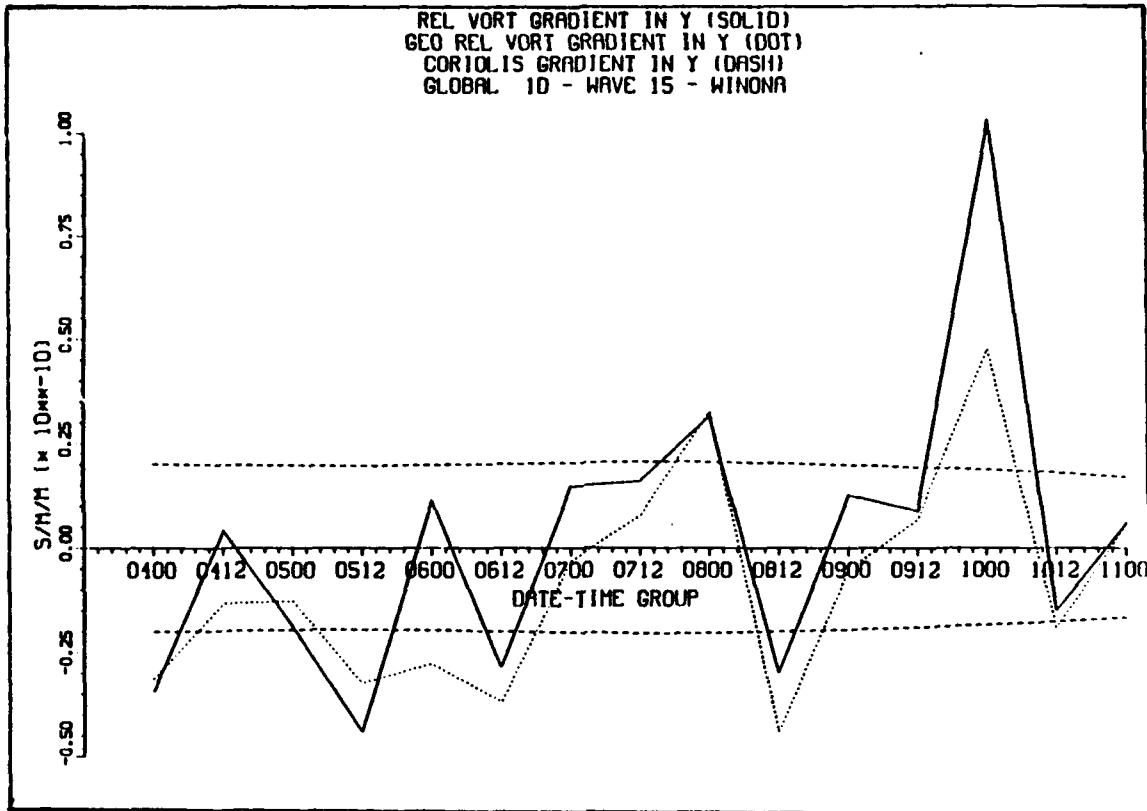


Figure 10. Y components (solid) and geostrophic (dashed) y components of relative vorticity gradients, and plus/minus beta values, for Typhoon Winona during 4 - 11 August 1990.

selected to illustrate the relationships between the absolute vorticity gradients and directions of propagation vectors (Fig. 12). The propagation vectors at 12 UTC 4 August and 00 UTC 5 August were outside the 90° arc, most likely due to Winona's disorganization during its initial phase. On the other hand, the propagation vectors at 12 UTC 7 August and 00 UTC 8 August were well within the 90° arc. The propagation vectors after 12 UTC 9 August were not tested due to Winona's landfall and resulting orographic distortion.

In conclusion, it appears that the environmental steering flow in the case of Winona is well represented by the low-pass filtered NOGAPS analyses. The magnitudes of the relative vorticity gradients in both the x and the y directions are large relative to beta. In most cases, the derived propagation vector directions are consistent with the absolute

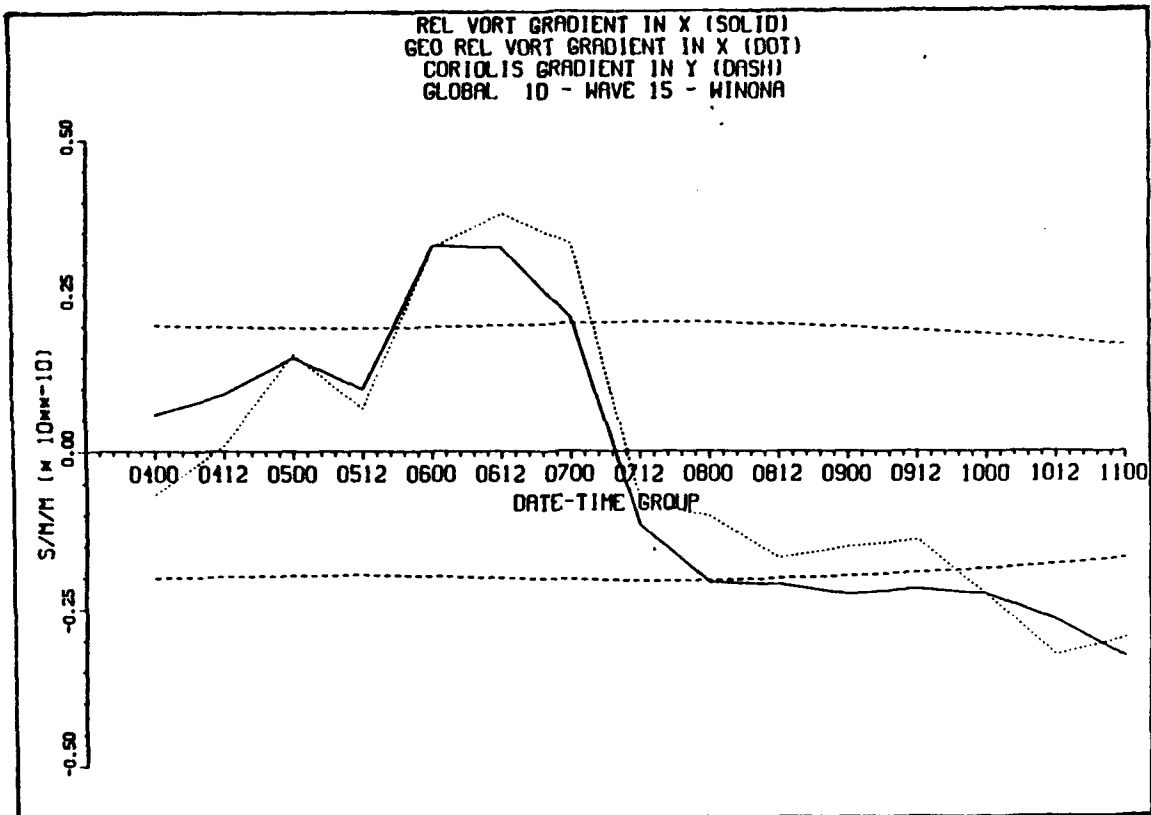


Figure 11. X components (solid) and geostrophic (dashed) x components of relative vorticity gradients, and plus/minus beta values, for Typhoon Winona during 4 - 11 August.

vorticity gradients.

2. Typhoon Yancy

Typhoon Yancy (Fig. 13) was active in the western Pacific from 9 August through 21 August 1990. Yancy formed well east of the TCM-90 operations area at around 162°E near the axis of a large and strong monsoon trough (ATCR 1990). Yancy did not reach typhoon intensity until 12 UTC 16 August, and its maximum intensity of 90 kt was achieved on 18 August just east-southeast of Taiwan. Since Yancy was one of the larger of the TCM-90 tropical cyclones, it was expected to have a larger propagation vector. The initial movement of Yancy was erratic due to the development, dissipation, and reformation of multiple mesoscale systems. Afterwards, it turned west on 13 August and tracked smoothly with

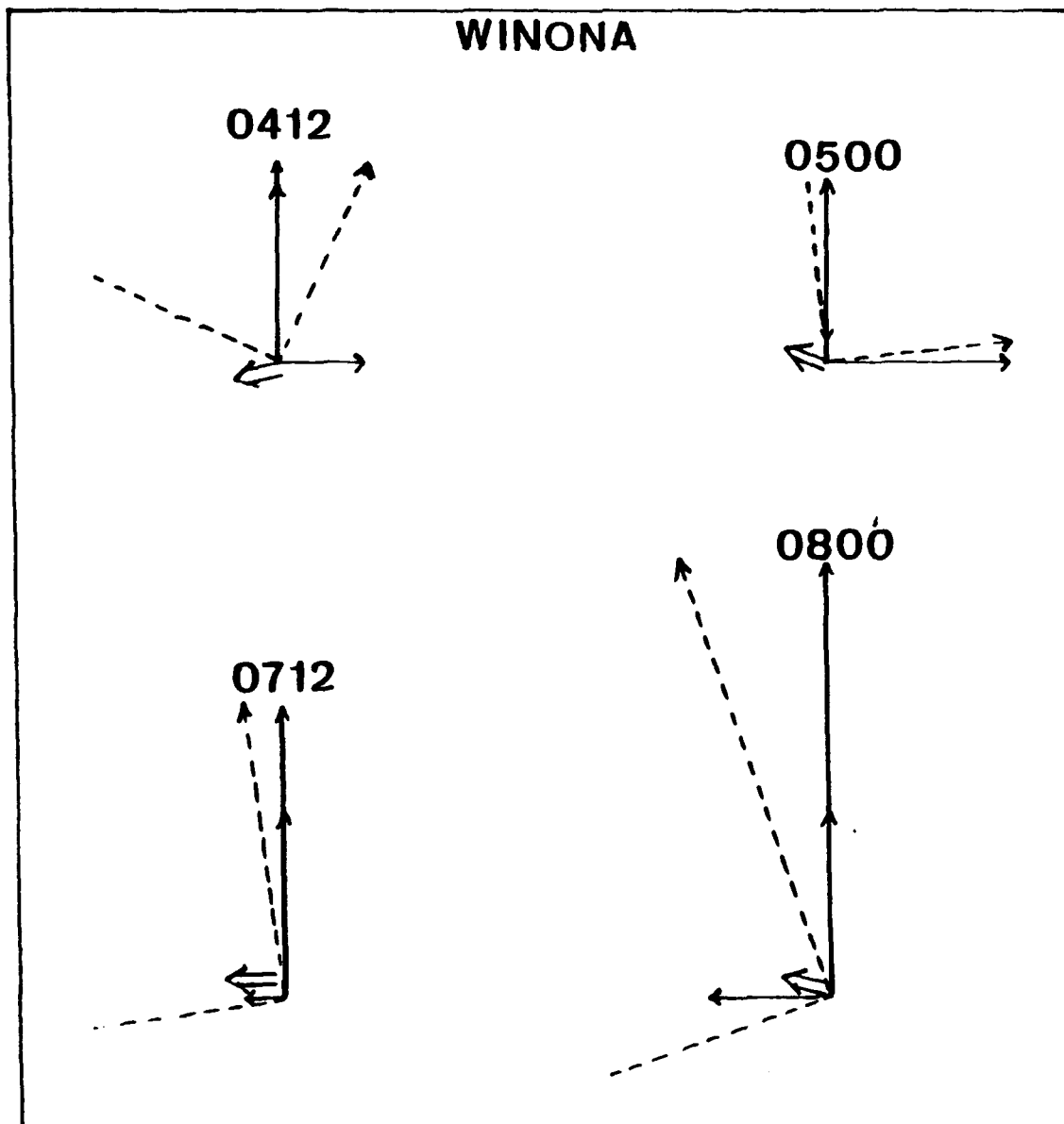


Figure 12. Propagation vectors (double arrow) and the gradients of absolute vorticity (dashed arrow) at four selected date-times for Typhoon Winona, based on relative vorticity gradients in Figs. 10 and 11.

translation speeds of up to 18 kt due to a strong subtropical ridge to the north.

The translation vectors, analyzed environmental steering flow and propagation vectors for the early and late periods of the long-lived Yancy are shown in Figs. 14a and 14b respectively. Significant angular

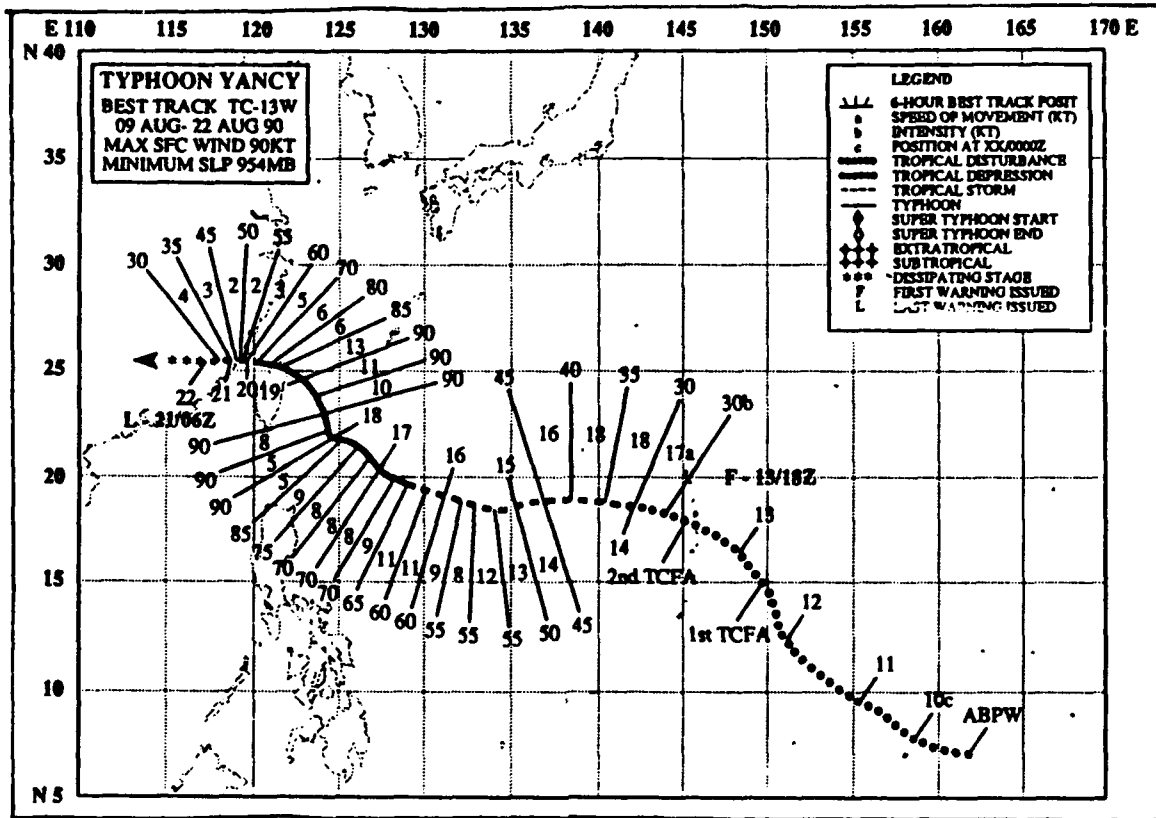


Figure 13. Best track for Typhoon Yancy from JTWC (ATCR 1990).

departures of the steering flow from the translation vectors are noted through 12 UTC 13 August. This could very well be attributed to the relocation of Yancy's center to the strongest northern mesoscale convective center during this time period. Such relocations would result in poor propagation vector estimations. Following 00 UTC 14 August, the predominate portion of Typhoon Yancy's track is environmental steering. Since Yancy was such a large storm, it had one of the largest mean magnitudes of propagation vectors derived for the six TCM-90 storms (2.91 m/s). The time consistency in the environmental steering flow estimates and the propagation vectors is also noticeable. One exception is the 00 UTC 16 August environmental steering vector, which has a very different direction, but its magnitude is small. Another erratic propagation vector occurred at 12 UTC 18 August, which was near the time that the environmental flow increased rapidly toward the northwest. In addition,

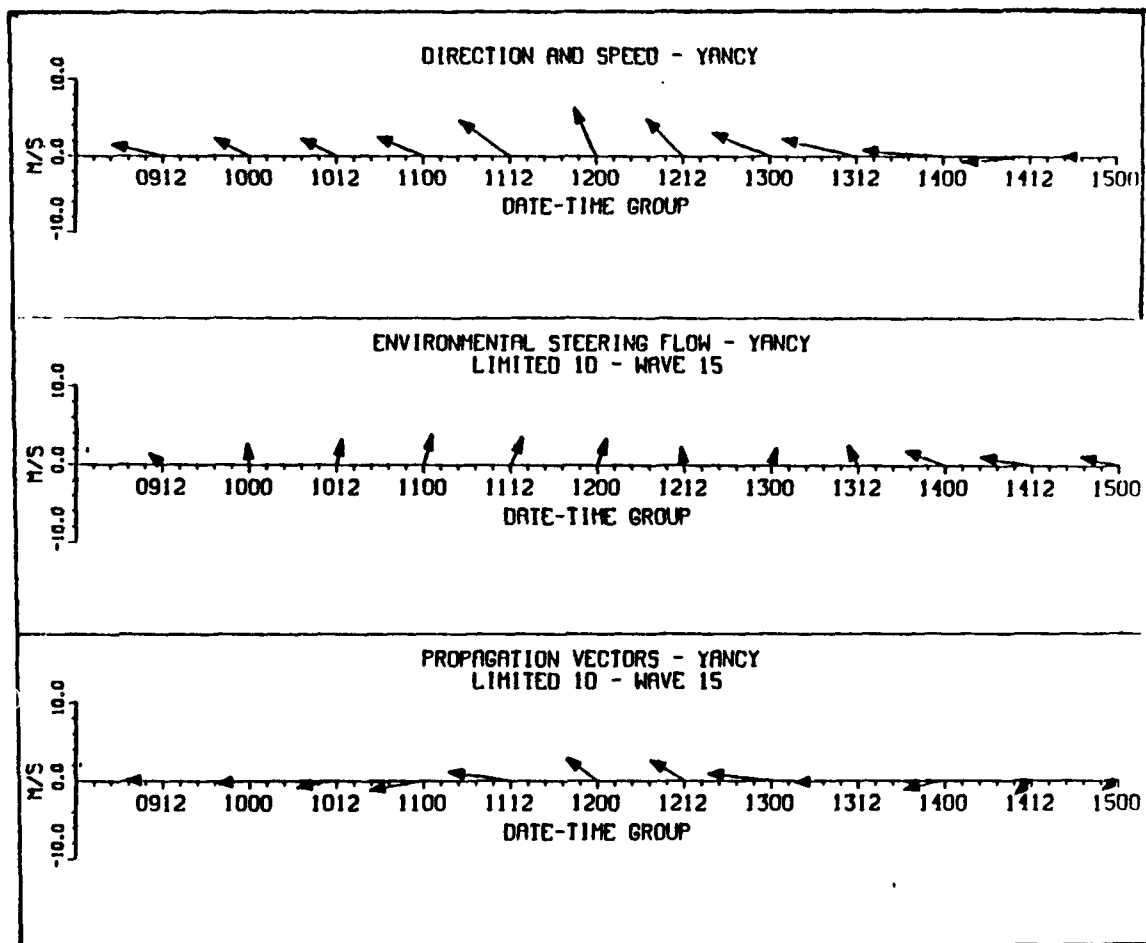


Figure 14a. Translation vectors, environmental steering and propagation vectors as in Figure 8, except for Typhoon Yancy during 12 UTC 9 August through 00 UTC 15 August 1990.

Yancy's low-level circulation began interacting with the mountainous orography of Taiwan during this period. Orographic influences continued until landfall on the mainland around 12 UTC 20 August.

During the formation period of Yancy, the relative vorticity of the environment was positive (Fig. 15a), and about $0.5f$. The basic trend of the geostrophic relative vorticity throughout the period matches that of the relative vorticity. However, the geostrophic values are more erratic and generally larger. The total horizontal wind shear vectors were generally erratic until after 00 UTC 14 August. From that time until 00 UTC 19 August, the horizontal shear of the environmental flow increased

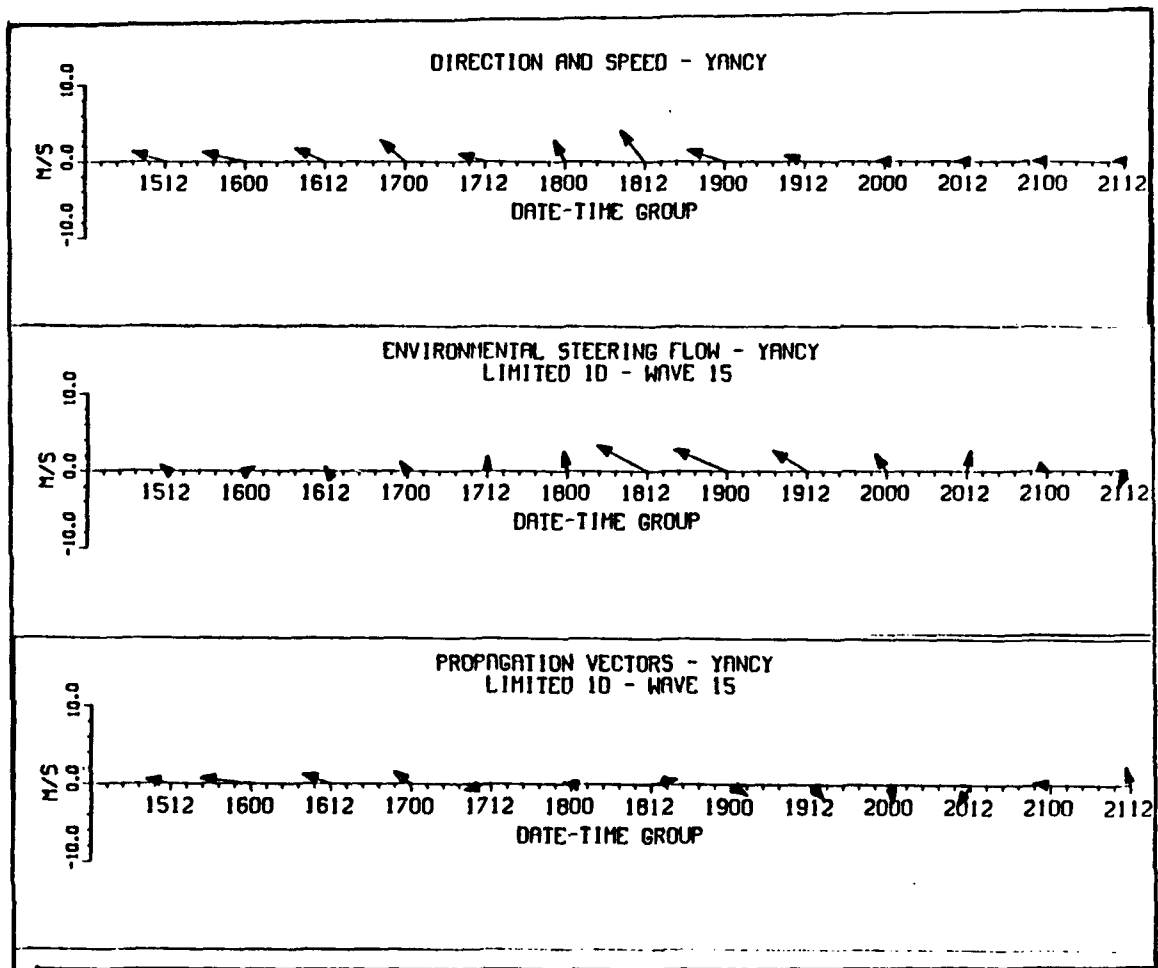


Figure 14b. As in Fig. 14a, except for Typhoon Yancy during 12 UTC 15 August through 12 UTC 21 August.

(Fig. 15b). The steady increase in positive x-shear ($\partial v/\partial x$) and negative y-shear ($\partial u/\partial y$) corresponds to the large values of relative vorticity, which exceeded f during this period. This relative vorticity may have been associated with the large outer circulation of Yancy, or represent the environmental flow of strong equatorial westerlies or southwesterlies and the strong trade flow on the poleward side. This is an example of the difficulty in separating the tropical cyclone circulation from the monsoon trough shear flow within which Yancy developed and grew. As the total horizontal shear became more strongly cyclonic between 14 - 15 August, the propagation vectors (Fig. 14) had a more southwestward direction as opposed to its previous westward propagation. However, the propagation

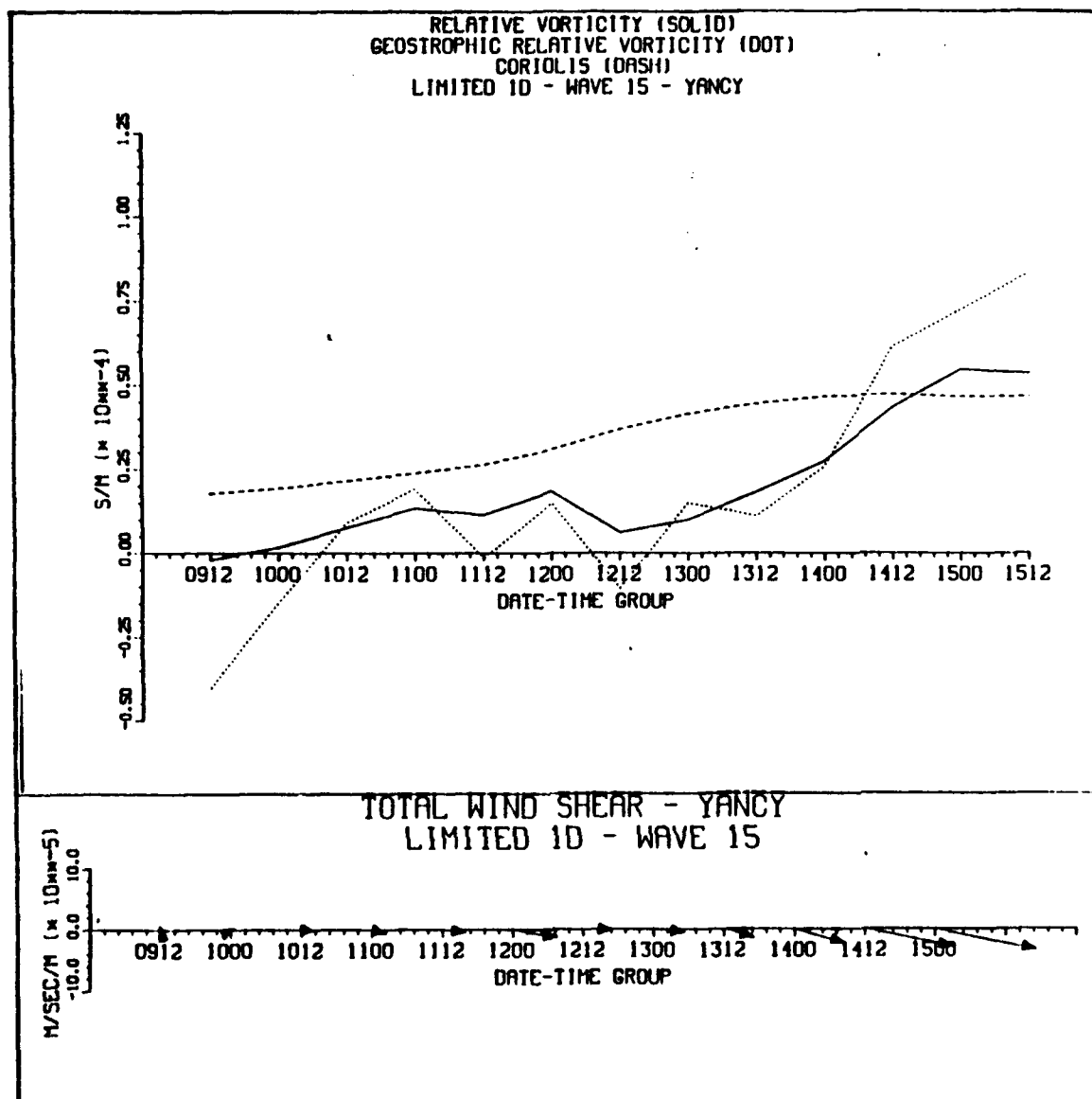


Figure 15a. Relative vorticity and horizontal wind shear as in Fig. 9, except for Typhoon Yancy during 12 UTC 9 August through 00 UTC 15 August 1990.

vectors again became more westward until 12 UTC 18 August.

The relative vorticity gradients in y and x are given in Figs. 16 and 17 respectively. Throughout the period of Yancy, the y gradient of relative vorticity seldom exceeded the magnitude of beta. The only points of significant excess were 00 UTC 18 August through 00 UTC 19 August, due to a midlatitude trough passing to the north. For the most part, the y

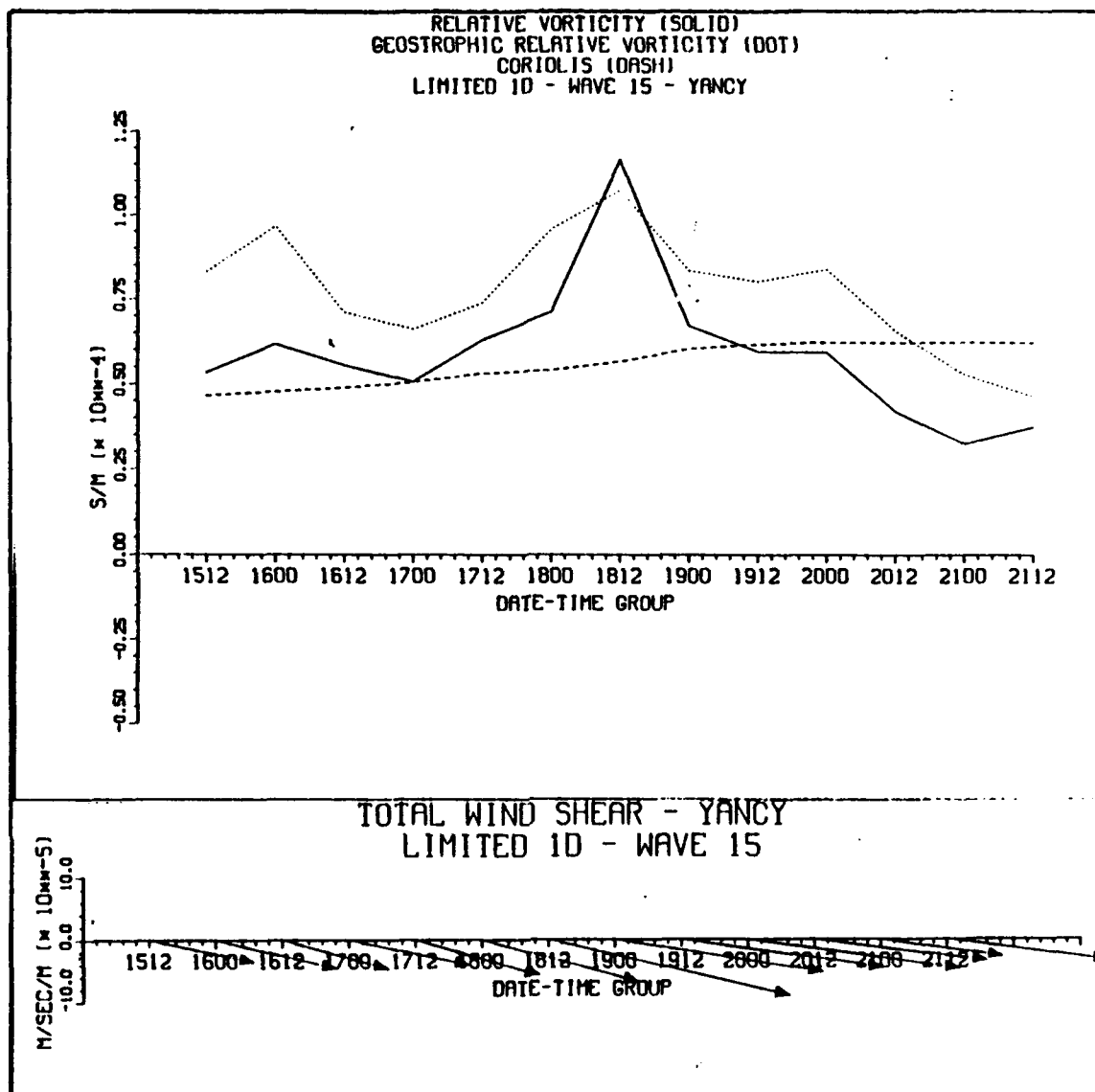


Figure 15b. Same as in Fig. 15a, except for Typhoon Yancy during 12 UTC 15 August through 12 UTC 21 August.

gradient alternated fairly evenly between positive and negative contributions to beta. The early positive contributions are questionable due to the uncertainty of Yancy's position. The negative contributions between 12 UTC 13 August and 12 UTC 15 August correspond to the westward and southwestward propagation vectors at this time. Between 12 UTC 15 August and 00 UTC 17 August, the relatively minimal contribution by the y gradient in relative vorticity correlate to northwestward propagation

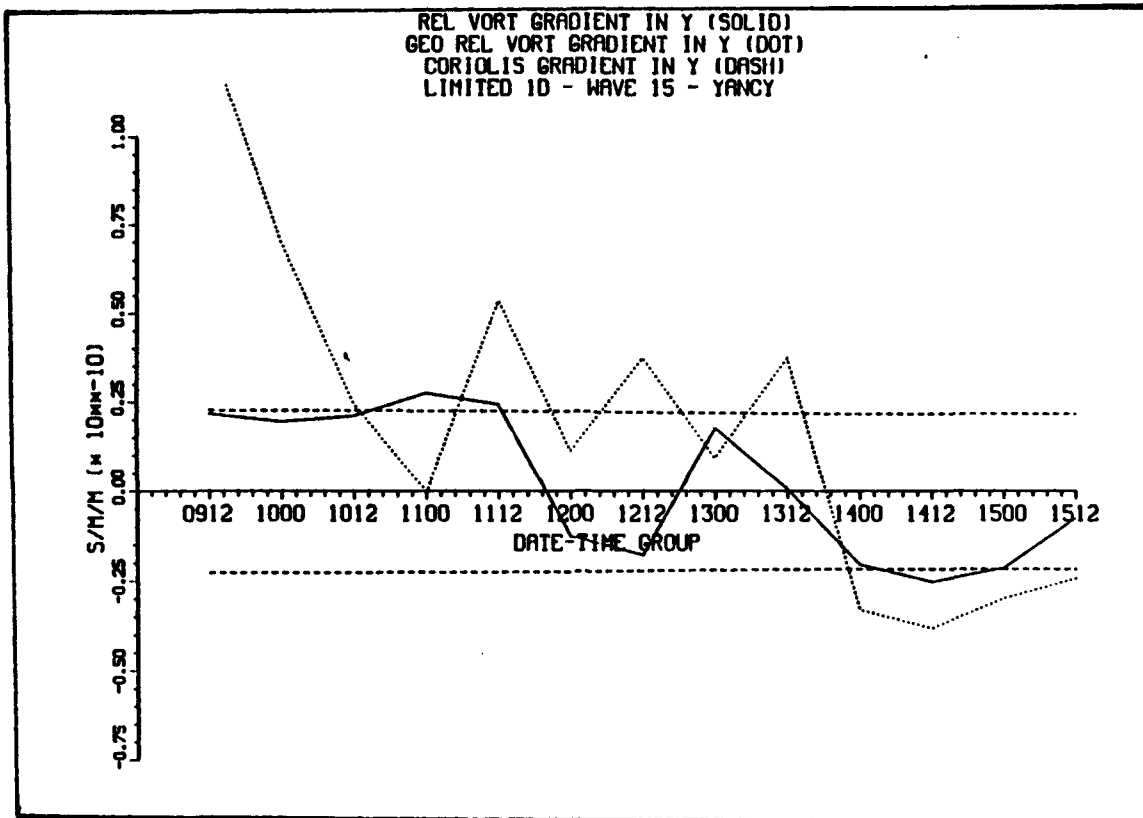


Figure 16a. Relative vorticity gradients in y direction as in Fig. 10, except for Typhoon Yancy during 12 UTC 9 August through 12 UTC 15 August 1990.

vectors. The negative contributions after 12 UTC 18 August are consistent with the southward propagation vectors. The geostrophic y gradients tended to be larger and more erratic. The x gradients of relative vorticity (Fig. 17) are comparatively weaker than the y gradients, but occasionally have significant magnitudes. The values that equal and exceed beta at 12 UTC 18 August and 12 UTC 20 August may not be representative. Just as in the y gradients, the geostrophic values tend to be larger and more erratic than do the gradient values based on the wind fields. The dominance of the y gradient over the x gradient was probably due to the elongated northwest-southeast monsoon trough that had been displaced poleward with Typhoon Yancy.

As in the Winona case, the beta and the relative vorticity gradients are added vectorially to compare the gradient of absolute

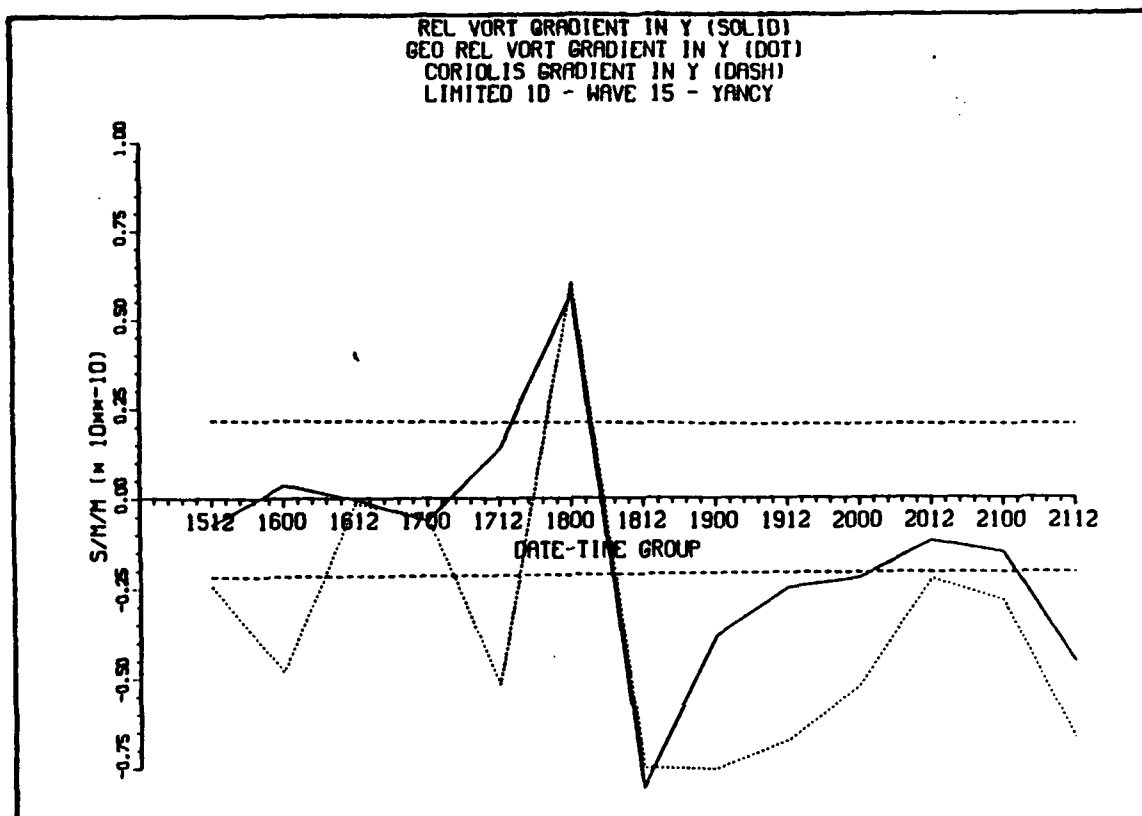


Figure 16b. Same as in Fig. 16a, except for Typhoon Yancy during 12 UTC 15 August through 12 UTC 21 August.

vorticity for selected date-times (Fig. 18). These date-times were chosen to illustrate the various relative vorticity gradient regimes. Of these seven date-times, five propagation vector directions fell within 90° to the left of the absolute vorticity gradient (Elsberry and Abbey 1991). The two exceptions were 12 UTC 14 August and 12 UTC 18 August. At 12 UTC 18 August, Yancy's track was nearing the orography of Taiwan, and therefore possibly subject to other steering effects. These two exceptions follow rapid fluctuations in the y relative vorticity gradient (Fig. 16), and modelling studies (Chan and Williams 1986, Fiorino and Elsberry 1989) have shown that the tropical cyclone propagation takes on the order of a day to adjust to sudden changes in vorticity gradients. The five vectors that fell within the arc were close to the 90° component to the absolute vorticity, which is indicative of a strong relative

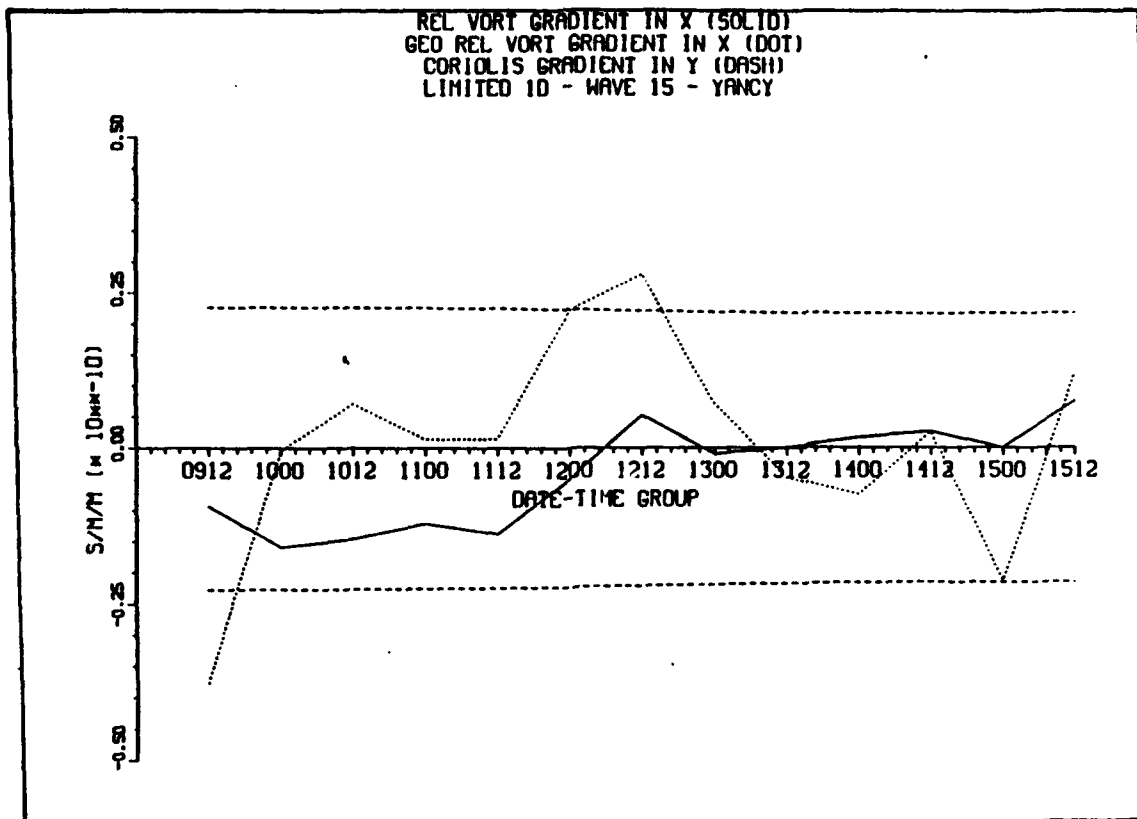


Figure 17a. Relative vorticity gradients in x direction as in Fig. 11, except for Typhoon Yancy during 12 UTC 9 August through 12 UTC 15 August 1990.

vorticity gradient influence.

3. Typhoon Zola

Typhoon Zola formed over the Philippine Sea just west of the Marianas Islands on 15 August 1990 (Fig. 19). Accurate positioning of Zola prior to 16 August was difficult due to several mesoscale circulations embedded in the monsoon trough. During this period Yancy was about 600 km to the northwest of Zola and was tracking toward the west. Prior to reaching typhoon strength, Zola made a sharp left turn near 20°N, 146°E just prior to 12 UTC 18 August and subsequently tracked to the northwest. The sharp turn may have been associated with the strengthening of the subtropical ridge around 33°N. Zola continued to intensify and reached typhoon strength on 20 August. The maximum intensity of Zola was

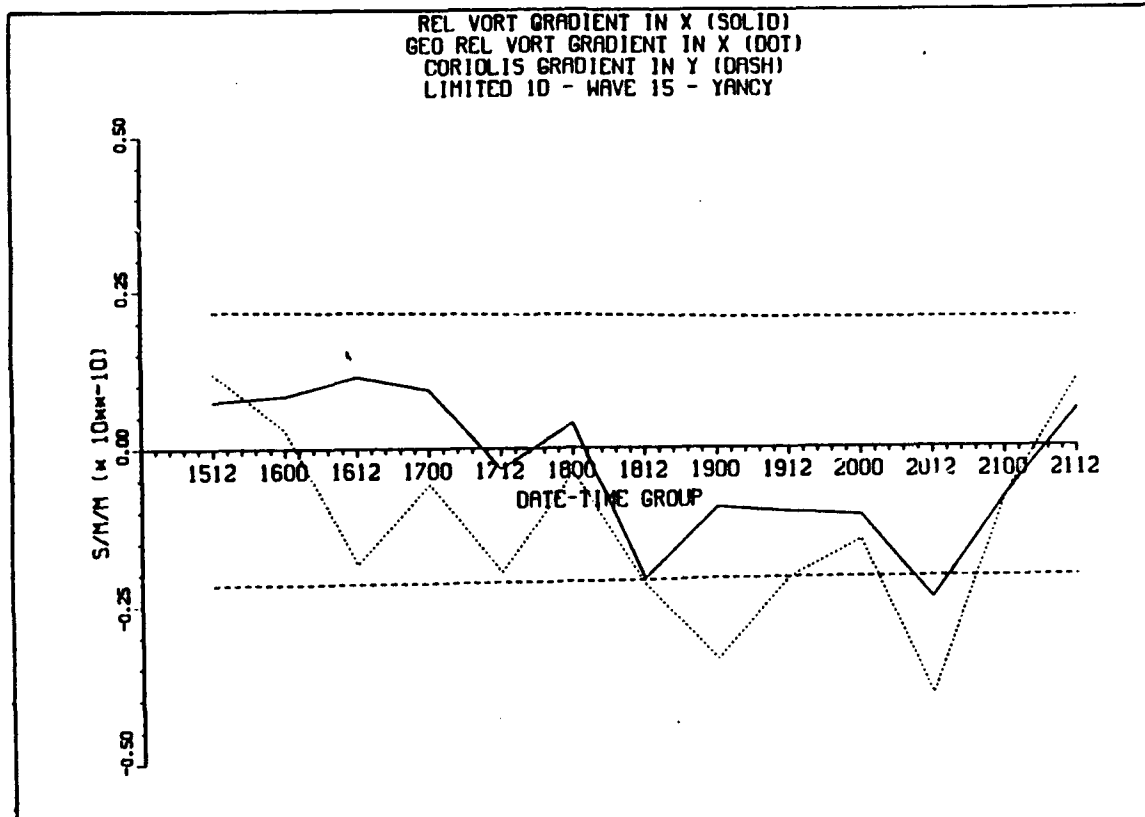


Figure 17b. Same as in Fig. 17a, except for Typhoon Yancy during 12 UTC 15 August through 12 UTC 21 August.

100 kt around 06 UTC 21 August, and then Zola began weakening prior to landfall in southern Japan on 22 August.

The translation vectors for Zola are compared with the environmental steering flow and propagation vectors in Fig. 20. The larger steering vectors toward the northeast at the beginning of Zola may be associated with the outer circulation of the large Typhoon Yancy, or it may be connected to the eastern end of the monsoon trough. Although Zola did track northeastward during this early period, the steering vectors are much greater in magnitude than the storm motion vectors. Thus, the propagation vectors are clearly excessive, which is further evidence of an unrealistic steering vector. This may be due to the uncertainty of Zola's position mentioned earlier. This may also be a result of a likely tendency of NOGAPS to underestimate the magnitude of significant changes

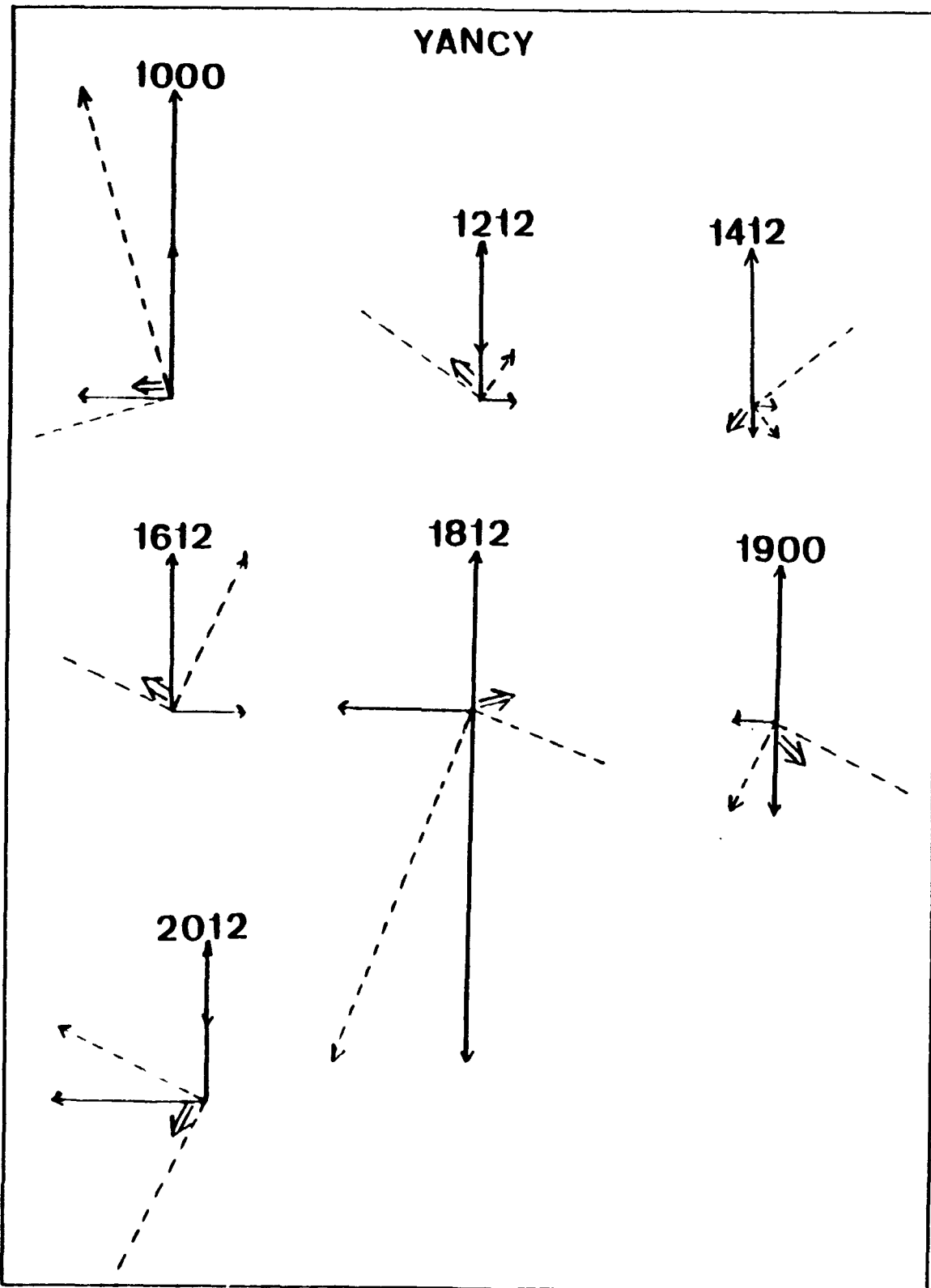


Figure 18. As in Fig. 12, except for seven selected date-times for Typhoon Yancy.

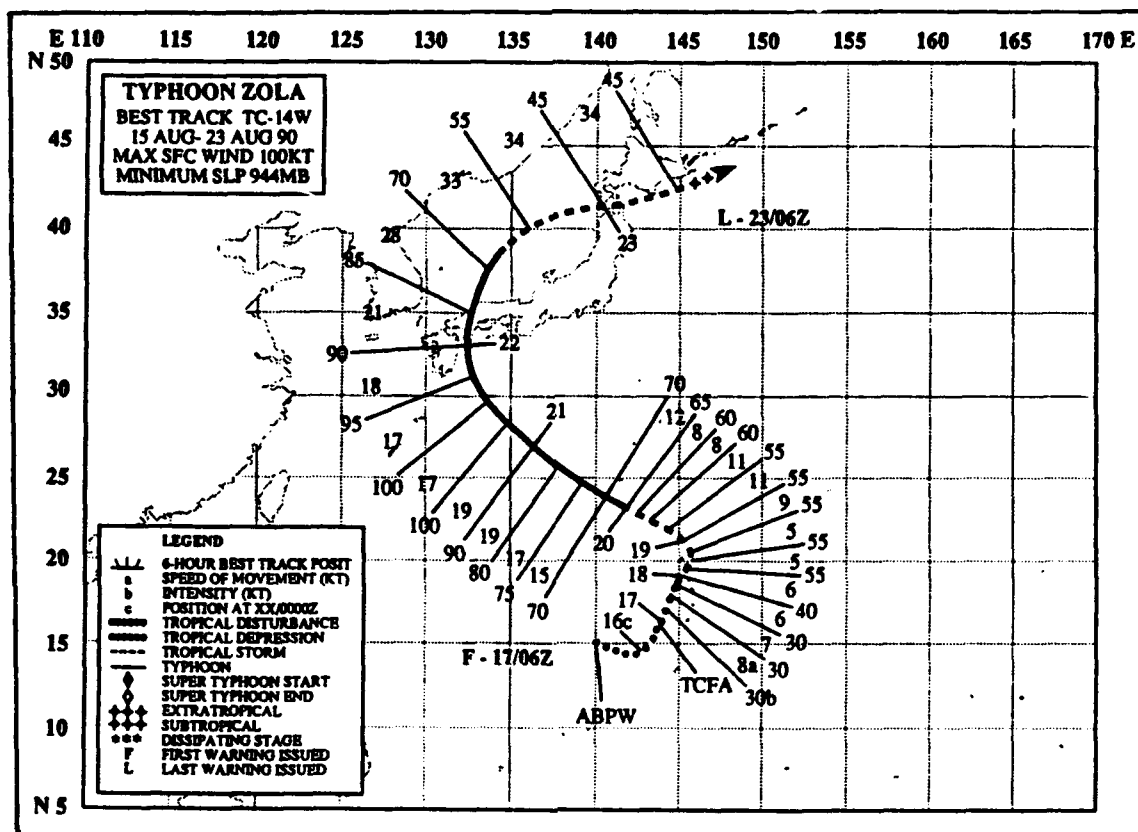


Figure 19. Best track for Typhoon Zola from JTWC (ATCR 1990).

in environmental flow (ie intensification of subtropical ridge). Between 12 UTC 16 August and 00 UTC 18 August, the agreement between the steering vectors and the storm translation vectors is much better. The storm motion is clearly to the left of the steering vector, therefore the propagation vector is westward. A failure of the steering estimates may have occurred again during the turning point between 12 UTC 18 August and 12 UTC 20 August, which could account for the excessive propagation vectors. The NOGAPS fields probably did not have a realistic analysis of the environmental flow during this period. From 00 UTC 21 August to the end, good agreement exists between the translation vectors and the steering motion, especially during recurvature. However, the magnitudes may not be as good, since the propagation vectors are southward and large. These propagation vectors are small compared to the steering vectors, and

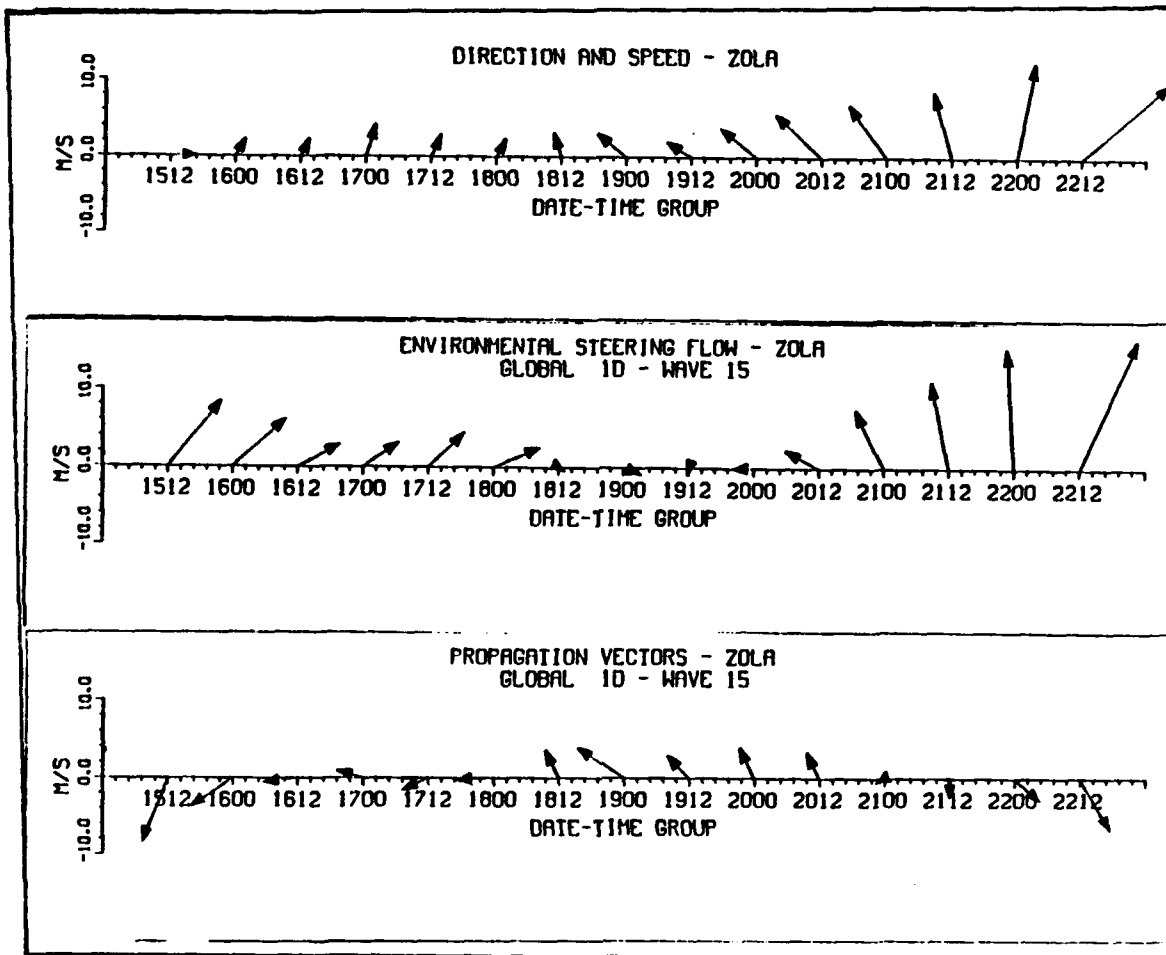


Figure 20. Translation vectors, environmental steering flow and propagation vectors as in Fig. 8, except for Typhoon Zola during 12 UTC 15 August through 12 UTC 22 August 1990.

therefore do not contribute significantly to the storm motion. The possible reason the westward component of the propagation vector diminishes after 12 UTC 21 August may be due to the outer wind structure of Zola beginning to interact with the mountainous terrain over southern Honshu. The mean magnitude of Zola's propagation vectors (2.83 m/s) is on the order of Yancy. However, this may not be very realistic considering the unrepresentative 12 UTC 15 August and 00 UTC 16 August vectors, and those associated with the sharp left turn around 12 UTC 18 August. These excessive values contribute to the large (3.6 m/s) standard deviation about the mean for Zola's propagation vectors.

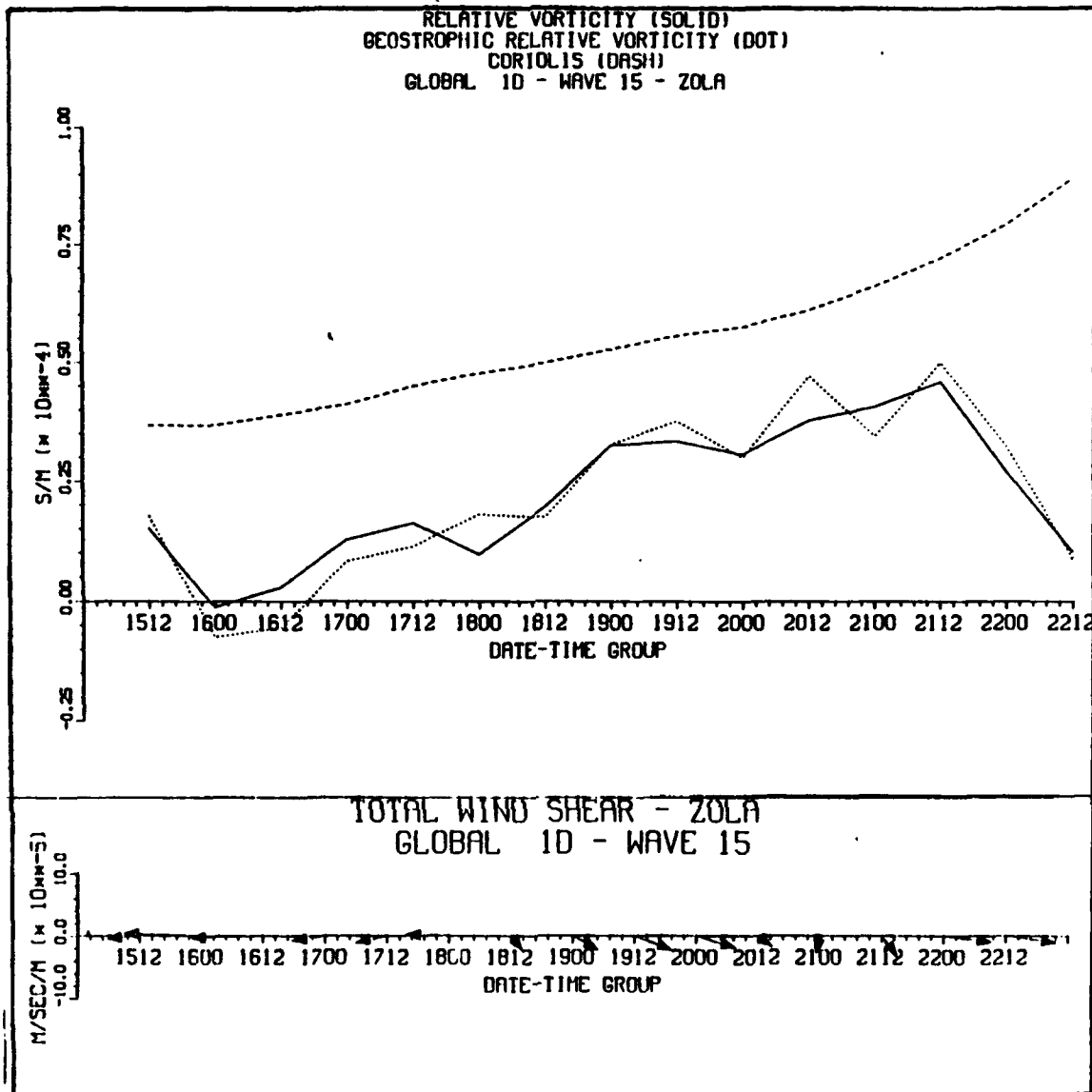


Figure 21. Relative vorticity and horizontal wind shear as in Fig. 9, except for Typhoon Zola during 12 UTC 15 August through 12 UTC 22 August 1990.

The total horizontal wind shear and relative vorticity have consistent time variations (Fig. 21). In addition, the geostrophic and actual relative vorticity of the environmental flow agree closely throughout the period. Compared to Yancy, the magnitudes of the horizontal wind shear and relative vorticity for Zola are considerably smaller. Both components of the shear reversed sign at 12 UTC 18 August,

and the relative vorticity increased. Zola's peak in relative vorticity at 12 UTC 21 August occurs during the brief period of maximum intensity. A detailed comparison of the total horizontal wind shears with the propagation vectors is probably not appropriate due to the small magnitudes of the wind shear. There are no significant increases in cyclonic or anticyclonic wind shear to induce a noticeable change in the direction of the propagation vectors.

The components of the relative vorticity gradient are plotted in Figs. 22 and 23. The y gradients of relative vorticity (Fig. 22) are highly erratic. Although the geostrophic y gradients have similar time variations, the magnitudes are even larger. The y gradients at 12 UTC 15 August and 00 UTC 22 August do not appear to be representative. The corresponding x gradients of relative vorticity (Fig. 23) also do not appear to be representative. The trends in the geostrophic gradients parallel those of the actual x gradients, but the magnitudes once again are generally larger. The time variations in the x gradients appear smoother. Considering the periods of unrepresentative environmental flow, propagation vectors, and x and y gradients of relative vorticity throughout most of Zola, it is surprising that nearly every case of the propagation vectors and absolute vorticity gradients is consistent (Fig. 24).

4. Typhoon Dot

Typhoon Dot formed near 15°N, 145°E on 3 September, achieved tropical storm strength on 4 September, and typhoon strength was reached on 6 September (Fig. 25). Dot was a large typhoon as it approached the island of Taiwan. Maximum intensity of 80 kt at 00 UTC 7 September was achieved upstream of Taiwan. One of the major features of interest concerning Dot was the straight and steady track toward the west-northwest. One factor may have been that the subtropical ridge continued to develop westward to maintain a constant relative position to the

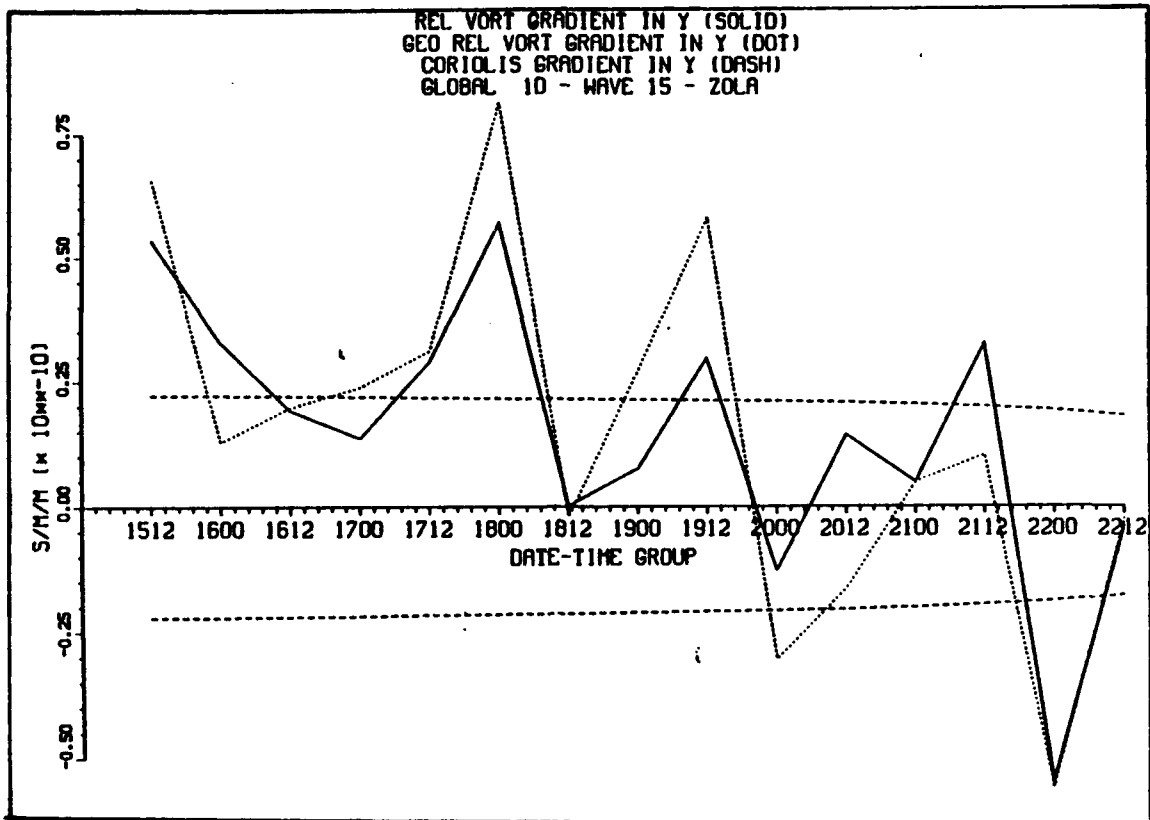


Figure 22. Relative vorticity gradient in y direction as in Fig. 10, except for Typhoon Zola during 12 UTC 15 August through 12 UTC 22 August 1990.

tropical cyclone during Dot's steady westnorthwest track.

The relationship between the direction and speed of Dot and the analyzed environmental steering flow and derived propagation vectors is shown in Fig. 26. Of particular note are the weak environmental flow and substantial propagation vector magnitudes from 12 UTC 2 September to 12 UTC 4 September. Since Dot was intensifying to tropical storm strength during this period, the propagation vectors are excessive. As in the early stages of Yancy, the environmental flow representation in NOGAPS appears to be unrealistic. After 00 UTC 5 September, the environmental steering flow was quite consistent in time. The storm motion was to the left of the northwestward steering flow from 00 UTC 6 September through 00 UTC 8 September as the subtropical ridge continued to build westward to the north of Dot. Thus, the propagation vectors were generally westward

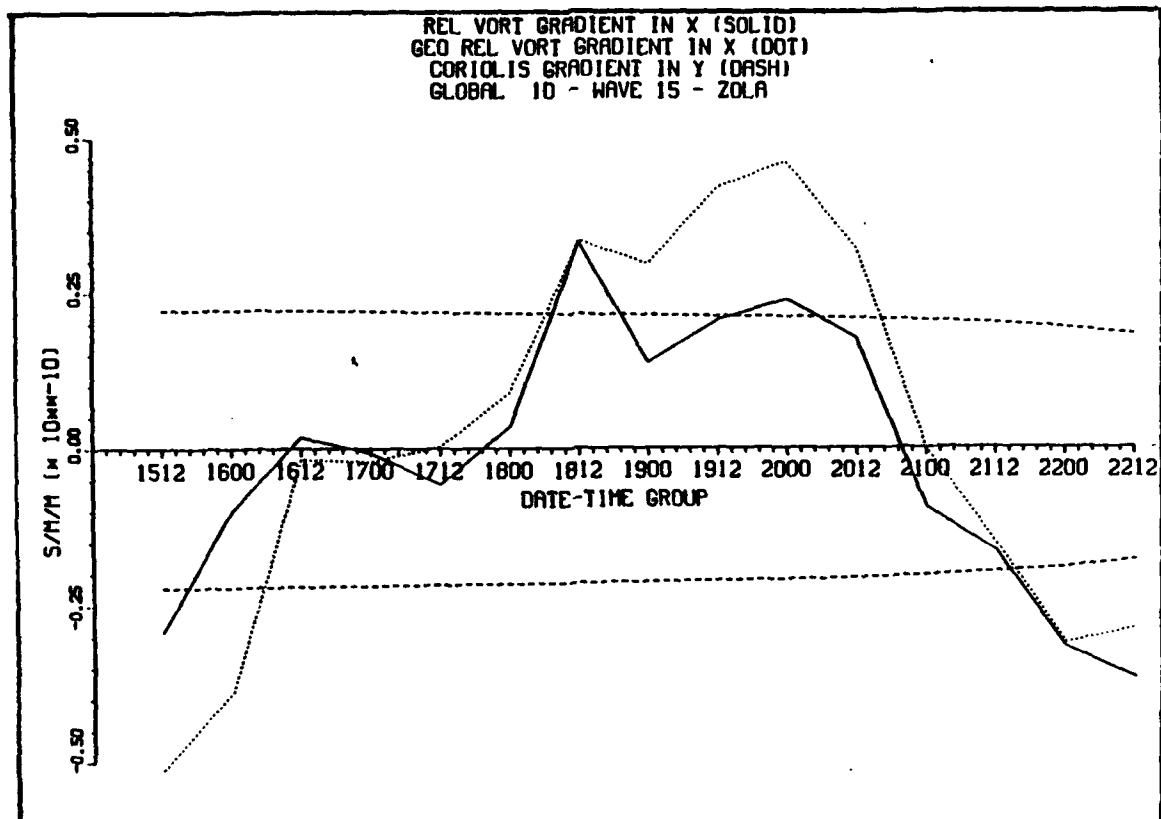


Figure 23. As in Fig. 22, except for relative vorticity gradient in x direction.

in this period. Notice also that the environmental flow vectors generally are faster than the storm motion, which is contrary to the results of prior studies (Elsberry and Abbey 1991). Dot struck Taiwan prior to 00 UTC 8 September and was over mainland China on 12 UTC 8 September, which may have distorted the propagation vectors at these times.

It is of interest that the relative vorticity of the environmental flow (Fig. 27) was approximately the same magnitude as the Coriolis parameter throughout Dot's existence. The geostrophic vorticity was even larger and had consistent (but larger) variations as the relative vorticity. The total horizontal wind shear vectors indicate this large positive relative vorticity was due to positive $\partial v/\partial x$ and negative $\partial u/\partial y$ that steadily increased in time. Thus, Dot remained on the cyclonic side of the wind maximum between the subtropical high and the lower pressures

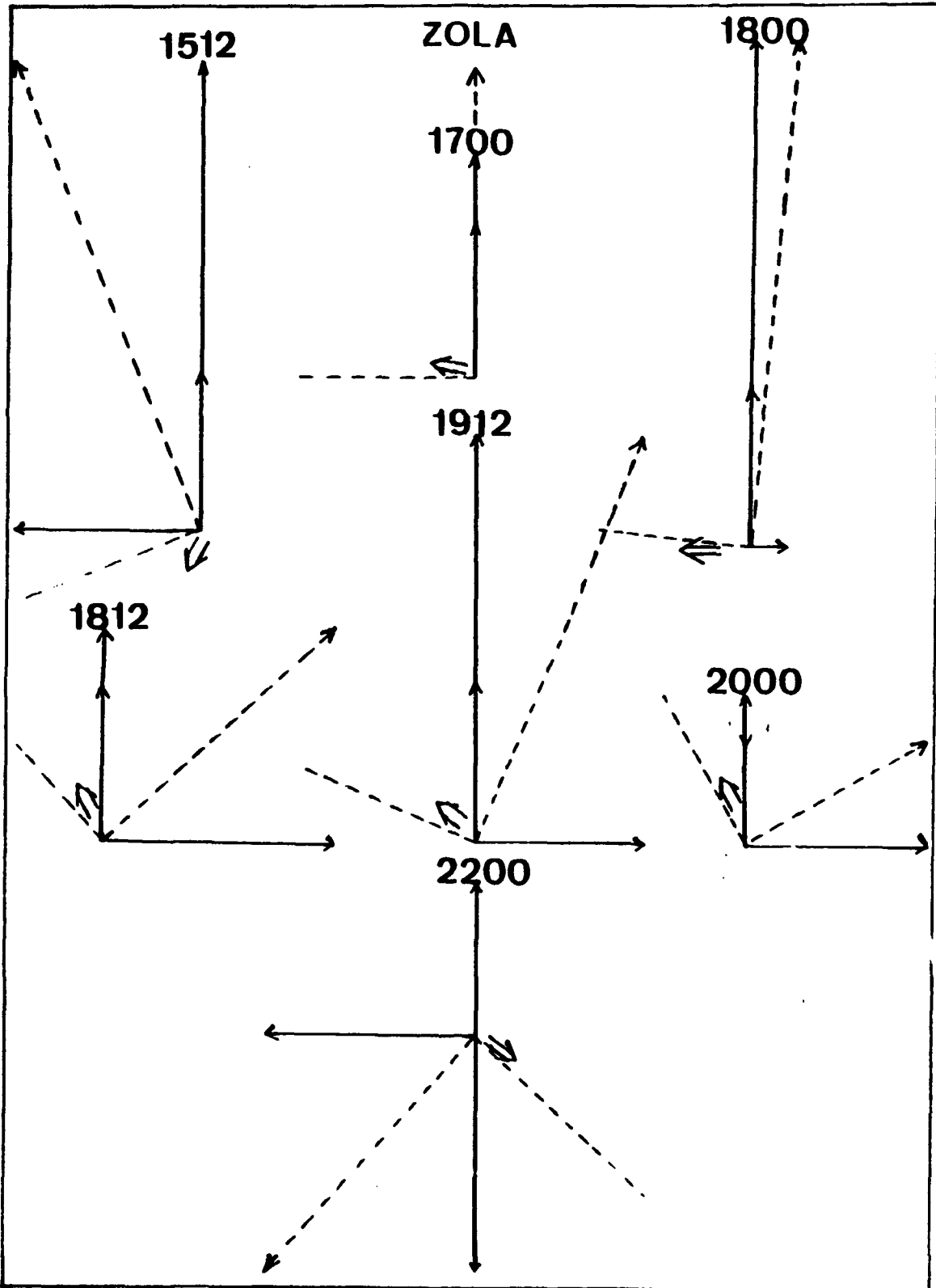


Figure 24. As in Fig. 12, except for seven selected date-times for Typhoon Zola.

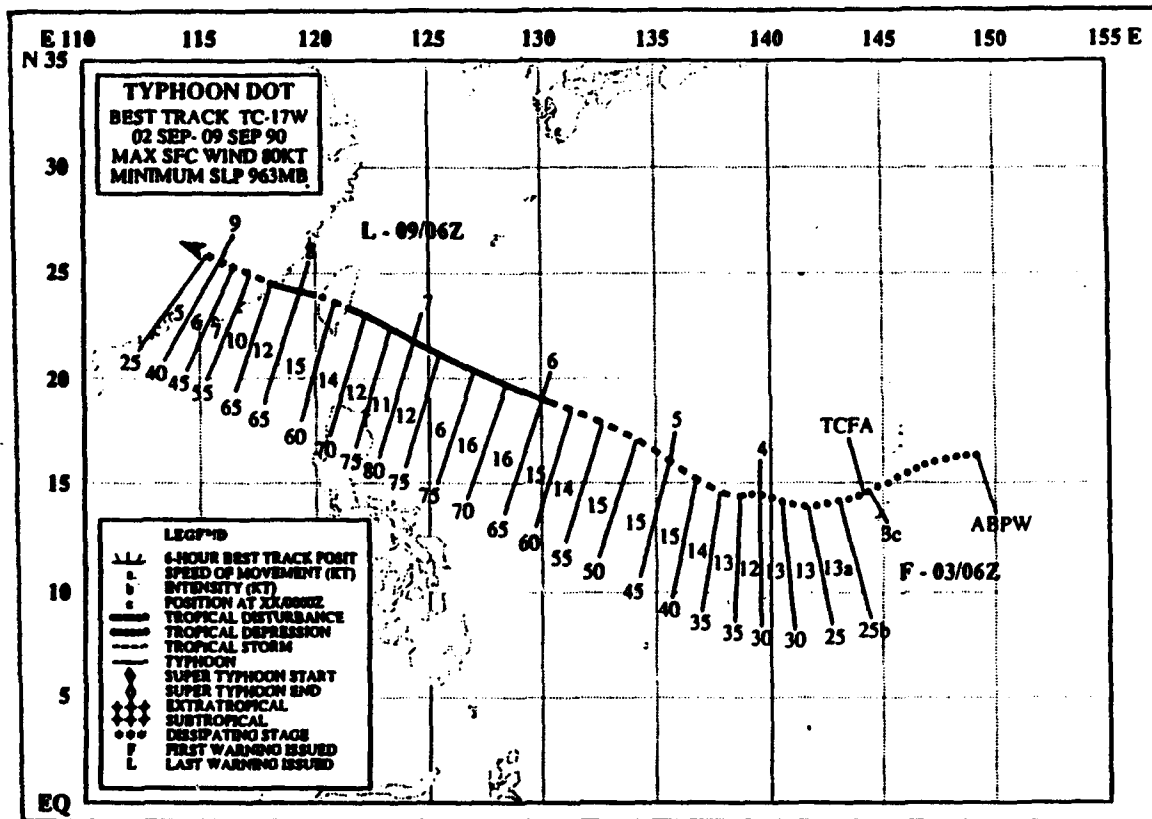


Figure 25. Best track for Typhoon Dot from JTWC (ATCR 1990).

in the monsoon trough over China. Only in Typhoons Dot and Flo (to be discussed below) did the relative vorticity increase subsequent to the period of maximum intensity.

The magnitudes of the y and x components of the relative vorticity gradients with respect to beta are displayed in Figs. 28 and 29. The y gradients are large and positive during the early stage. However, this is the period during which the NOGAPS representation of the environmental flow appears to be unrealistic. Between 00 UTC 5 September and 12 UTC 6 September, the y gradients become large and negative. The geostrophic values are extreme during this period. Subsequently, the y gradients assume a positive value through 12 UTC 8 September, except at 12 UTC 7 September. The values at 00 UTC and 12 UTC 8 September may include land effects and are therefore subject to question. The positive values

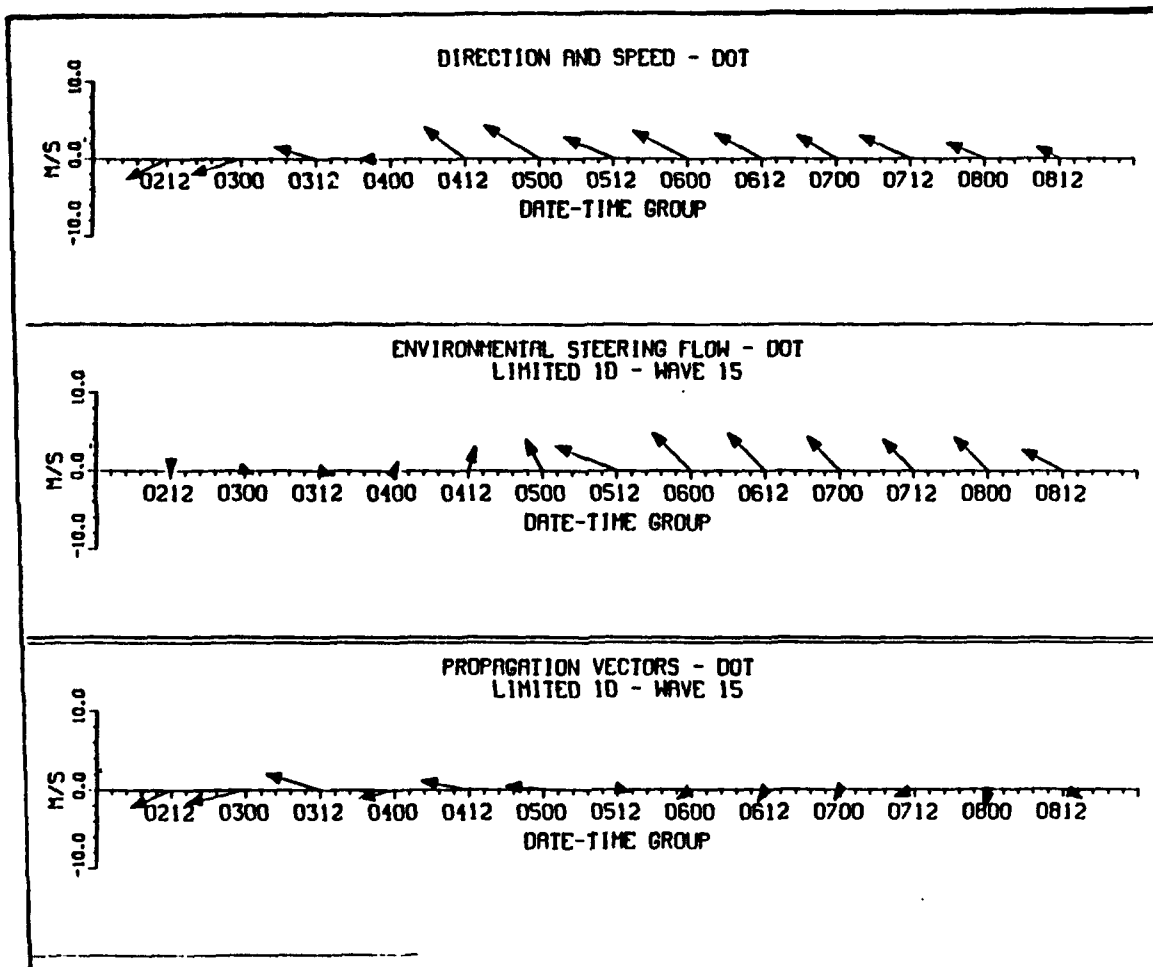


Figure 26. Translation vectors, environmental steering flow, and propagation vectors as in Fig. 8, except for Typhoon Dot during 12 UTC 2 September through 12 UTC 8 September 1990.

of relative vorticity in Fig. 27 combined with positive y gradient values at both ends of the time scale do not seem consistent with the subtropical high building westward with Dot. However, the predominately negative y gradient values between 00 UTC 5 September and 12 UTC 7 September would agree with the westward building to this ridge. The consistent negative values of the x gradient of relative vorticity (Fig. 29) are expected for a ridge to the east. As noted before, there is a greater time consistency with the x gradient as compared to the y gradient, and the geostrophic x gradients again are more erratic and generally larger in magnitude. Although the x gradient magnitudes are not as large as beta, they are not

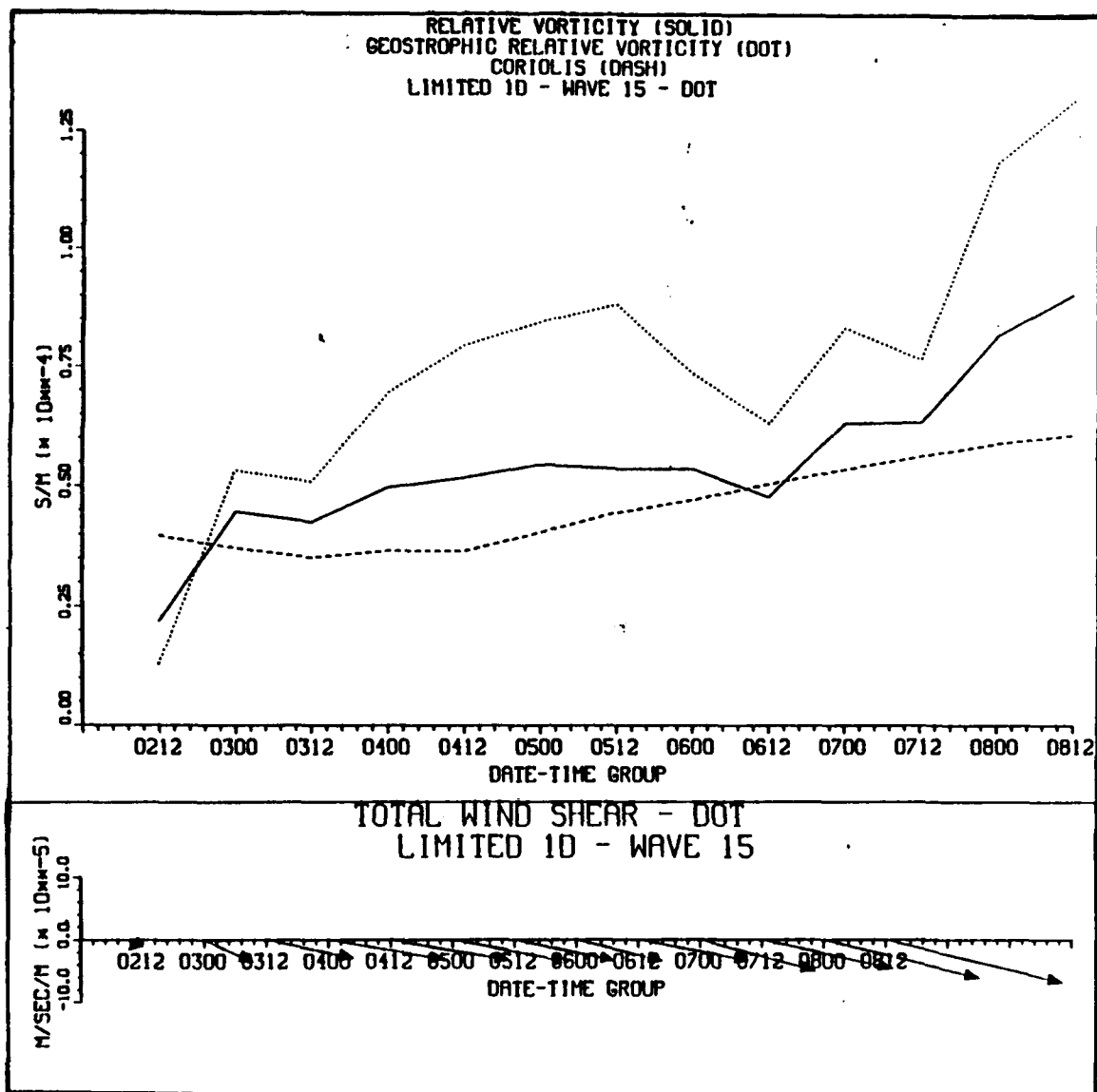


Figure 27. Relative vorticity and horizontal wind shear as in Fig. 9, except for Typhoon Dot during 12 UTC 2 September through 12 UTC 8 September 1990.

negligible.

The directions of selected propagation vectors are compared with the absolute vorticity gradients for various date-times in Fig. 30. These date-times were chosen to represent various relative vorticity gradient regimes. Four of the five date-times demonstrated that the propagation vector directions were consistent with the expected relationship (Elsberry

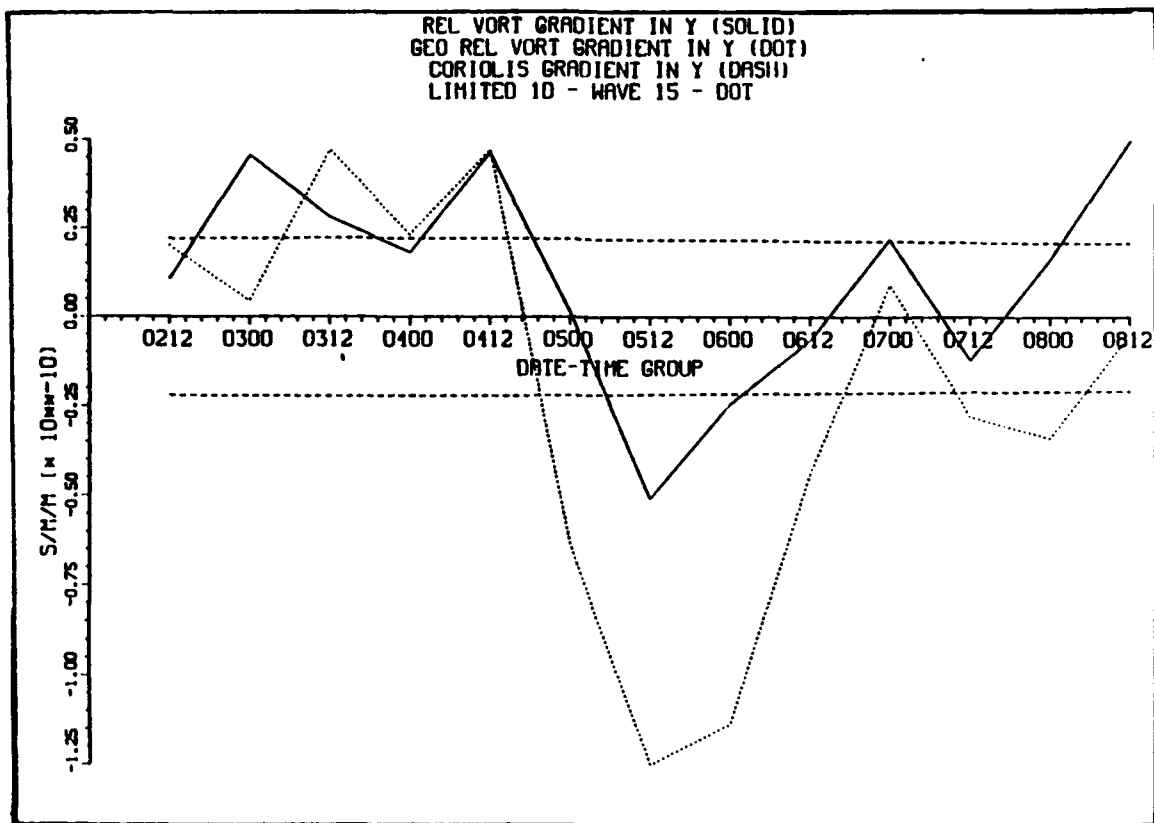


Figure 28. Relative vorticity gradient in y direction as in Fig. 10, except for Typhoon Dot during 12 UTC 2 September through 12 UTC 8 September 1990.

and Abbey 1991). The only exception was 12 UTC 8 September, where Typhoon Dot was over southern China. Thus the orographic influence may have distorted the expected relationship between the environmental steering flow and self-propagation.

5. Typhoon Ed

Typhoon Ed originated in the Marshall Islands east of Guam on 7 September 1990 and made landfall in Vietnam about 6,000 km and 12 days later (Fig. 31). Ed did not reach tropical storm strength until 11 September, and did not become typhoon strength until 14 September. Maximum intensity of 90 kt was reached at 18 UTC 16 September in the South China Sea, and then Ed weakened prior to making landfall in Vietnam.

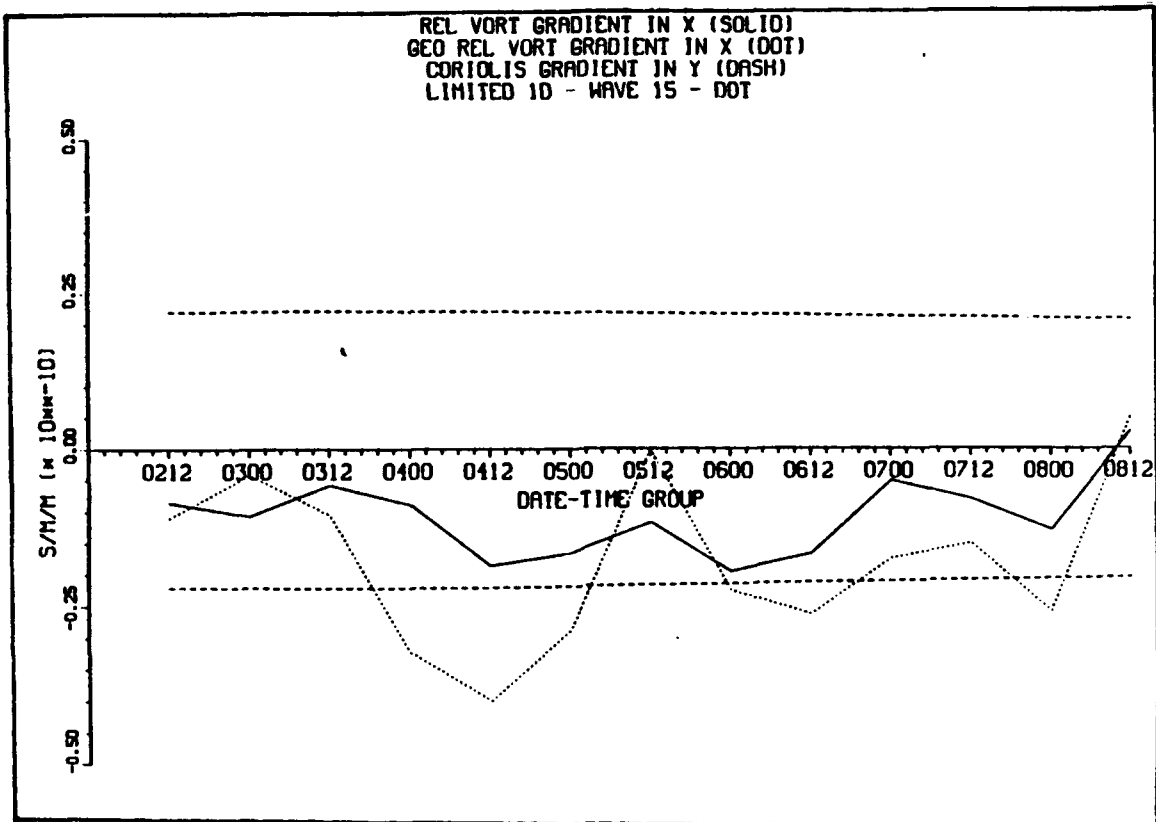


Figure 29. As in Figure 28, except for relative vorticity gradient in x direction.

Typhoon Ed formed from the northern-most convection cluster of a region of cloudiness in the monsoon trough. The emergence of this cluster as the dominant feature led to an apparent track displacement toward the northwest east of Guam. After 10 September Ed tracked due west along 20°N for four days while most objective aids were predicting a westnorthwest path. This westward track may have been due to the continual building of the subtropical ridge toward the west to the north of Ed. Another peculiar portion of the track was the westsouthwest path across the northern tip of Luzon. The WSW track of Ed subsequent to 14 September may be attributed to advection around a large monsoon trough to the southeast. Another possibility is an interaction with Tropical Storm Flo, which was also within the monsoon trough about 1700 km to the east.

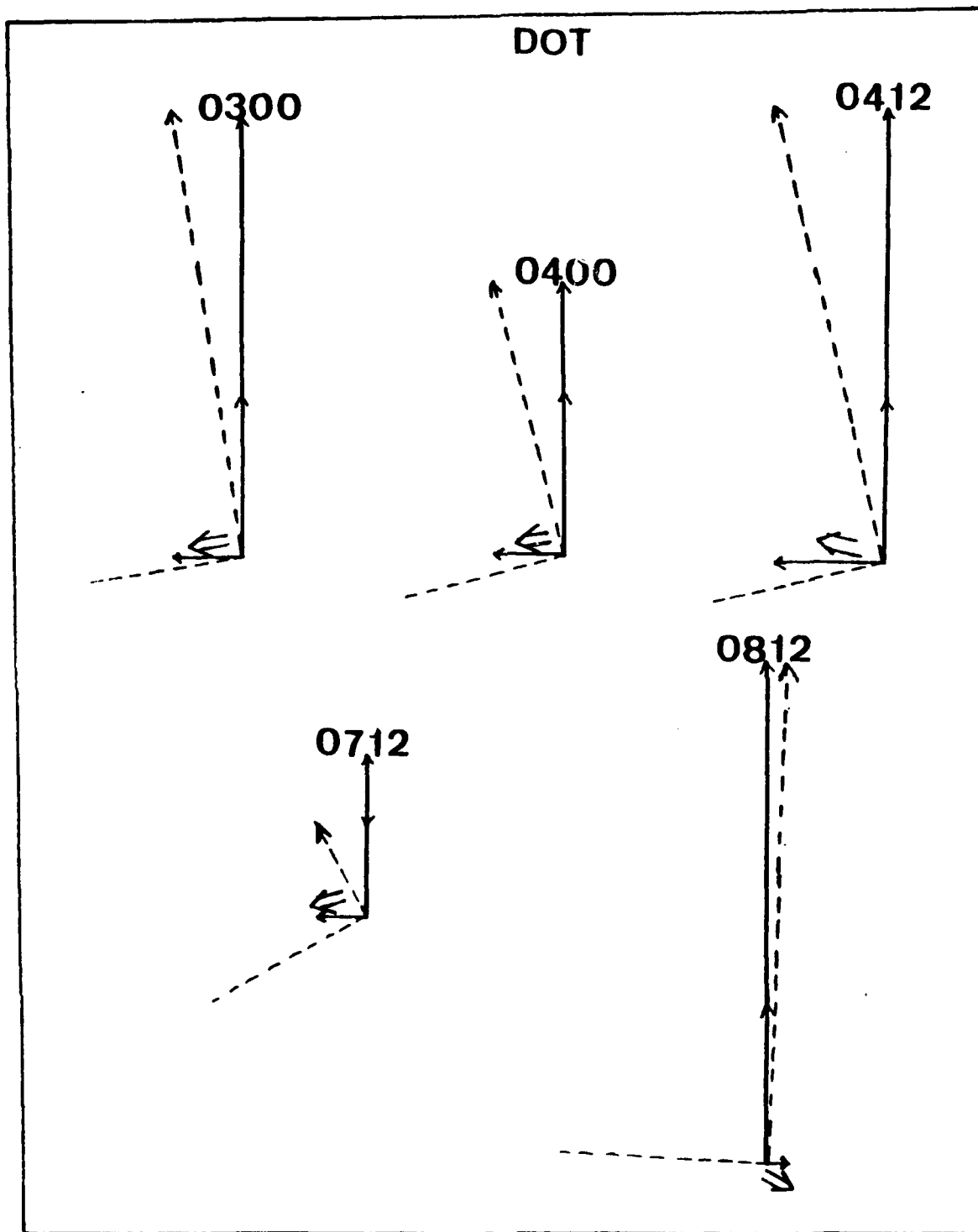


Figure 30. As in Figure 12, except for five selected date-times for Typhoon Dot.

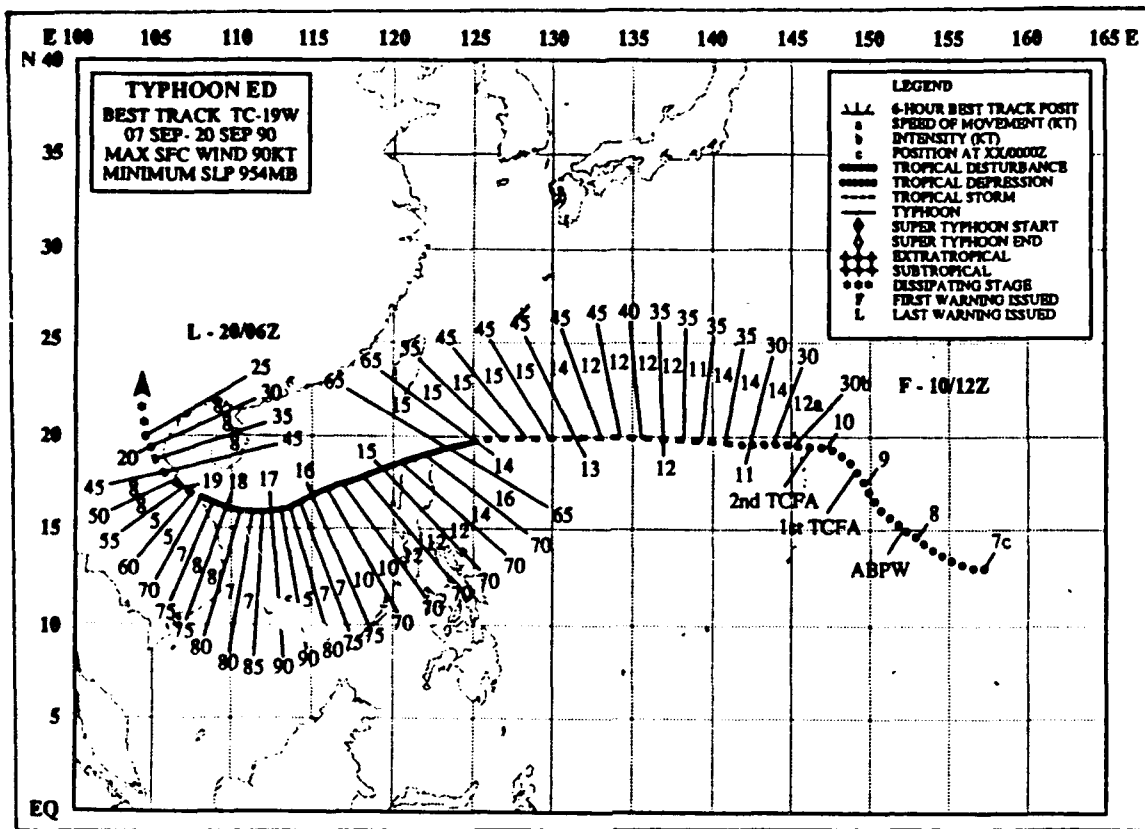


Figure 31. Best track for Typhoon Ed from JTWC (ATCR 1990).

Finally, a strong warm high-pressure system that intensified over China on 14 September may also have contributed to the westsouthwest track of Ed.

A comparison of the translation vectors, environmental steering flow, and propagation vectors for Ed is given in Fig. 32. The similarities between Ed's direction and speed and the environmental flow reveal how closely Ed tracked with the large-scale environment. Notice especially the period of westsouthwest flow from 12 UTC 13 September through 12 UTC 15 September. Although the directions of the NOGAPS low-pass filtered analyses are consistent with the westsouthwest track, the magnitudes are larger than the storm motion (except for 12 UTC 14 September). Thus, the derived propagation vectors are actually eastward rather than westward. The average magnitude (0.54 m/s) of Ed's propagation vectors was among the smallest of all the TCM-90 tropical

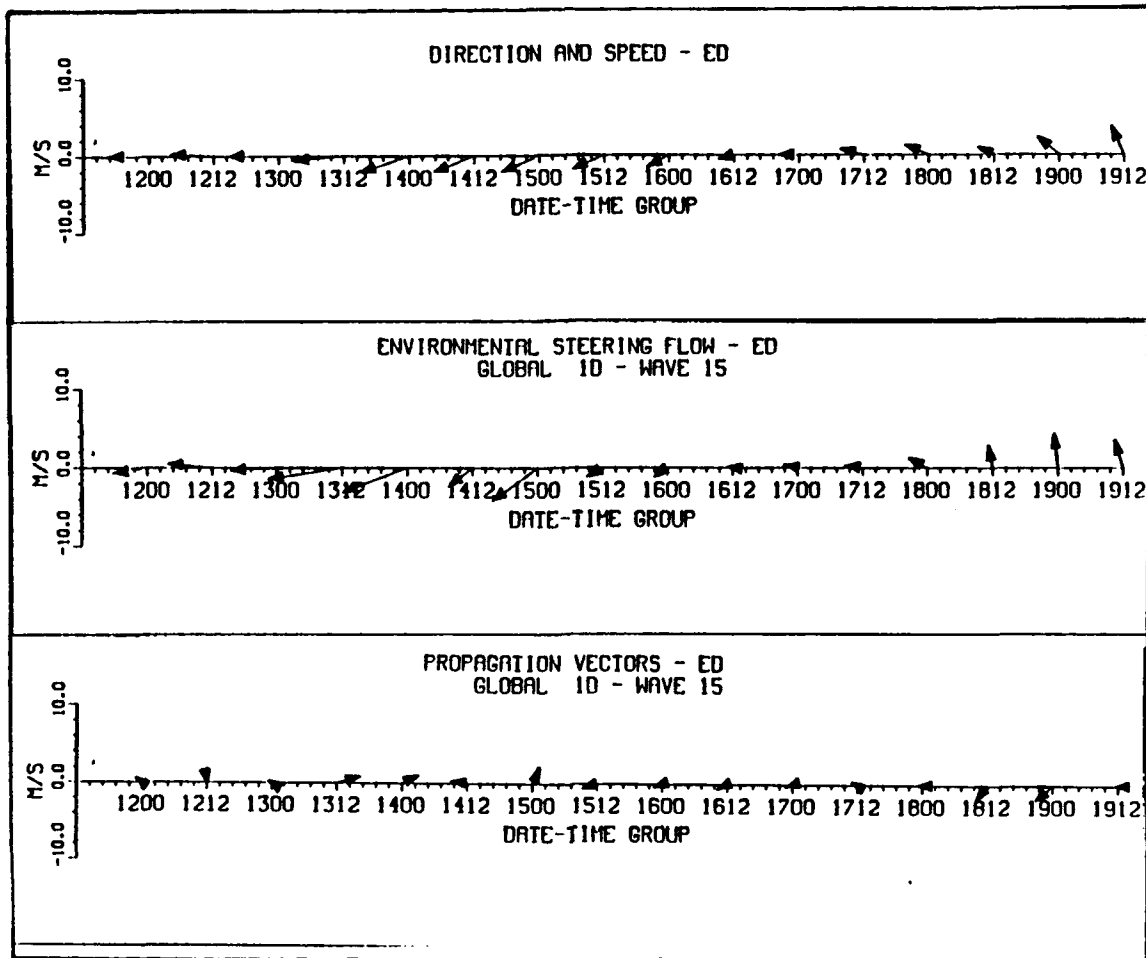


Figure 32. Translation vectors, environmental steering flow and propagation vectors as in Fig. 8, except for Typhoon Ed during 00 UTC 12 September through 12 UTC 19 September 1990.

cyclones.

Even though Ed formed and moved within a monsoon trough environment, the relative vorticity of the environmental flow was generally less than the Coriolis parameter until about 12 UTC 16 September (Fig. 33). The relative vorticity then exceeded the Coriolis magnitude during this period of maximum intensity. These relative vorticities are consistent with the total horizontal wind shear vectors (Fig. 33), which indicate positive $\partial v/\partial x$ and negative $\partial u/\partial y$ throughout most of the period. The exceptions are at 12 UTC 14 September and 00 UTC 15 September, when the relative vorticity values are small.

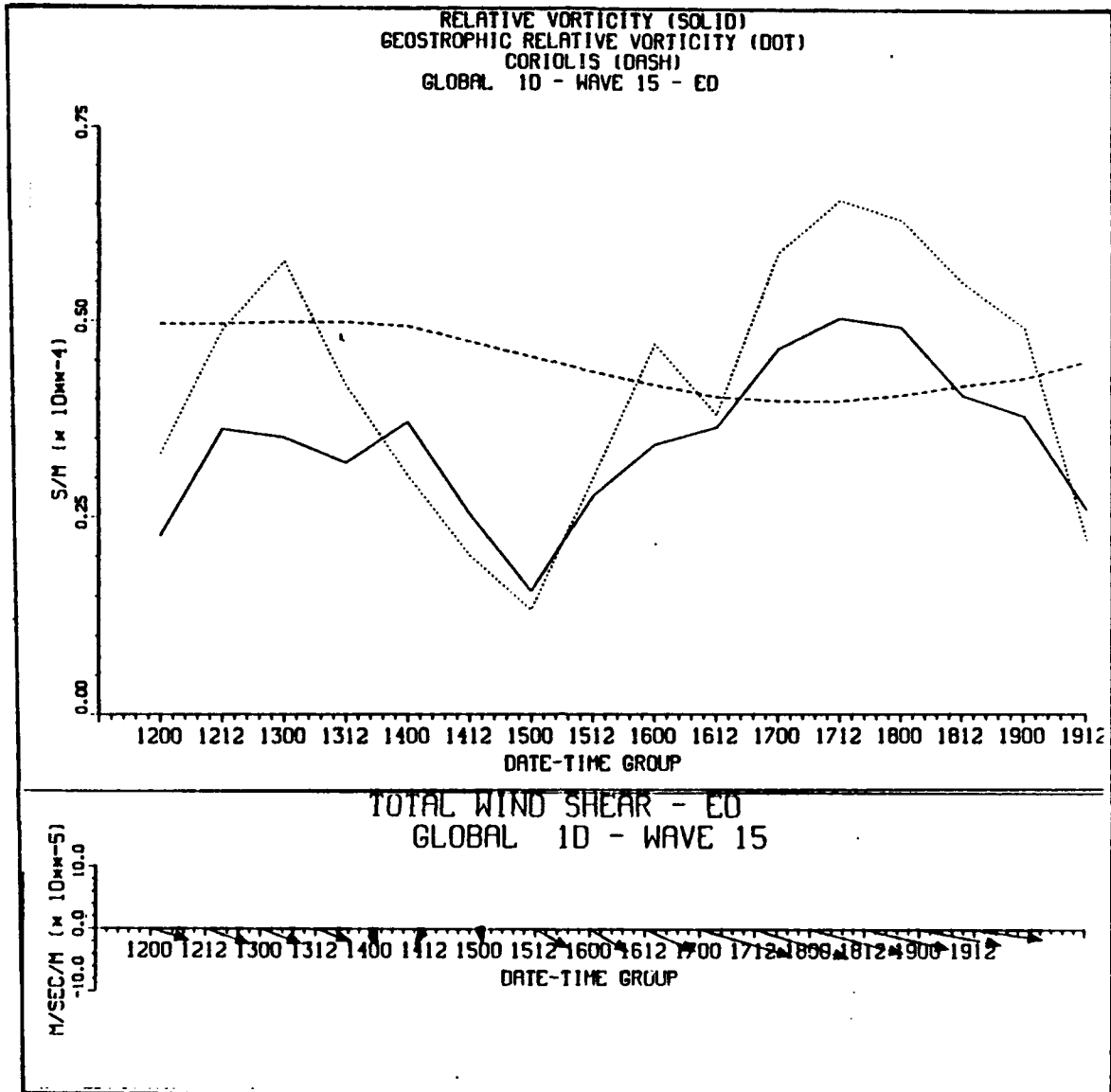


Figure 33. Relative vorticity and horizontal wind shear as in Fig. 9, except for Typhoon Ed during 00 UTC 12 September through 12 UTC 19 September 1990.

The x and y components of the relative vorticity gradients versus the magnitude of beta are given in Figs. 34 and 35. As previously, the y gradient values (Fig. 34) are large relative to beta and are erratic in time, especially during 12 UTC 14 September through 12 UTC 15 September when the environmental flow vectors were weak. Otherwise the period 00 UTC 13 September through 00 UTC 18 September would have negative y

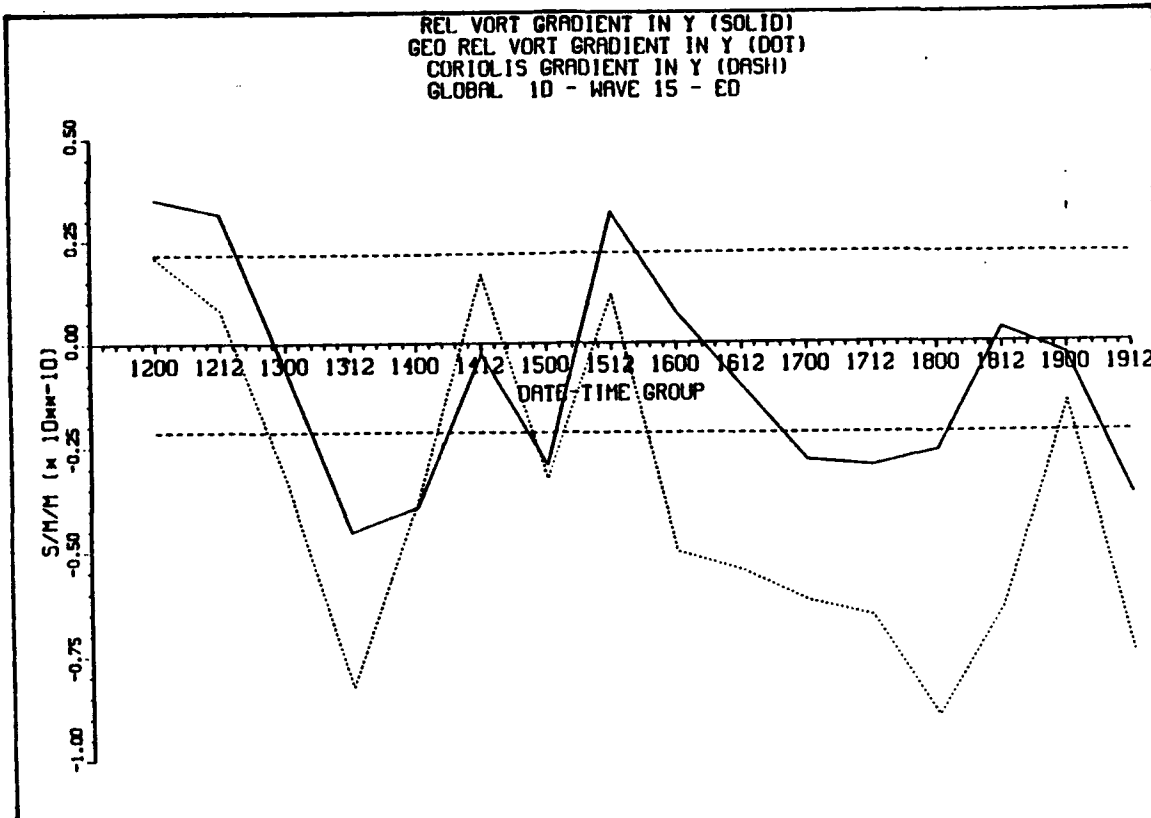


Figure 34. Relative vorticity gradient in y direction as in Fig. 10, except for Typhoon Ed during 00 UTC 12 September through 12 UTC 19 September 1990.

gradient values, which would be consistent with the subtropical ridge to the north. The geostrophic values, as seen previously, are quite large and have larger variations in time than do the y gradients calculated from the wind fields. The x gradient values (Fig. 35) are generally small and negative, with the exception of the period between 00 UTC 14 September and 12 UTC 15 September, when other aspects of the environmental flow (discussed above) were also erratic. The geostrophic x gradient values again had larger variations.

The relationships between the absolute vorticity gradients obtained from Figs. 34 and 35 with the directions of the propagation vectors are shown in Fig. 36 for seven date-times. The 12 UTC 13 September, 00 UTC 14 September, and 00 UTC 15 September propagation vectors are consistent with the gradient of absolute vorticity as

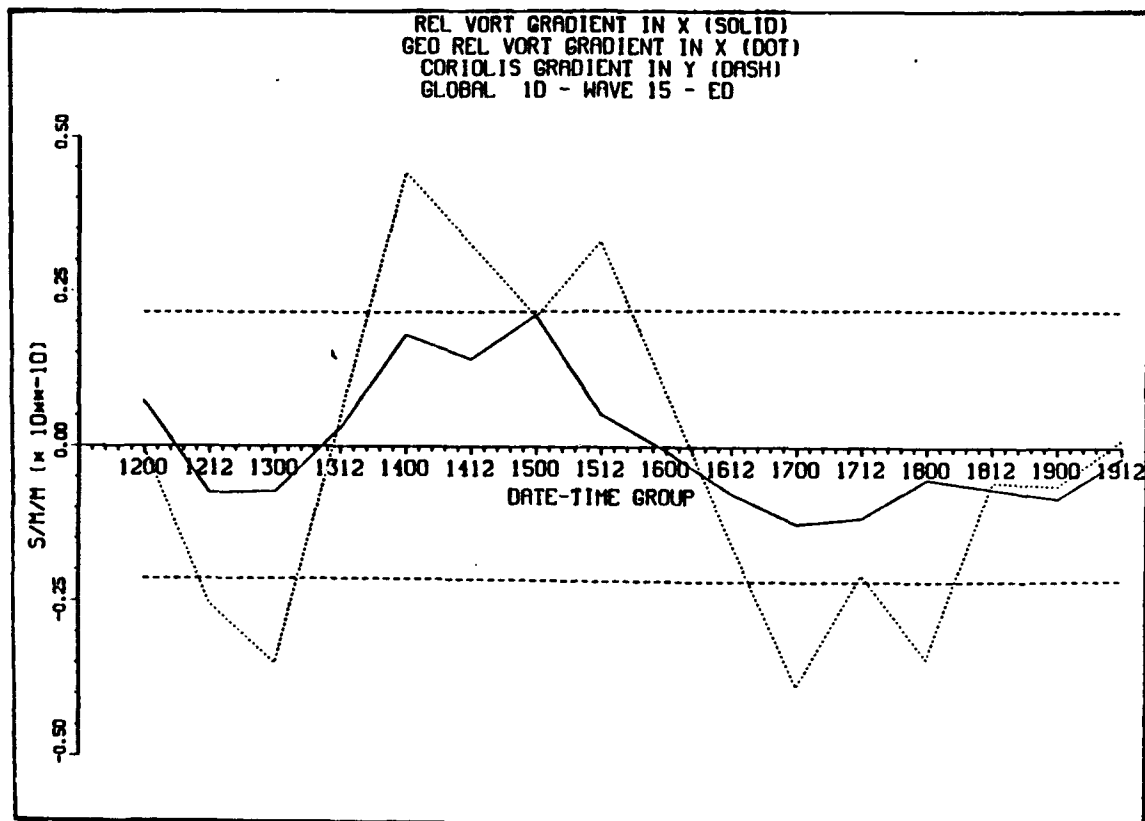


Figure 35. As in Fig. 34, except for relative vorticity gradient in x direction.

discussed in Elsberry and Abbey (1991). However, the 12 UTC 14 September and 12 UTC 15 September vectors are not. This may be due to the erratic nature of the environmental flow discussed earlier during this time period. The 12 UTC 18 September and 00 UTC 19 September vectors may have been affected by the mountainous orography of Vietnam.

6. Supertyphoon Flo

Supertyphoon Flo formed to the southeast of Guam on 8 September 1990 (Fig. 37). Rapid consolidation of Flo from a disorganized cluster of convection to a spiral banded structure occurred around 12 September, and as a result Flo was upgraded to a tropical depression. Flo reached tropical storm strength at 12 UTC 13 September and steadily intensified to typhoon strength on 00 UTC 15 September. Subsequently, a rapid

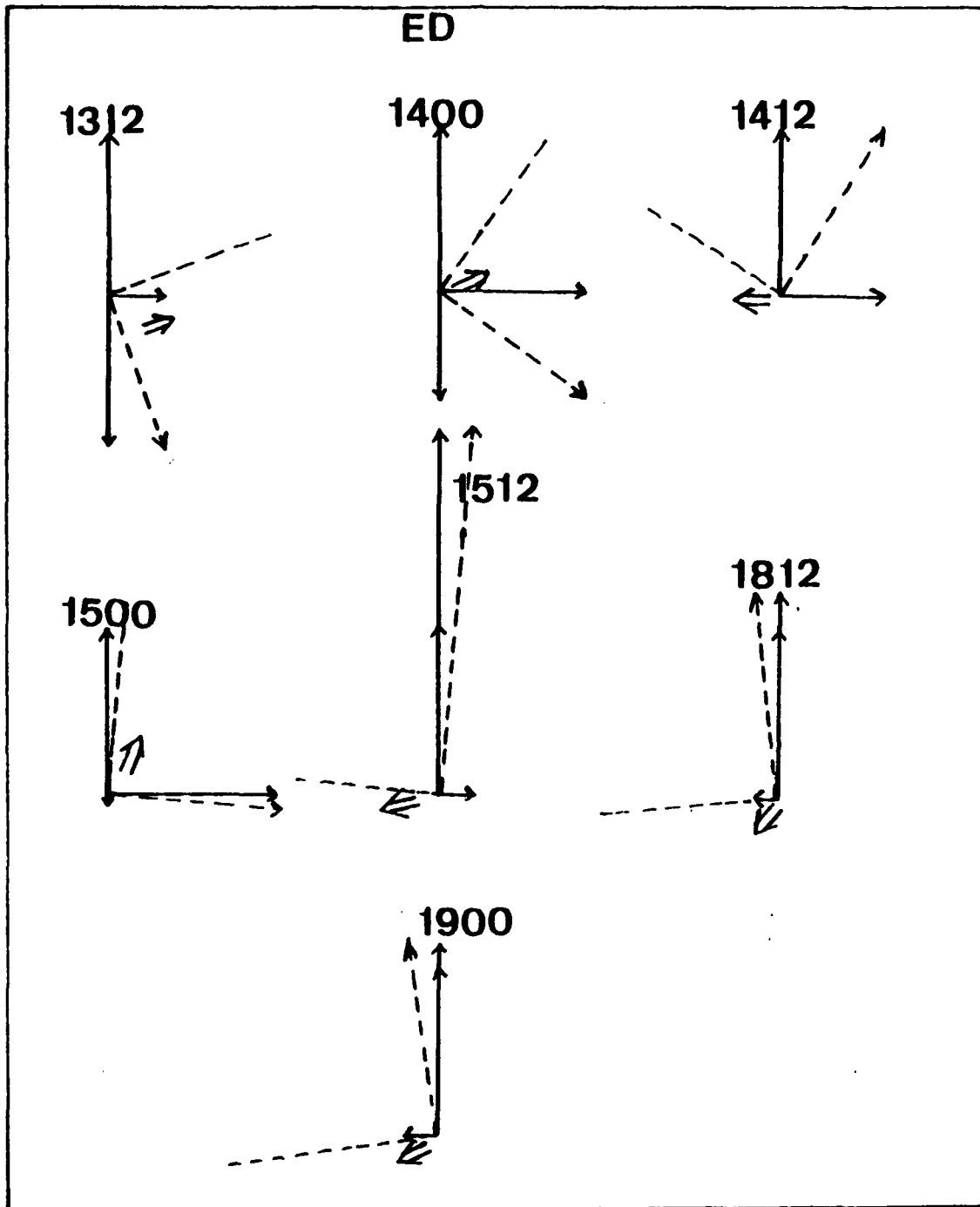


Figure 36. As in Fig. 12, except for seven selected date-times for Typhoon Ed.

intensification period occurred, and Flo reached supertyphoon strength at 12 UTC 16 September. Both the intensification and subsequent maintenance

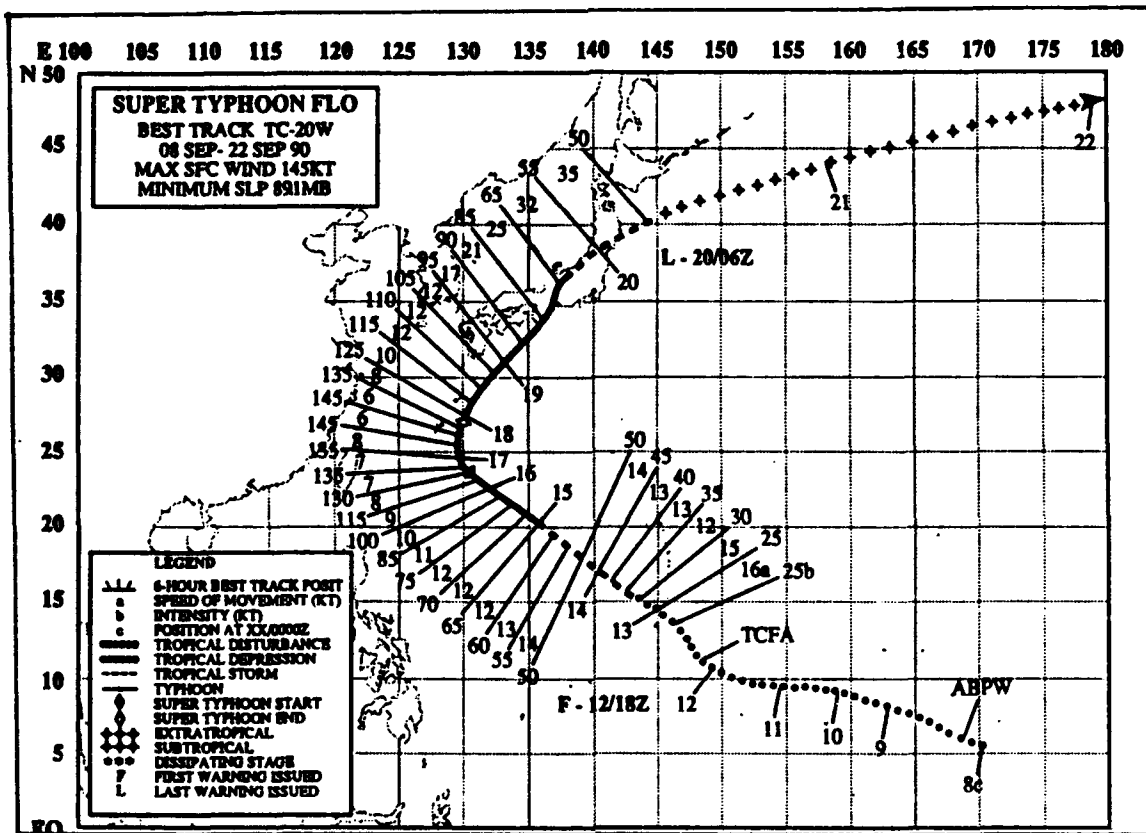


Figure 37. Best track for Supertyphoon Flo from JTWC (ATCR 1990).

of the high intensity were primarily due to a ready access to the midlatitude westerlies via outflow jets. The maximum intensity was 145 kt, with a minimum sea-level pressure of 891 mb.

The northwestward track between Guam and Saipan on 13 September was predominantly influenced by a large monsoon trough to the west that was subsequently contributing to Typhoon Ed's southwestward track over northern Luzon (Fig. 31). A series of complex interactions occurred around the time of recurvature between Supertyphoon Flo, a strong meridional subtropical ridge to the northeast, a developing midlatitude trough to the northwest, and a large, intense Tropical Upper Tropospheric Trough (TUTT) cell to the east.

The comparison of translation vectors, environmental steering flow, and propagation vectors for Supertyphoon Flo is presented in Fig.

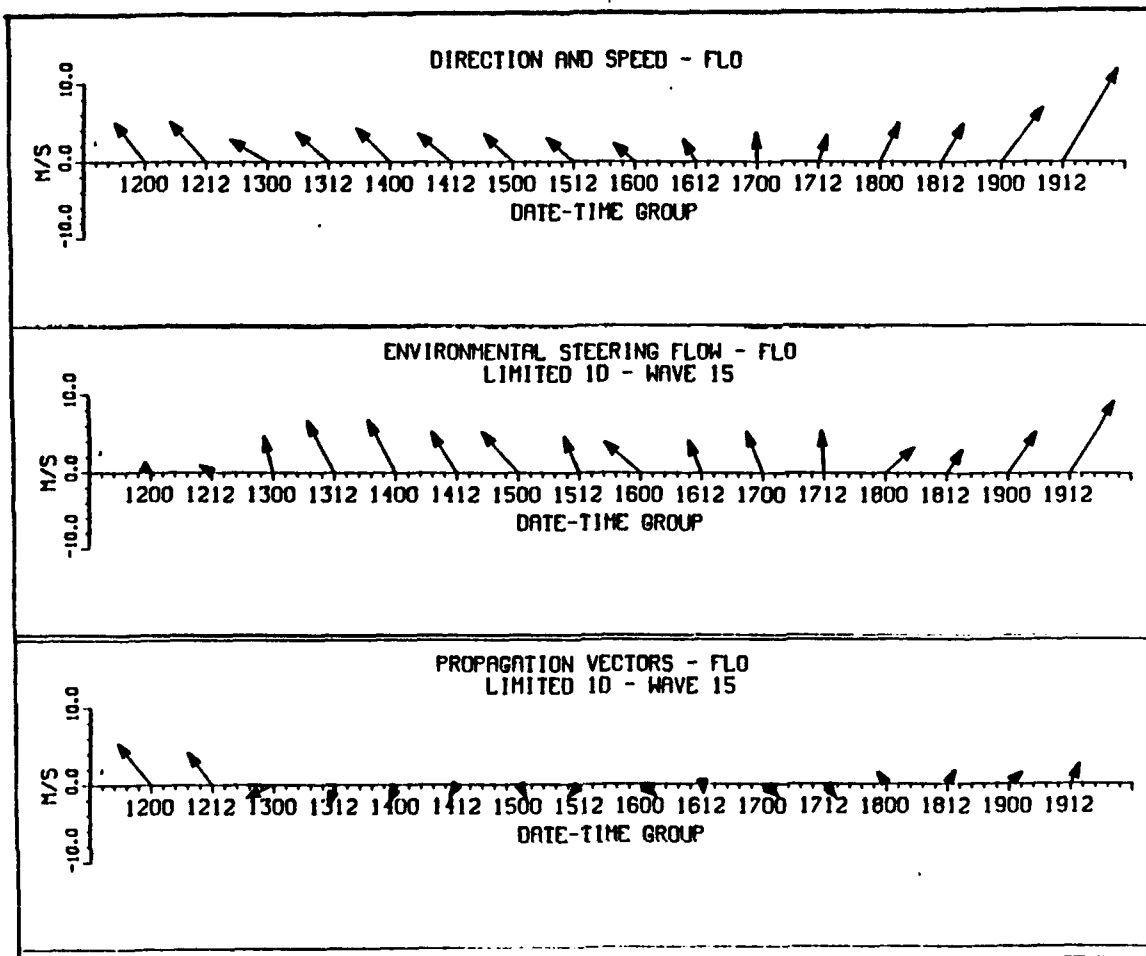


Figure 38. Translation vectors, environmental steering flow and propagation vectors as in Fig. 8, except for Supertyphoon Flo during 00 UTC 12 September through 12 UTC 19 September 1990.

38. Except for the very weak steering vectors at 00 UTC and 12 UTC 12 September, the time variations of the environmental flow directions are quite consistent. However, the magnitudes are larger than the storm motion. Two factors may have contributed to the anomalous characteristics on 12 September. First, the sudden northward displacement of the track on this date (Fig. 37) is in part due to a relocation of the center to the northernmost portion of the cloud cluster. Thus, the large northwestward motion vectors on this date are probably unrepresentative. Second, the environmental flow from the NOGAPS low-pass filtered analyses again appears to be erratic in low latitudes. The derived propagation vectors

on 12 September therefore are too large to be realistic. The almost 90° change in direction of the steering between 12 UTC 16 September and 12 UTC 17 September is consistent with the recurvature of Flo around 25°N. A large fraction of Flo's direction and speed is accounted for by these steering flow estimates. The southward components of propagation vectors between 00 UTC 13 September and 12 UTC 17 September are due to larger steering vectors than the storm motion vectors, which is opposite most prior studies (Elsberry and Abbey 1991). Later in the period, the storm motion vectors were larger, and the propagation vectors rotate with the storm motion. However, the propagation vectors are only a small contribution to the total storm motion on 19 September.

The relative vorticity of the environmental flow generally was equivalent to the Coriolis parameter after the anomalous period on 12 September (Fig. 39). That is, Flo formed on the cyclonic shear side of the monsoon trough and remained on the cyclonic side of the maximum in the environmental flow. Both the magnitude and the time variations of the geostrophic relative vorticity were larger than for the relative vorticity.

The time history of Flo's total horizontal wind shear (Fig. 39) is generally marked with a steady increase in cyclonic shear that is consistent with the increase in relative vorticity. The exceptions are at 12 UTC 17 September and 00 UTC 18 September just following recurvature, when the large-scale environmental flow was changing rapidly. The significant increases in positive $\partial v/\partial x$ at 12 UTC 13 September and in positive $\partial v/\partial x$ and negative $\partial u/\partial y$ at 00 UTC 15 September correspond to cyclonic rotation of the respective propagation vectors.

The relative vorticity gradients in the x and y directions are shown in Figs. 40 and 41 respectively. Although generally negative after 12 September, the y gradient values (Fig. 40) are highly erratic in time. Many of the negative values are of the same order as beta, which is a significant factor in the calculation of the propagation vector. The

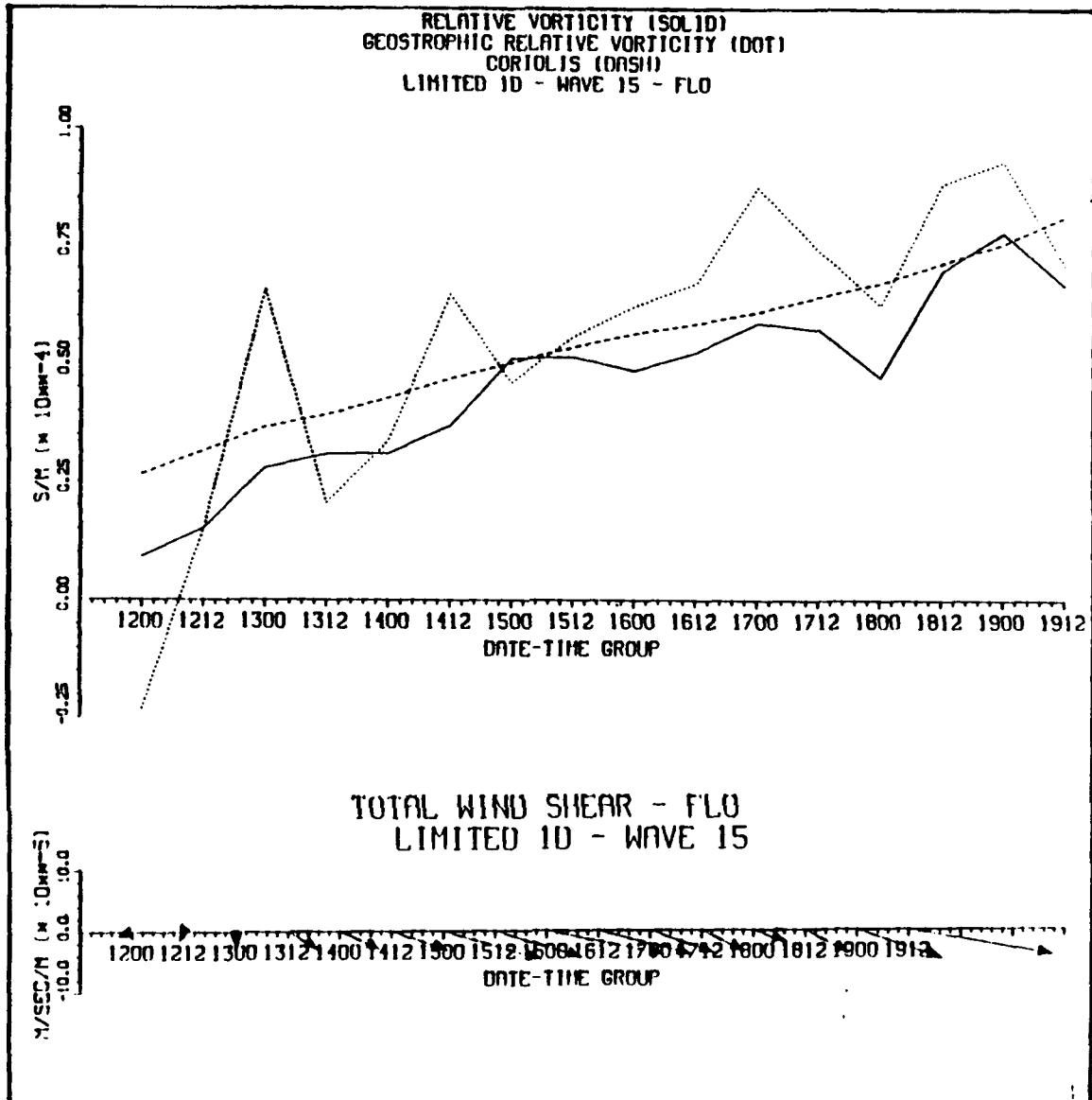


Figure 39. Relative vorticity and horizontal wind shear as in Fig. 9, except for Supertyphoon Flo during 00 UTC 12 September through 12 UTC 19 September 1990.

geostrophic values, as before, are quite large and erratic in time. As in previous cases, a positive relative vorticity with negative y gradient values would be consistent with a subtropical ridge to the north (or northeast). The positive values at recurvature time (00 UTC 17 September) and later (00 and 12 UTC 18 September) would be consistent with troughing to the north. As printed out earlier, the flow pattern near recurvature

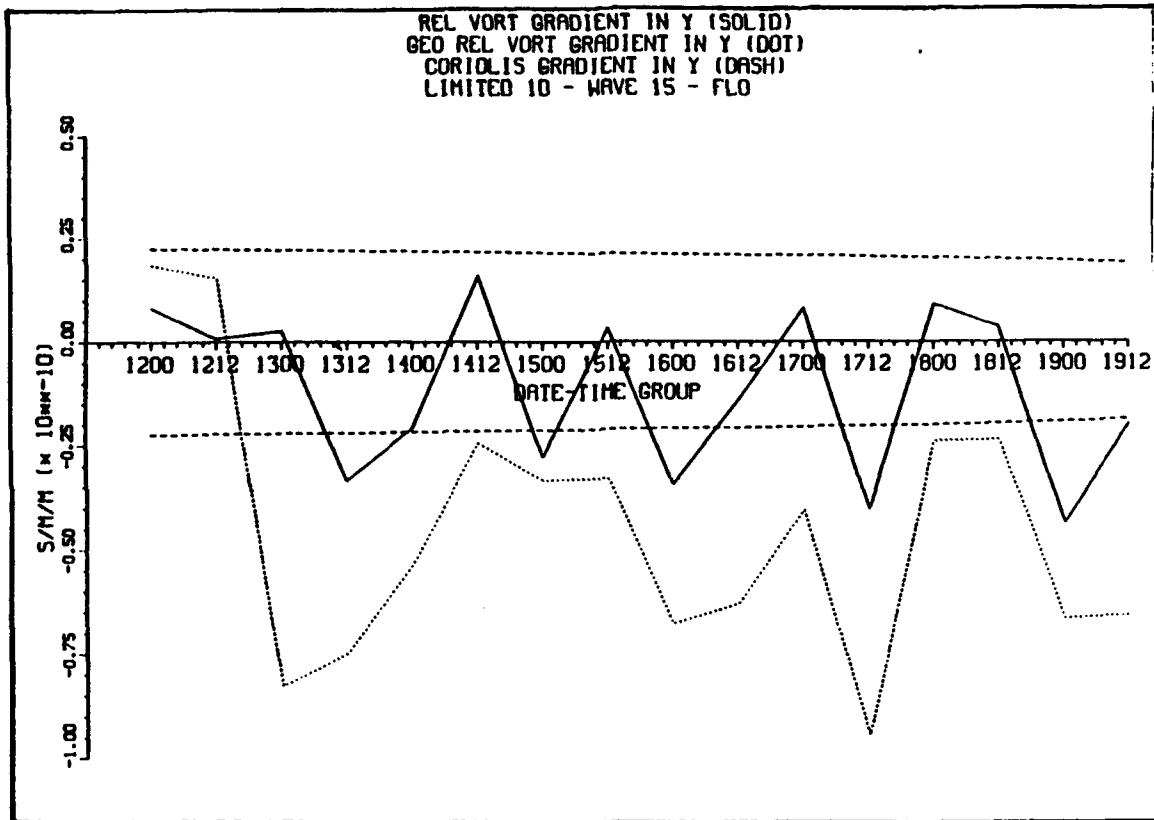


Figure 40. Relative vorticity gradient in y direction as in Fig. 10, except for Supertyphoon Flo during 00 UTC 12 September through 12 UTC 19 September 1990.

time was quite complex. Magnitudes (both actual and geostrophic) of the x gradients of relative vorticity (Fig. 41) are reasonable. The general negative trend, as in previous cases, is consistent with the subtropical ridge to the east (or northeast). The positive values between 00 UTC 18 September and 00 UTC 19 September occur after recurvature.

Propagation vectors are compared the absolute vorticity gradients in Fig. 42 to determine consistency with Elsberry and Abbey (1991). As before, date-times were chosen to represent the different gradient regimes in Figs. 40 and 41. Three of the seven comparisons agreed with Elsberry and Abbey, and three of the four that did not agree did not deviate significantly. The 00 UTC 17 September propagation vector was anomalous, probably due to the complex nature of the environmental flow around the time of recurvature.

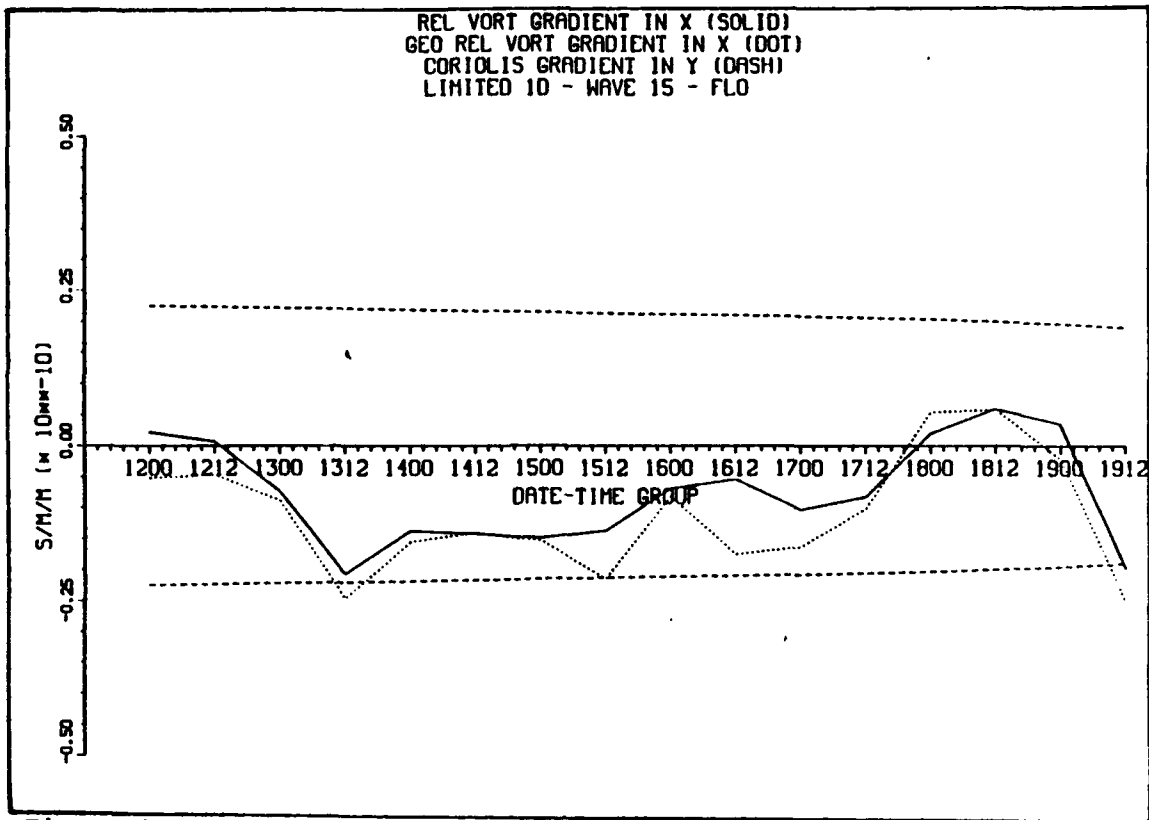


Figure 41. As in Fig. 40, except for relative vorticity gradient in x direction.

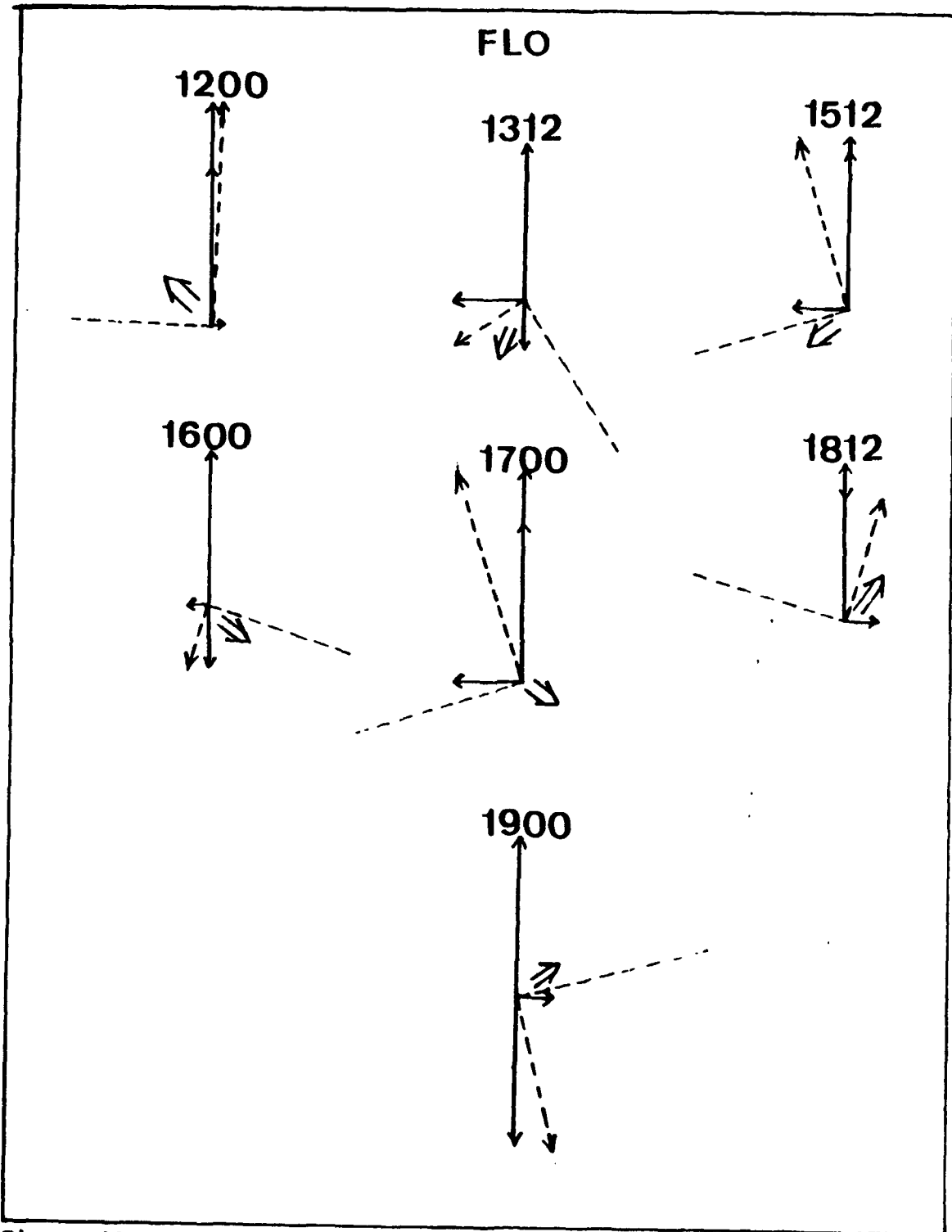


Figure 42. As in Fig. 12, except for seven selected date-times for Supertyphoon Flo.

V. CONCLUSIONS AND RECOMMENDATIONS

This study indicates that filtering 850 - 300 mb layer-mean NOGAPS global u and v wind fields, or a limited region of these global NOGAPS fields, provides an effective definition of the large-scale environmental steering flow in the region of the TCM-90 tropical cyclones. The measure of goodness was the steering flow vector that most closely agreed with the storm motion vector over an ensemble of storms. Thus, the search was for the minimum standard deviation of the propagation vector, which was defined to be the difference between the storm motion and the steering vector. When analyzing each of the six storms individually, zonal wavenumbers 1 - 15 was the best low-pass filter in representing the large-scale environmental wind field. Using wavenumbers 1 - 21 as the low-pass filter gave the worst representation. When considering the ensemble of six storms, wavenumbers 1 - 12 best represented the environmental wind field. However, this wavenumber low-pass filter did not perform quite as well in the individual storm analyses. Filtering only in the zonal direction provided a better representation of the large-scale environmental flow than doing a two-dimensional Fourier decomposition (zonally and meridionally). An Errico detrending procedure to introduce periodicity, and then restoring that trend once the filtering was accomplished, appeared to be an effective means of handling the non-periodicity in the limited region. However, filtering meridionally was not performed because of the degradation in the layer-mean geopotential height gradients in the meridional direction if the higher wavenumbers were removed. The limited region and global one-dimensional low-passed analyses provided equivalent steering flow estimates for the six TCM-90 tropical cyclones.

The directly interpolated layer-mean u and v wind fields provided more accurate steering estimates than the calculated geostrophic wind fields

for five of the six cases. The exception was Supertyphoon Flo, which had a size and northern track for which geostrophy perhaps would provide just as accurate a representation of the steering flow.

The low-passed NOGAPS analyses provided a large-scale environmental steering flow, propagation vectors, and total horizontal wind shear vectors that usually varied consistently in time. A notable exception occurred for storms in low latitude monsoon trough environments, when the magnitude of the steering flow vectors was too small. This exception corresponds to the early stages of the tropical cyclones, when position errors were also likely. In other cases, the influence of adjacent synoptic features could clearly be seen in the environmental steering flow. The linear environmental shear and relative vorticity variations were consistent because the low-passed fields contained little divergence. Although the absolute vorticity gradients and propagation vectors were generally consistent in direction, no attempt was made to compare magnitudes. The NOGAPS steering flow estimates did appear to be faster than the storm motion, which generally led to more westward propagation vectors.

One weakness of this study is the 2.5 deg. lat/lon resolution of the NOGAPS analyses. It is recommended that a similar wavenumber low-pass filtering in the zonal direction be applied to the final TCM-90 high resolution (50 km) limited region analyses. If operational NOGAPS analyses are found to provide similar steering flow estimates as the higher resolution TCM-90 analyses, then use of NOGAPS (including forecast fields) for other tropical cyclone motion studies might prove to be beneficial.

It is hoped that an accurate representation of the large-scale environment will lead to further advances in understanding tropical cyclone motion, and through those advances a greater confidence in tropical cyclone forecasting. These results show that the best representation of the large-scale flow peaks at wavenumbers 1 - 15, and

worsens rapidly with the use of larger wavenumbers. Thus a test is recommended of the use of wavenumbers 1 - 15 as a definition of the large-scale environmental flow as opposed to wavenumbers 1 - 20 that are currently being employed by Fleet Numerical Oceanography Center (FNOC) and the National Meteorological Center (NMC).

Since the environmental flow and the cyclone are a continuum, an optimum representation of the environmental steering flow in the vicinity of tropical cyclones is probably case dependent. The results provided in Table V give a preliminary indication that lower (higher) wavenumber low-pass filters are associated with the larger (smaller) tropical cyclones. Therefore, it is recommended that a case dependent study of the higher-resolution TCM-90 analyses be done using the best wavenumber low-pass filter for each storm.

APPENDIX A: DISCUSSION ON FFT2D/FFT2B SUBROUTINES

The purpose of the IMSL subroutine FFT2D is to compute Fourier coefficients of a complex periodic two-dimensional array. The call to FFT2D is

```
FFT2D(NRA, NCA, A, LDA, COEF, LDcoef),
```

where

NRA = number of rows of the two-dimensional array A (input),
NCA = number of columns of the two-dimensional array A (input),
A = the complex two-dimensional array to be analyzed via Fourier analysis (input),
LDA = leading dimension of A as called in the dimension statement of the calling program (input),
COEF = complex matrix containing the Fourier coefficients of A. Its dimensions are NRA by NCA (output),
LDA = leading dimension of COEF as called in the dimension statement of the calling program (input).

The routine computes the discrete complex Fourier transform using a variant of the Cooley-Tukey algorithm. Of note, an unnormalized inverse is found in the IMSL routine FFT2B, whose call is

```
FFT2B(NRCOEF, NCCOEF, COEF, LDcoef, B, LDB),
```

where

NRCOEF = number of rows of the coefficient array COEF (input),
NCCOEF = number of columns of the coefficient array COEF (input),
COEF = the complex coefficient array obtained from FFT2D that contains the Fourier coefficients to be transformed (input),
LDcoef = leading dimension of COEF as called in the dimension statement of the calling program (input),

B = the complex two-dimensional array containing the inverse Fourier coefficients of COEF. Its dimensions are NRCOEF by NCCOEF (output),

LDB = leading dimension of B as called in the dimension statement of the calling program (input).

The key to using FFT2D and FFT2B as a filter in knowing how the two-dimensional coefficient array, COEF, is filled. The elements of COEF are complex, where the "real" component of each element represents the cosine coefficient, and the "imaginary" component represents the sine. In Fourier analysis, filtering beyond the Nyquist frequency produces aliasing, and the Nyquist frequency in each dimension is defined as one-half of the number of data points in that dimension. The first coefficient in Fourier analysis represents the mean (average) value of the data. Therefore, the number of coefficients in each dimension representing the data will be the Nyquist frequency in that dimension plus 1, after rounding to the nearest whole number. These coefficients, only occupy one-fourth of the array, and the array fills from top to bottom and from left to right in this quadrant. There are 144 rows and 73 columns of data in the array. Therefore, the space in the array occupied by the Fourier coefficients is 73 rows and 37 columns.

Element 1,1 (row,column) is the element that contains the mean value of the data. The remaining elements in row 1 and column 1 contain coefficients that represent wavenumbers 0 in the north/south and east/west directions respectively. Similarly row 2 and column 2 contain the wavenumber 1 coefficients for their respective directions, and so on through row 73 and column 37. For example, the cosine and sine coefficients representing wavenumber 10 in the north/south direction and wavenumber 18 in the east/west direction will be housed in element 18,10 (row,column).

The remaining three quadrants of the array mirror this first quadrant, with symmetry about row 73 and column 37 if row 1 and column 1 are

neglected. That is, row 2 coefficients representing wavenumber 1 in the north/south direction are seen also in row 144, and column 6 coefficients representing wavenumber 5 in the east/west direction are also mirrored in column 69. Therefore, each pair of cosine and sine coefficients in an element of the coefficient array in quadrant one will also be present in the remaining three quadrants. All quadrants must be represented in order for an accurate filtering to be achieved.

LIST OF REFERENCES

- Carr, L. E., III, and R. L. Elsberry, 1990: Observational evidence for predictions of tropical cyclone propagation relative to steering. *J.Atmos.Sci.*, 47, 542-546.
- Chan, J. C.-L., 1985: Identification of the steering flow for tropical cyclone motion from objectively analyzed wind fields. *Mon.Wea.Rev.*, 113, 106-116.
- Chan, J. C.-L., and W. M. Gray, 1982: Tropical cyclone movement and surrounding flow relationships. *Mon.Wea.Rev.*, 110, 1354-1374.
- Chan, J. C.-L., and R. T. Williams, 1986: Analytical and numerical studies of the beta-effect in tropical cyclone motion. Part I. Zero mean flow. *J.Atmos.Sci.*, 44, 1257-1265.
- DeMaria, M., 1985: Tropical cyclone motion in a nondivergent barotropic model. *Mon.Wea.Rev.*, 113, 1199-1210.
- Dong, K., and C. J. Neumann, 1986: The relationship between tropical cyclone motion and environmental geostrophic flows. *Mon.Wea.Rev.*, 114, 115-122.
- Elsberry, R. L., 1990: International experiments to study tropical cyclones in the western North Pacific. *Bull.Amer.Meteor.Soc.*, 71, 1305-1316.
- Elsberry, R. L., and R. F. Abbey, Jr., 1991: Recent advances in understanding tropical cyclone motion. Technical Report NPS-MR-91-003, Naval Postgraduate School, Monterey, CA. 93943, 92 pp.
- Errico, R. M., 1985: Spectra computed from a limited area grid. *Mon.Wea.Rev.*, 113, 1554-1562.
- Errico, R. M., and D. Baumhefner, 1987: Predictability experiments using a high-resolution limited-area model. *Mon.Wea.Rev.*, 115, 488-504.
- Feuer, S. E., and J. L. Franklin, 1991: Nested analysis of hurricane Gloria from dropwindsonde and Doppler radar data. Preprints of 19th Conference on Hurricanes and Tropical Meteorology, Amer. Meteor. Soc., Boston, MA. 02108, 130-133.
- Fiorino, M., and R. L. Elsberry, 1989: Some aspects of vortex structure in tropical cyclone motion. *J.Atmos.Sci.*, 46, 979-990.
- Franklin, J. L., 1990: Dropwindsonde observations of the environmental flow of hurricane Josephine (1984): Relationships to vortex motion. *Mon.Wea.Rev.*, 118, 2732-2744.
- George, J. E., and W. M. Gray, 1976: Tropical cyclone recurvature and nonrecurvature as related to surrounding wind-height fields. *J.Appld.Meteor.*, 16, 34-42.

- Gray, W. M., 1989: Summary of ONR sponsored tropical cyclone motion research and future plans. Appendix D of Technical report NPS 63-89-002, Naval Postgraduate School (R. L. Elsberry, Ed.), Monterey, CA 93943, 68-79.
- Gross, J. M., 1991: The effect of shallow, medium, and deep layer mean wind in the beta and advection model. Preprints of 19th Conference on Hurricanes and Tropical Meteorology, Amer. Meteor. Soc., Boston, MA. 02108, 104-106.
- Holland, G. J., 1984: Tropical cyclone motion: A comparison of theory and observation. *J.Atmos.Sci.*, 41, 68-75.
- Holland, G. J., and J. L. Evans, 1991: Interactions between a barotropic vortex and an idealized subtropical ridge. II. Structure changes. *J.Atmos.Sci.*, (accepted).
- IMSL, 1989: IMSL Math/Library User's Manual. Fortran subroutines for mathematical applications. IMSL, Inc., 501-510.
- Joint Typhoon Warning Center, 1990: Annual Tropical Cyclone Report 1990. NOCC, Guam, Marianas Islands, 94-151.
- Kaplan, J., and J. L. Franklin, 1991: The relationship between the motion of tropical storm Florence (1988) and its environmental flow. Preprints of 19th Conference on Hurricanes and Tropical Meteorology, Amer. Meteor. Soc., Boston, MA. 02108, 93-97.
- Kasahara, A., and G. W. Platzman, 1963: Interaction of a hurricane with the steering flow and its effect upon hurricane trajectory. *Tellus*, 15, 321-335.
- Keenan, T. D., 1982: A diagnostic study of tropical cyclone forecasting in Australia. *Aust.Meteor.Mag.*, 30, 69-80.
- Lord, S. J., and J. L. Franklin, 1987: The environment of Hurricane Debby (1982). Part I: Winds. *Mon.Wea.Rev.*, 115, 2760-2780.
- Marks, F. D., Jr., R. A. Houze, Jr. and J. F. Gamache, 1991: Dual-aircraft investigation of the inner core of Hurricane Norbert. Part I. Kinematic structure. Submitted to *J.Atmos.Sci.*
- Neumann, C. J., 1979: On the use of deep-layer-mean geopotential height fields in statistical prediction of tropical cyclone motion. 6th Conference on Prob. and Stat. in Atmos. Sci., Amer. Meteor. Soc., Boston, MA 02108, 32-38.
- Roux, F., and F. D. Marks, Jr., 1991: Eyewall evolution in hurricane Hugo deduced from successive airborne Doppler observations. Preprints of 19th Conference on Hurricanes and Tropical Meteorology, Amer. Meteor. Soc., Boston, MA. 02108, 558-563.
- Velden, C. S., and L. M. Leslie, 1991: The basic relationship between tropical cyclone intensity and the depth of the environmental steering layer in the Australian region. *Wea.and Fcst.*, 6, 244-253.

INITIAL DISTRIBUTION LIST

	No. Copies
1. Defense Technical Information Center Cameron Station Alexandria, VA 22304-6145	2
2. Library, Code 52 Naval Postgraduate School Monterey, CA 93943-5000	2
3. Chairman (Code OC/Co) Department of Oceanography Naval Postgraduate School Monterey, CA 93943-5000	1
4. Chairman (Code MR/Hy) Department of Meteorology Naval Postgraduate School Monterey, CA 93943-5000	1
5. Prof. R. L. Elsberry (Code MR/Es) Department of Meteorology Naval Postgraduate School Monterey, CA 93943-5000	2
6. Lcdr. Richard H. Bohner Jr. 3339 Michael Dr. Marina, CA 93933-2464	1
7. Director Naval Oceanography Division Naval Observatory 34th and Massachusetts Avenue NW Washington, DC 20390	1
8. Commander Naval Oceanography Command Stennis Space Center MS 39529-5000	1
9. Commanding Officer Fleet Numerical Oceanography Center Monterey, CA 93943-5005	1
10. Director Naval Research Laboratory Monterey, CA. 93943-5006	1
11. Chief of Naval Research 800 N. Quincy Street Arlington, VA 22217	1
12. Commanding Officer Naval Oceanography Command Center, Guam Box 12 FPO San Francisco, CA 96630	1